UNIVERSITÀ DEGLI STUDI DI PAVIA

DOTTORATO IN SCIENZE CHIMICHE E FARMACEUTICHE E INNOVAZIONE INDUSTRIALE (XXXVI Ciclo)

Coordinatore: Chiar.mo Prof. Giorgio Colombo

Gel Cleaning Application to Historical Musical Instruments

Tesi di Dottorato di
Chaehoon Lee

AA 2022/2023

Tutor
Chiar.mo Prof. Maurizio Licchelli

Co-tutor
Chiar.mo Prof. Marco Malagodi

Abstract

Cleaning historical musical instruments requires special attention to the delicate nature of their materials. Especially those made of wood are prone to absorb water, risking damage. Players who frequently use these instruments can accumulate unwanted contaminants such as sweat and dirt, affecting their functionality and exhibiting beauty. Traditional cleaning methods that involve water can effectively remove contaminants from surfaces. However, they can also lead to solvent diffusion and residue issues. To overcome these challenges, conservators and restorers have started using gels as cleaning tools. Gel cleaning tools can contain solvents and prevent their diffusion on the surface of historic artworks due to their chemical or physical cross-linking networks.

This research focuses on the cleaning application of newly formulated, differently cross-linked gel systems based on natural polysaccharides such as sodium alginate and konjac glucomannan. The study aims to determine whether gels formulated from these biopolymers can be used to clean soil, sweat, and restored adhesives on historical musical instruments' hydrophobic and hydrophilic surfaces. The study examines the network of the newly formulated gels through spectroscopic techniques, thermal analysis, electron microscopy, moisture, and mechanical properties of the gels. In addition, cleaning was performed on mock-ups and original musical instruments, and analysis was conducted using noninvasive tools such as stereomicroscopy, profilometry, colorimetry, and noninvasive spectroscopic analysis.

Overall, this 3-year project succeeded in formulating and examining physical and chemical gels, evaluating their characteristics, and analyzing their cleaning efficacy before and after application, using a comprehensive methodological approach at the microscale level

Contents

Abstract **1**

List of Abbreviations **7**

Preface **11**

Introduction **13**

Chapter 1. Context of the Research Project **15**

1.1. Historical Wooden Musical Instruments and Surface Contaminants 16

1.1.1. East Asian Musical Instruments 16

1.1.2. Western Musical Instruments 17

1.1.3. Unwanted Contaminants on the Surface of Musical Instrument 19

1.2. Cleaning Procedures and Gel Systems in the Cultural Heritage Field 22

1.2.1. Cleaning Procedures and Cleaning Issues 22

1.2.2. Gel Systems and Cleaning Applications 26

1.3. Sodium Alginate and Konjac Glucomannan Materials in Cultural Heritage 33

Chapter 2. Experimental: Materials, Mock-ups, and Analytical Methods **35**

2.1. Gel Materials 36

2.1.1. Sodium Alginate Studies 36

2.1.2. Konjac Glucomannan Studies 36

2.2. Mock-ups and Case Study 37

2.2.1. East Asian and Western Wooden Mock-ups with Soiling 37

2.2.2. East Asian and Western Wooden Mock-ups with Sweat 38

2.2.3. Wooden Mock-ups with Restoration Adhesive 38

2.2.4. Case Study 40

2.3. Analytical Evaluation of the Gel Characteristics 41

2.3.1. Fourier Transform Infrared Spectroscopy with Attenuated Total Reflection (FTIR-ATR) 41

2.3.2. Liquid Nuclear Magnetic Resonance (NMR) 41

2.3.3. Thermogravimetric Analysis (TGA) 42
2.3.4. Scanning Electron Microscopy with Energy-dispersive X-ray Spectroscopy (SEM-EDS) 42
2.3.5. Mechanical Properties 43
2.3.6. Determination of Moisture Properties of the Gels 44
2.4. Non-invasive Analytical Setup for the Evaluation of the Cleaning and Removal Efficacy 45
2.4.1. Imaging 45
2.4.2. Stereomicroscopy 45
2.4.3. Profilometry 46
2.4.4. Colorimetry 47
2.4.5. External Reflection FTIR (ER-FTIR) 47
2.4.6. XRF Spot and Mapping Measurements 48
2.5. Cleaning System Evaluation 49

Chapter 3. Sodium Alginate-based gels 51

3.1. Sodium Alginate Properties and Applications 52
3.2. Calcium alginate 55
3.2.1. Gel Preparation 57
3.2.2. Gel Characterization 57
3.2.3. Cleaning Application and Evaluation of the Efficacy 60
3.2.3.1. Stereo microscopy and profilometry 60
3.2.3.2. Colorimetric Measurements 64
3.2.3.3. XRF 66
3.2.3.4. ER-FTIR 69
3.3. CA-GPTMS 73
3.3.1. Gel Preparation 74
3.3.2. Gel Characterization 75
3.3.3. Cleaning Application and Evaluation of the Efficacy 81
3.3.3.1. Gel residue examination 81
3.3.3.2. Cross-section 82

3.3.3.3. ER-FTIR 83
3.3.3.4. Case study 84
3.4. CA-XAMA7 85
3.4.1. Gel Preparation 87
3.4.2. Gel Characterization 88
3.4.3. Cleaning Application and Evaluation of the Efficacy 93
3.4.3.1. XRF mapping 93
3.5. Evaluation and Optimisation of Alginate-based Gels 94

Chapter 4. Konjac Glucomannan-based gels 97

4.1. Konjac Glucomannan Properties and Applications 98
4.2. Konjac Borax 98
4.2.1. Gel Preparation 100
4.2.2. Gel Characterization 101
4.2.3 Cleaning Application and Evaluation of the Efficacy 104
4.2.3.1. Stereo Microscopy and Profilometry 104
4.2.3.2. Colorimetric Measurements 107
4.2.3.3. XRF 109
4.2.3.4. ER-FTIR 111
4.3. Konjac borax-PVA-PVP 113
4.3.1. Gel Preparation 114
4.3.2. Gel Characterization 115
4.4. Konjac-Polyphenols 118
4.4.1. Gel Preparation 121
4.4.2. Gel Characterization 122
4.4.3. Cleaning Application and Evaluation of the Efficacy 125
4.4.3.1. XRF 125
4.4.3.2. ER-FTIR 127
4.5. Evaluation and Optimisation of Konjac-based Gels 129

Chapter 5. General Conclusion and Further Perspectives 131

Bibliography **134**

List of Figures **156**

List of Tables **163**

Acknowledgements **165**

List of Abbreviations

3D	Three-dimensional
CA	Calcium alginate
CA-GPTMS	Calcium-alginate-3-glycidoxypropyltrimethoxysilane
CA-XAMA7	Calcium-alginate-3-pentaerythritol tris[3-(1-aziridinyl)propionate]
DSC	Differential scanning calorimetry
EAM	East Asian mock-ups
ECH	Epichlorohydrin
ER	External reflection
EWC	Equilibrium water content
FTIR	Fourier transform infrared spectroscopy
FTIR-ATR	Fourier transform infrared spectroscopy with attenuated total reflection
G	Guluronic acid
GPTMS	3-glycidoxypropyltrimethoxysilane
IPN	interpenetrating polymer network
KG	Konjac glucomannan

KGB	Konjac-borax crosslinked hydrogel
KGPPB	Konjac-PVA-PVP-borax crosslinked hydrogel
KG-SKL	Konjac-soft kraft lignin polyphenol crosslinked hydrogel
KG-Vv	Konjac-*vitis vinifera* polyphenols crosslinked hydrogel
KK	Kramers-Kronig
LASER	Light amplification by stimulated emission of radiation
M	Mannuronic acid
NMR	Nuclear magnetic resonance
PP	Polyphenols
PVA	Polyvinyl alcohol
PVP	Polyvinylpyrrolidone crosslinked hydrogel
SA	Sodium alginate
Sa	Arithmetic mean height
SC	Swelling capacity
SCE	Specular component excluded
SEM-EDS	Scanning electron microscopy with energy-dispersive X-ray spectroscopy
SKL	Softwood kraft lignin

Ssk	Skewness
Sv	Maximum valley depth
TGA	Thermogravimetric analysis
THF	Tetrahydrofuran
TSP	Sodium salt of 3-(trimethylsilyl)propionic acid-2,2,3
UV	Ultraviolet
VIS	Visible
Vv	*Vitis vinifera*
WM	Western mock-ups
WR	Water Release
XAMA®7	Pentaerythritol tris[3-(1-aziridinyl)propionate]
XRF	X-ray fluorescence

Preface

The research for this thesis began with an investigation into the gel system, a colloidal material that has been widely used in the US and Europe cultural heritage field since the 1980s. However, to the best of my knowledge and experience, the gel cleaning system has not yet been widely introduced in Asian countries. Surprisingly, even today, in 2023, only one publication on the subject of gel cleaning has been published in Korea, the country where I come from.

In addition, the conventional approach to cleaning musical instruments involves using a damp cloth or cotton swab soaked in water or solvent to clean surfaces of unwanted contaminants such as soil, sweat, and adhesive residues. However, this method can be potentially aggressive as it may not control the interaction of the solvent with the surface material. It is particularly important to be attentive when applying aqueous methods to hydrophilic materials, which have a strong affinity for water.

For sensitive surfaces (e.g., paper with organic binders, wood with adhesives), the development in the last decades of gel system tools was highly demanded as the structure entanglement of gels is solvent retentive and ensures the amount of used solvent while improving cleaning efficiency. Nevertheless, the water-based physical gel systems (cellulose ethers, agar, and gellan gum) still offer a strong affinity for hydrogen-bonded materials such as paper, wood, and glues. However, limitations of using water-based physical gel systems also persist. The discontinuous fluid phase (water) can easily overflow on surfaces, and sometimes the stiffness and brittleness characteristics may leave gel residues on the artwork's surface.

Over this concern, in this thesis, two natural polysaccharides, sodium alginate and konjac glucomannan were chosen as the basis for the study and the goal was set to tailor the two polymers into a suitable cleaning tool. The chemical structure of alginates contains hydroxyl and carboxyl groups that can participate in multiple chemical reactions to modify the final characteristics. The chemical structure of konjac glucomannan contains hydroxyl and acetyl groups that can share the characteristics of high-water absorption. Moreover, both materials are biocompatible, biodegradable, non-toxic and widely used in the biomedical, pharmaceutical, and food fields.

The project branched out among different institutions and included relevant collaborations at the national level. The research conducted within the Department of Chemistry and the Department of Drug Sciences at the University of Pavia was focused on the formulation of the gels and the analysis of their chemical and mechanical characteristics. Moreover, within a scientific collaboration with the University of Milan Bicocca, novel gel formulations with antioxidant properties were developed. The determination of the cross-linkage of the formulated gels were examined by spectroscopic techniques, thermal analysis, electronic microscopy, and the evaluation of the moisture and mechanical properties of the gels were carried out.

The analytical investigation on the cleaning performance of the gels on mock-ups and original musical instruments was conducted at the Arvedi Laboratory of Non-Invasive Diagnostics in Cremona (CISRIC, University of Pavia) in collaboration with the National Enterprise for nanoScience and nanoTechnology (NEST) at Scuola Normale Superiore of Pisa.

Introduction

The thesis deals with differently cross-linked gel formulations based on natural polysaccharides, sodium alginate and konjac glucomannan, which so far are not the gel substances commonly used by conservators and restorers (agar and gellan gum). On this regard, the research study aimed:

i) to understand the materials (sodium alginate and konjac glucomannan) and their crosslinking characteristic and the derived gel characteristics (moisture and mechanical properties) by different chemicals and network systems (physical to chemical networks)

ii) to perform cleaning on representative mock-ups of historical musical instruments with soil, sweat, and restoration adhesive contaminants and systematic examination of cleaning efficacy.

To answer these aims, the discussion is divided into five chapters, organized from addressing the point of the theoretical background to in-depth investigation, experimental of gel characteristics and cleaning application of each sodium alginate and konjac glucomannan based gel.

Chapter 1 introduces East Asian and Western musical instruments, along with a description of unwanted contaminants on the musical instrument surfaces. Additionally, a cleaning procedure and brief concern about the cleaning process in cultural heritage is outlined.

Chapter 2 is dedicated to the experimental works that were composed and arranged for this thesis. It includes a description of representative musical instrument mock-up preparations and specific contaminants that conservators may intentionally seek to remove. Furthermore, analytical instrumentations and their analysis parameters are explained to understand the characteristics of the newly formulated gel substances (e.g., crosslinking system, moisture, and mechanical properties). To evaluate the cleaning effectiveness, the surfaces before and after cleaning were analyzed with noninvasive analytical instruments, and their analysis parameters are included.

Chapter 3 fundamentally explains sodium alginate material and concerns the synthesis of physical (ionic) and chemical (ester bonding) crosslinking formulations. For the physical crosslinking, calcium cation was used for the ionic crosslinking, and for the chemical

crosslinking, 3-glycidyloxypropyltrimethodxysilane (GPTMS) and Pentaerythritol tris(3-(1-aziridinyl)propionate) (XAMA7) were used for oxirane ring and aziridine ring opening and carboxylic group of alginate reaction. The chapter also includes the results of each newly formulated gel's chemical characteristics as well as features of moisture and mechanical properties. Practical cleaning performance and the results are also presented as well as the approach of the evaluation to understand the cleaning efficacy.

Chapter 4 fundamental explains cross-linking formulations of konjac-glucomannan with different types of chemicals. To improve the structural condition of the gel and the mechanical and moisture properties, interpenetrating polymer network (IPN) chemicals and polyphenols were used for crosslinking. Following the understanding of the formulated gel, a specific gel was selected to be used for cleaning, taking into account the corresponding properties of the gel. As in Chapter 3, a cleaning test was performed on the included mock-ups and a systematic evaluation to understand its effectiveness.

In the last chapter, a general conclusion and future perspective of the gel synthesized with sodium alginate and natural polysaccharide konjac glucomannan.

These threads allowed to grasp a comprehensive understanding of the different synthesis of natural polysaccharide gels. In line with this, extensive analytical techniques enabled the evaluation of cleaning efficiency on specifically prepared mock-ups and case studies.

Chapter 1. Context of the Research Project

1.1. Historical Wooden Musical Instruments and Surface Contaminants

1.1.1. East Asian Musical Instruments

East Asian musical instruments closely harmonize with nature, as evidenced by the derivation of raw materials from natural elements (Sahoon 1990; Korea National Gugak Center 2014). Traditionally, following the materials and their resulting sounds, they are mostly classified into eight sounds/tones (八音), which include metal (金), stone (石), silk (絲), bamboo (竹), gourd (匏), clay (土), skin (革), and wood (木) (Sahoon 1990; Korea National Gugak Center 2014). The music and instrumental tradition shared by China, Japan, and Korea originates from the same connection to the raw materials and the eight tones but simultaneously differs through historical and geographical peculiarities.

Among these musical instruments, a large number are made of organic materials such as wood, bamboo, and silk, due to easy access to raw materials and ease of processing. Musical instruments that are mainly made of organic materials are commonly found at archaeological sites, where anoxic environments help to slow down the decay of the material. As a representative example, in Korea, at Sinchang-dong Gwangju, a submerged musical instrument with wooden strings dating back to around 100 B.C. was excavated, of which the zither-like characteristic remained, making it recognizable as a musical instrument. This zither musical instrument was preserved by the wood conservator of the Gwangju National Museum with a careful examination of its condition and treatment that included cleaning, adhesive treatment, and drying (Gwangju 2002). Besides the archaeological findings, some musical instruments are well preserved from their previous use and are displayed and stored in the museum. The most important example of a long historical collection of wooden musical instruments in East Asia is preserved in an official warehouse of the imperial house Shōsōin (正倉院, also read as Zhengchangyuan, Nara, Japan). Shosoin's collection includes collections of musical instruments used by Emperor Shomu (聖武天皇, Shōmu-tennō, 701-756 CE, 45th emperor of Japan) and collections from other countries such as the Tang dynasty (唐朝, 618-907 CE, China) and the Silla dynasty (신라, 新羅, 57 BC - 935 CE, Korea)

(Akihiko Nishikawa 2009; Dien AE 2007). In Shōsōin (正倉院), the collections of musical instruments include biwa, koto, bamboo musical instruments, etc.

For musical instruments whose soundboard is made of organic materials (e.g. wood, bamboo), generally the construction ends with a surface treatment. The role of the final surface treatment is to protect the surface from scratches by musicians (Wilder 2010; Pollens 2015) and to protect the object from certain environmental factors (e.g. temperature, humidity, insects, microorganisms, etc.). For historical East Asian stringed musical instruments, mainly *Paulownia tomentosa* or *Paulownia coreana* are used. On the paulownia soundboard, the surface is treated with natural or organic pigments mixed with animal glue, lacquer and a traditional method of heat treatment called Nakdong technique (낙동법, 烙棟法). Nakdongbub has the meaning of Nak (낙; 烙; Lao) scorching, Dong (동; 棟; Tong) paulownia wood, and Bub (법; 法; Fa) is the term for the technique. It is a method of scorching the entire surface of dried paulownia wood to obtain a visible wood structure (Johnson 2004; Lee et al. 2021). The Nakdong technique is conventionally used in most East Asian string musical instruments (e.g., gayageum in South Korea, koto in Japan, and guzheng in China), historical ships, and furniture (Yoshikawa and Waltham 2014). In addition, there are evident oral and literature records about the beneficial effects for aesthetic purposes of treating this technique on the surface of paulownia wood to darken the colour and protect against pests and degradation caused by improper storage conditions and management (Kim 2010).

1.1.2. Western Musical Instruments

Western musical instruments were classified and structured by Erich Moritz von Hornbostel and Curt Sachs as the Hornbostel-Sachs classification in 1914. The division principle is based on the structure and physical properties of the instrument and, consequently, the way it produces sounds (Murray Campbell, Clive Greated 2004). There are four categories of idiophones, membranophones, chordophones, and aerophones, and the classification expands to five categories by including electrophones. The development of musical instruments is strongly linked to the gradual and continuous history of the cultural movement in Europe, particularly in Italy. At the beginning of the 14th century in Italy, there was a demand for

faster and more rhythmically complex music than that produced by the composers of the Ars Nova. Consequently, the musical instruments of the 15th-16th centuries developed in response to the change in musical style and became essential factors in the musical life of Europe (Geiringer 1978). In addition to the evolution of musical ideas and the new possibilities that composers and musicians could explore, musical instruments were modified into new forms and developed into a precursor version of many modern instruments (including violin, guitar, lute, and keyboard instruments) (Geiringer 1978; Bruce Carlson, Fausto Cacciatori 2006). Instrumental music flourished and established its form the most in the period between 1600 and 1750, which we can broadly define as the Baroque era. This is also evidenced by the golden age of the most modern string quartets (violin, viola, and cello) in Brescia and Cremona, which originated from Italy through Europe. Valuable string musical instrument makers include such notables as Andrea Amati, Antonio Stradivari, and Guarneri del Gesù, who devoted their working lives experimenting and establishing the model that has served as an example for makers ever since (Geiringer 1978; Bruce Carlson, Fausto Cacciatori 2006).

Their work also includes varnish treatment which is a finishing treatment after the construction of the musical instrument structure. Varnish is applied to beautify the appearance of the maple and spruce wood as well as give a unique color to the surface and protect the surface from biological attacks, which consequently results in a particular tone to the musical instruments. The distinctive tone of an instrument, which derives from the materials that are used (wood, ground layer, varnish, etc.) is also known to impact a wide range of discussions that give different characteristics in sound. Additionally, even though there was conservation and restoration work on wearing out areas repeatedly by the player's use, the ground varnish and some traditional varnish areas still remain (Bruce Carlson, Fausto Cacciatori 2006).

To the recent research results of the 17th-18th centuries historical musical instruments, most of the studies were held with maple (mostly with European maple *Acer platanoides*) as a base material as it is used as the resonance wood, side, neck, rib, bridge, head part and bow of the stringed instruments (Bruce Carlson, Fausto Cacciatori 2006; Wegst 2006; Bucur 2016). Also, spruce (mostly with European spruce *Picea abies*) is an important species as the main part of the soundboard (Bucur 2016; Lämmlein et al. 2019; Stanciu et al. 2020). On these maple and spruce woods, a finishing layer is applied, which, as is generally known, is primarily treated

with a ground layer of protein binders such as casein or animal glue with silicate compounds on the wood material. Following this, some research identified the varnish layer, composed of siccative oil dissolved with resin. Then the polishing and restoration layers are applied (Tirat et al. 2017; Spinella et al. 2017; Invernizzi et al. 2018b, 2020a; Kasprzok et al. 2020; Fiocco et al. 2021c). Furthermore, string musical instruments uphold until the present period their established pleasant sound, indeed they are still played by performers. The exposed usage by the performers necessitates continuous examination for the maintenance of the instrument and documentation of sound recording, as well as defining the techniques and materials used in restoration or conservation procedures (Barclay 1997).

1.1.3. Unwanted Contaminants on the Surface of Musical Instrument

Dust is one of the most common unwanted substances on musical instrument surfaces, which is found on objects stored and exhibited in museums. It is mostly considered to be “soiling on the surface”, which represents a dirty surface that is caused by the solid particle matter sitting on (or bonded to) the surface of an object.

Frequently, these particles can be seen by the naked eye in the museum's storage and on the collections laid on open shelves, which will require cleaning at the end. These soil particles are mostly airborne particles, derived from indoor conditions (e.g., enter and exit of passengers to the exhibition hall) or concrete buildings (that is one of the widely used construction materials from the 19th century) and from outdoor conditions (e.g., soot and gas) (Dost 1996; Tetreault 2003; Abbasi et al. 2016). Pollutants emitted from building materials could be a problem, as the air in a new concrete building is usually alkaline due to the presence of aerosol particles. For most parts, the soil may also contain higher levels of organic acids, particularly formic and acetic acids and low-level concentrations of both sulfur dioxide and nitrogen oxides (Sterling et al. 2000; Yeung et al. 2003; Bonaduce et al. 2016; Abbasi et al. 2016). This is because the materials are used in confined spaces, where any emissions become trapped and their concentration increases. Some sources of airborne particles could be present indoors, and concentrations of soil matter could be much higher than those outdoors. If enclosed with inappropriate materials, metal artifacts can corrode, and inorganic objects can suffer adverse reactions such as forming mixed salts. Organic materials suffer adverse effects when exposed to some pollutants. Cellulose-based materials such as paper, wood, and some

textiles may degrade due to acid or alkaline material, which eventually becomes brittle and susceptible to damage by handling.

Compromising the airborne particles both from outdoor and indoor conditions, the reason for the retention of soil on the surface of artworks is the size and the variety of interaction forces of the particles (Wolbers 2000). In museums, if particles of different sizes (0.03-0.5 μm and 5-100 μm, sharp and in crystalline form) are deposited on a surface that is not very uniform, the larger and lighter particles can be partially blown away with an air current, but very small particles, such as elemental (black) carbon and heavier particles, cannot be dislodged in this way. If the particles are still laid, they may become a permanent part of the structure. Therefore, since some dust may contain detrimental particles and if they are not removed and stored for a long time, the collections will certainly be damaged in the near future. Accordingly, the soil particles that accumulate may be bonded to the surface by molecular forces (ionic, dipolar, hydrogen bonding, or Van der Waals interactions), electrical, coulombic forces (attractive to the opposite charges of the particles), and mainly to the relative moisture current, and sparsely by oil (fat): all these factors may exist on the surface of the artwork (Cushman 1992; Wolbers 2000).

Other than dust, musical instruments are particularly concerned with unwanted substances as they are functional. It is distinctive from other artworks as it has “playability” (Barclay 1997). It means that during players' performances and practices, there is always pressure (mechanical stress) as well as players' body fluid (e.g., sweat) on the collection. As museum instruments are often vital sources of representing the historical existing practices and object materials, often museum instruments are played to remind the authenticity of the ability of the sound. On the other side, it is questioned for the potential wear and original substance alterations. Even from the past to the present with several generated players, restoration work was inevitable.

Music performers mostly play in an enclosed room or concert hall with a full audience. The enclosed space, with the air breathed by the audience and the humidity, is susceptible to making the performer sweat, and at the same time, direct body contact of the performer delivers moisture to the surface of musical instruments. Sweat, being composed mainly of water, small amounts of metal and nonmetal ions (Na^+, K^+, Ca^{2+}, Cl^-, and Mg^{2+}), metabolites (lactate, pyruvate, and xenobiotics), and nitrogen compounds (amino acids and urea), could

be a problematic factor for the surface of musical instruments (Patterson et al. 2000; Montain et al. 2007), particularly on hydrophilic surfaces (e.g., wood). One of the research works conducted an X-ray fluorescence spectrometry (EDXRF) examination of violin soundboards, the area on which violinists rest their chins directly. The examination detected the presence of traces of chlorine, potassium, and copper in the area where the violinist rests his or her chin directly, which are presumed to come from the musicians' sweat drops (Echard and Bertrand 2010).

Another necessary point is the long-term playing of the objects. Due to the periodic mechanical use, constant and vigorous vibrations, and continuous hand-to-hand physical contact, the body of the musical instrument often undergoes mechanical friction, such as cracks and wear, and delamination of the decorative elements (Bucur 2016). In addition, a long storage period and incorrect relative humidity and temperature management often lead to shrinkage and curvature. Particularly, these evident issues appear on wooden-bodied musical instruments. In order to maintain the aesthetic and acoustic style, violin restoration work was abundantly encouraged with constant repair work from the past.

Another unwanted material present on the surface of a musical instrument can be considered a restoration intervention. Until today, repeated restoration interventions were carried out, such as treating the new varnish on the surface of the violin where it was worn and applying adhesives to the cracks and splits in the plate to attach each joint of the wood structure as an additive to hold the material together, particularly on the internal unvarnished side of the plate with lining (e.g., linen and Japanese paper) together (H. Weisshaa 1988; Wilder 2010). For these adhesives, historically, glues based on -collagen and -proteins derived from animal hides, bones, and milk are widely applied due to their advantages of reversibility, non-toxicity, and water solubility (Schellmann 2007; Adams 2021). In particular, the most commonly used glues for wood manufacturing are protein-based and chemically structured with amino acids and peptide bonds. These glues, when aged on the artwork, oxidize and structurally deform, turning yellow, especially in the case of hide glue, darkening the colour (Schellmann 2007; Petrella et al. 2016). Furthermore, due to the decrease in protein hydrogen bonds (e.g. peptide bonds, carboxyl, and amine groups), old glues form flakes and cracks that cause the material to lose compactness and weaken adhesion over time, resulting in a loss of functionality (Petrella et al. 2016). Therefore, old glues are usually removed for conservation and

restoration operations and new, reversible glues are applied.

1.2. Cleaning Procedures and Gel Systems in the Cultural Heritage Field

1.2.1. Cleaning Procedures and Cleaning Issues

In general terms, cleaning means 'removing dirt or dust from something'. But for heritage artworks, cleaning is not a dogmatic application and must be tailored to the type of unique and valuable artwork and its material. In fact, the compound of the material to be cleaned (unwanted material) is complex; sometimes, the original layer underneath has brittle features due to environmental exposure. The practical cleaning of artworks requires a case-by-case examination and the ensuring of removing the unwanted material without causing stress to the original layers. For this reason, cultural heritage cleaning procedures require a comprehensive discussion of the challenges and critical issues.

The cleaning purpose usually determines the cleaning method. The cleaning procedures used in the cultural heritage field include mechanical, chemical (aqueous and nonaqueous), and non-contact (laser) (Cushman 1992; Umney and Rivers 2003; Stulik and Dorge 2004). Mechanical cleaning is carried out by the method of abrasive or rubbing the material with a certain range of handling by vacuuming or using tools like a brush, cotton swab, sponge, eraser, and scalpel (Daudin-Schotte et al. 2013; Valtierra et al. 2020). Generally, it is used for removing the accumulated substances derived from natural pollution, such as surface dirt, grime, and soil. As an alternative to the abrasive, Light Amplification by Stimulated Emission of Radiation (LASER) cleaning delivers short laser pulses to clean complex black pollution layers, particularly for sculpture conservation (Moretti et al. 2019). Chemical cleaning can be performed by using a variety of solvents (ethanol, methanol, acetone, benzyl alcohol, xylene, mineral spirits, or a mixture of one or more of these), water and water solutions containing soluble ions, soaps, enzymes, detergents, chelating agents, surfactants. Microemulsions containing organic solvents can also be applied for cleaning (Cushman 1992; Umney and Rivers 2003; Stulik and Dorge 2004). These solvents are carried out with a cotton swab or small brushes on the surface to remove soil, restoration adhesives, an aged layer of varnish, or retouched areas.

Concerning mechanical cleaning, it is sometimes aggressive toward organic materials, especially those composed of fibers. In addition to removing contaminants, the original layer of fiber structure of wood, textiles, and paper materials can be loosened and removed by compressed air or handling pressure (Ahmed 2011). In addition, mechanical abrasion can cause changes in gloss or loss of pigment and decoration particles for inorganic materials, such as metals and stone materials (Valtierra et al. 2020). The application of wet cleaning methods is intended to effectively clean soils adhering to the surface or aged restoration materials that are difficult to remove with mechanical cleaning, which causes intense stress to the surface. Moreover, applying water or solvents softens or loosens the adhesion strength of many dirt particles, facilitating their easy removal. However, although the intention is to deliver a small amount of solvent, wet systems with cotton swabs and brushes sometimes do not control the solvent capacity on water-sensitive surfaces. Especially when the surface is permeable to moisture (e.g., wood, paper), there is a possibility that the solvent can diffuse and cause swelling, particularly on the surface layer.

The cleaning procedure of musical instruments, it is deemed to be a minor cleaning and routine care. Generally, wooden musical instruments begin with the least aggressive cleaning and then move on to the necessary cleaning systems (Barclay 1997). In most cases, dust is brushed from the surface to the cloth-wrapped nozzle with a vacuum cleaner. In some circumstances, the damp swab is rolled until it is completely dried, at the same time lifting dirt from the surface and barely depositing water on the surface. In addition, on the inside part of the soundboard, restored glue joints and excess glue from the restoration work require cleaning. For this purpose, a damp swab with distilled water is repeatedly applied until the glue swells and softens (Barclay 1997; Umney and Rivers 2003). After, the softened glue is mechanically removed with a small spatula.

Cleaning issues that may occur when using an aqueous cleaning method and issues that must be addressed in conservation and restoration work on musical instruments are outlined here with examples 1) and 2).

Example 1) (Figure 1)

As an example of cleaning the restored area on the internal side of the violin with the animal glue, a damp swab is commonly passed over repeatedly on the animal glue-layered wood surface. As a description of the physical phenomenon, due to the certain retention of solvent/water used and the solvent delivery by swab, a solvent (or water) is delivered to the interface (glue). At the same time, the solvent (or water) diffuses inwards and outwards of the surface as well as wetting the interface and resulting swelling of the surface substances (glue).

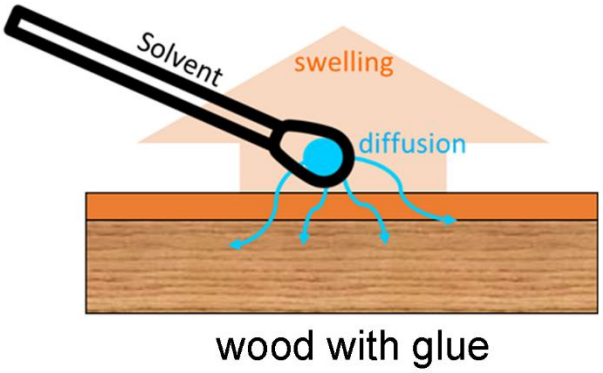

Figure 1. Example 1), schematic drawing of physical phenomena occurring simultaneously while cleaning glue on wood with solvent (water).

Retention is a material's ability to keep the solvent within or on its structure and is determined by the solvent/water diffusion rate towards the surface material (Phenix and Sutherland 2001). This is a physical phenomenon, the speed of which is governed by the surface tension and viscosity of the solvent. It means that a liquid with high surface tension and low viscosity will exhibit high retention. On the other hand, a liquid with low surface tension will exhibit higher wettability and low penetration on the surface (Cremonesi 2019; Volpi 2017).

Diffusion is a net movement of solvent transport occurring in open space, and this physical phenomenon is easily modeled in Fick's law if there are no external influencing factors (Phenix and Sutherland 2001; Baij et al. 2020; Di Tullio et al. 2023). Fick's law of diffusion, presented in equation (1), is described as the amount of flow of active substances is independent of the concentration of the applied substances and the diffusion coefficient.

$$J = -D\frac{d\varphi}{dx} \quad (1)$$

J: diffusion flux, D: diffusion coefficient, $\frac{d\varphi}{dx}$: concentration gradient

This means that the diffusion rate will increase if a solution with a high concentration and a substance with a high diffusion coefficient is used. The diffusion coefficient is a parameter of the inherent property (e.g., viscosity) and the medium in which it flows.

Swelling is a tangible effect of expanding the interacting area to a significant degree and softening the organic materials (e.g., paint layer, varnish area, animal glue, starch glue, and other types of adhesives) (Phenix and Sutherland 2001; Canevali et al. 2016; Baij et al. 2020, Baglioni and Chelazzi 2013). The interaction between the helical structure of glue reduces as water molecules bind to the interchain bond, which, in this case, is described as the glue being swelled by water. Once it swells the glue, the hydrophobic side group of helical chains arranges itself, which causes the material structures to shrink. As a result, the glue layer becomes loose and is reversible from the wood surface. However, at the same time, the support material of the violin soundboard, which in this case is wood, also absorbs the water as the wood is a hygroscopic and permeable material, and once it swells, the internal moisture of the wood can affect physical (e.g., split, curve, crack), and biological (e.g., microorganism growing) damages.

Example 2) (Figure 2)

When cleaning dust on wood (water-sensitive surface) with an aqueous cleaner involves the interaction between a liquid phase (aqueous cleaner) and a solid phase (wood surface). An issue with this process is that, due to the structure of the wood material (porous material), capillary permeation of the fluid is likely to occur, which will strongly correlate with the spread ability of the liquid to wet the solid surfaces. Diffusion rates are strongly correlated with substances from a monolithic porous material, which can easily be described by the fact that the liquid can easily diffuse into the porous material (Phenix and Sutherland 2001; Canevali et al. 2016; Baij et al. 2020; Baglioni and Chelazzi 2013).

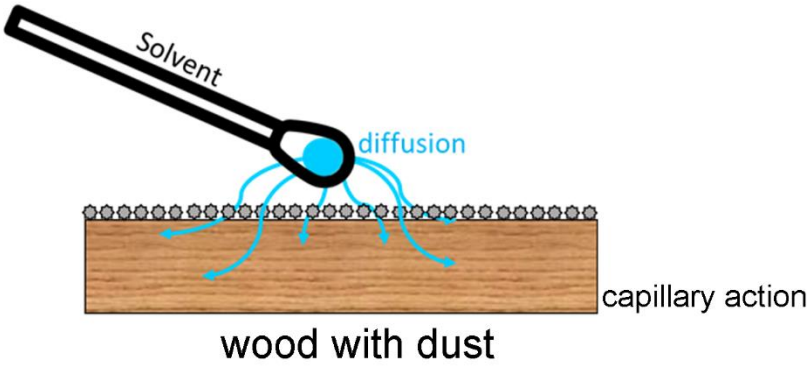

Figure 2. Example 2), schematic drawing of physical phenomena occurring simultaneously while cleaning dust on wood with a solvent (water).

For these complex issues, beginning with Richard Wolbers in the mid-1980s, an optional cleaning system, gel-based aqueous methods of cleaning painted surfaces, was introduced (Wolbers 2000).

As an excerpt from Wolbers 2000, an aqueous gelled system may offer:

- *control of the organic solvent evaporation rate and capillary flow into surrounding areas and underlying layers*
- *control of the surface contact time to increase the effectiveness of the cleaning agent and reduce potential effects on the surface.*
- *minimizing human exposure to toxic organic solvents*

The system began to offer a comprehensive approach to selecting a system for specific cleaning problems. However, at the same time, residue of the gel substances and leach from the aqueous agent were also addressed (Stulik et al. 2004).

1.2.2. Gel Systems and Cleaning Applications

A gel is a 3D structured polymer, either liquid or solid, with small or large colloidal particles interacting with liquid vehicles (G. O. Phillips and P. A. Williams 2009; Baglioni and Chelazzi 2013). The network system is classified through cross-linked physical and chemical bonds, and the gelators may be discrete small molecules, polymers, inorganic particles, or colloidal particles (Zhang et al. 2018; Baglioni and Chelazzi 2013). The matrix of gel networks has the characteristic of swelling, which means that the gel system takes

in fluids and retains them simultaneously. For hydrogel, the swelling arises from the hydrophilic functional groups attached to the polymer chains, while the resistance to discontinuation results from the cross-links between the polymer chains. This characteristic of gel encourages it to be considered an ideal substance for the absorption and adsorption of materials used in numerous applications.

The gels are classified into physical gels (physical linking) and chemical gels (chemical linking) (Figure 3) (G. O. Phillips and P. A. Williams 2009; Ibrahim et al. 2018). Physical gels are gel-like networks built by molecules cross-linked through non-covalent interactions, which also can be subdivided into strong and weak gels. The physical bonds include hydrogen bonds, ionic bonds, and self-assembly of small molecules. Physically crosslinked networks can mostly reverse their structure based on changes in temperature, pH, or solvent composition. Chemical gels are cross-linked and networked with covalent bonds, i.e., replacing hydrogen bonds with stronger and stable covalent bonds, which may provide permanent bonding (Rubinstein and Colby 2003; Gulrez et al. 2011; Ibrahim et al. 2018). It is an irreversible gel and can be formulated by addition, condensation, and cross-linking of the polymer chain in random or end-linking processes (Rubinstein and Colby 2003; Gulrez et al. 2011). Considering these characteristics, physical gels have a drawback in application to surfaces, such as the possibility of leaving solid residues of gel substances, because they have weak bonding compared to chemical gels (Stulik et al. 2004). On the other hand, chemical gels can induce changes in some properties of the network, such as swelling and elasticity.

Gel materials started to be applied in cultural heritage conservation as thickening agents, by Richard Wolbers (described in section 1.2.1.), for cleaning procedures alternative to mechanical and direct solvent application systems. Afterward, different polymer materials such as polysaccharides and synthetic polymers were used, and different crosslinking methods were applied in the cultural heritage field. Diverse gels with solvents applied on mock-ups and artworks are organized as in Table 1.

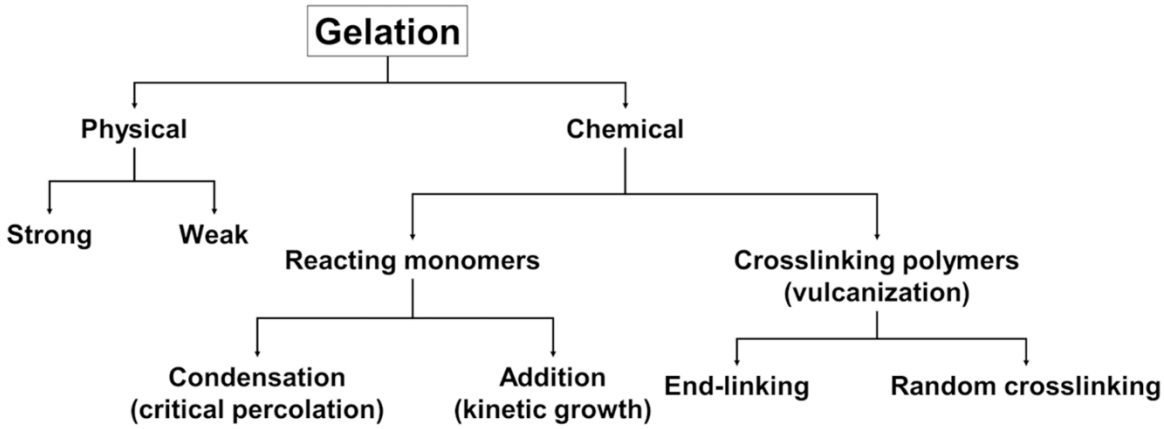

Figure 3. Classification of gelation mechanism (Rubinstein and Colby 2003).

An example of solvent gel is represented by Carbopol, a hydrophobically modified crosslinked polyacrylate polymer (Wolbers 2000; Stulik et al. 2004). For the application works, it is used by mixing with Ethomeen (surfactant), water, and organic solvents. Another widely used thickener agent used as the solvent gel is Klucel G, made of non-ionic cellulose ethers. It is remarkably used also by book conservators for consolidation treatments (Casoli et al. 2013; Moretti et al. 2020; Martínez-Domingo et al. 2020). Klucel G is soluble in water below 38 °C, insoluble in water above 40 °C, and soluble in many polar organic solvents, including methyl alcohol, ethyl alcohol, and isopropyl alcohol (95%). It is insoluble in poorly polar solvents such as toluene, xylene, and trichloroethylene. Both solvent gels and aqueous gels are applied by a cotton swab, and after the application, they are removed by a clean swab.

Other than the thickening agent used with the organic solvents, natural polysaccharides such as agar and gellan gum were used as they were featured to control the diffuse of liquid more than the solvent gels (Gorel 2010; Tireni et al. 2011; Scott 2012; Gulotta et al. 2014; Mazzuca et al. 2014; Canevali et al. 2016; Hughes and Sullivan 2016; Cremonesi 2016; Kanth et al. 2018; Smets et al. 2019; Di Napoli et al. 2020; Sansonetti et al. 2020; Bertasa et al. 2021; Cazzaniga et al. 2021).

A silicon-based gel, which displays a hydrophobic character, has been also used as a cleaning agent (Albano et al. 2020).

Besides the rigid gels, there was also an attempt of using soft featuring Polyvinyl alcohol (PVA)-borax gel, which showed cleaning effectiveness on irregular surfaces (Riedo et al. 2015; Al-Emam et al. 2019).

An organogel forming a gelator substance with organic solvent was also applied to selectively dissolve the specific type of contaminant present on the surface (Baglioni et al. 2015; Prati et al. 2018).

Moreover, the different features of the physical gel and chemical gel such as semi-IPN, PVA/PVP, and acrylamide hydrogels were also formulated and application tests were performed on the artworks (Domingues et al. 2014; Mazzuca et al. 2017; Bonelli et al. 2018, 2019; Bartoletti et al. 2020a).

Until now and still today, the gel cleaning procedure has been widely used by restorers, but due to the preciousness and uniqueness of each work of art, there is always a critical doubt about possible gel residue, solvent diffusion, and capillarity on the surface of different materials after application. This still represents a task to be validated and investigated. Furthermore, at the same time, the use of biopolymers and green gels has been particularly encouraged in the field of cultural heritage, as they will guarantee an environmentally friendly, biodegradable, non-hazardous, and consequently safe treatment for restorers', working environments and also for artworks (Gueidão et al. 2021; Passaretti et al. 2021, Volpi 2017).

Table 1. Diverse gels application in the cultural heritage field

Gel Classification	The main material of gel	Applied surfaces (materials and contaminants)	Solvents or compounds used together	Reference
Solvent gel	Carbopol	Varnish and unvarnished paint, 10 years old oil paint (polychrome surface)	Ethomeen C/12; C/25 in acetone and white spirit	(Moretti et al. 2020)
		Poly (vinyl acetate) fixative on the mural paintings	Acetone and dimethyl carbonate	(Yu et al. 2021)
	Klucel G (methylcellulose)	19th-century newspaper	followed by a treatment with a cotton swab using a hydroalcoholic solution (1:1 v/v)	(Casoli et al. 2013)
		Plaster with pigment and binders	distilled water; water and acetone (75:25)	(Martínez-Domingo et al. 2020)
		Varnish and unvarnished paint, 10 years old oil paint (polychrome surface)	ethanol, citric acid, EDTA	(Moretti et al. 2020)
Aqueous gel	Carbopol	Paper	-	(Warda et al. 2007)
	Klucel G (methylcellulose)	Industrial alkyd paints diluted in turpentine with soiling	-	(Bonelli et al. 2019)
Polysaccharide	Agar	Silk textiles with dye bleeding	D4 (octamethylcyclotetrasiloxane), D5 (decamethylcyclopentasiloxane)	(Smets et al. 2019)
		Marble with artificial staining	ethylenediaminetetraacetic acid (EDTA), triammonium citrate (TAC) or specific amino acid	(Sansonetti et al. 2020)
		Marble with artificial staining	Disodium EDTA, TAC	(Bertasa et al. 2021)
		Stone with copper stain	Disodium EDTA, TAC	(Canevali et al. 2016)

		-	Selective enzymes hydrolases, proteases, amylases	(Cremonesi 2012)
		-	water-in-oil emulsion and enzymes	(Cremonesi 2016)
		Wood with beeswax	micro-emulsion with SDS and Pentanol	(Gorel 2010)
		Sculpture with dark deposit covered on the surface	Tween 20, polysorbate surfactant; TAC, ammonium citrate tribasic; EDTA	(Gulotta et al. 2014)
		Wood with varnish	Ammonium and Sodium Citrate tribasic solution of synthetic saliva, tween 20, Vulpex™	(Cazzaniga et al. 2021)
	Gellan gum	Acrylic painted canvas	calcium acetate in ratio of 0.40g/L	(Kanth et al. 2018)
		Print works with yellow stains	calcium propionate, calcium propionate + TBAB	(Tireni et al. 2011)
		Modern paper	NaCl	(Di Napoli et al. 2020)
		Paper book	dilute calcium acetate solution (0.4g/L)	(Hughes and Sullivan 2016)
		Paper with starch paste	α-Amylase enzyme	(Mazzuca et al. 2014)
Silicon-based	Velvesil plus	Varnish layer on a lamina of brass with soiling and sweat	solvent cyclomethycaine D5	(Albano et al. 2020)
PVA-borax gel	a different formulation of PVA-borax and PEO	limestone coated with paraloid B72	30% 2-propanol, 30% acetone	(Riedo et al. 2015)

	PVA-borax-agar in different concentrations	Ancient Egyptian wall painting	EAPC system	(Al-Emam et al. 2019)
Organo gel	green PHB-GVL gel	Tempera and oil painting	Poly[(R)-3-hydroxybutyric acid], γ-valerolactone and other biodegradable solvents	(Samorì et al. 2016; Volpi 2017; Prati et al. 2018)
	pMMA gel (MMA-MEK, MMA-Cyclo, MMA-EA)	Easel painting	Methyl methacrylate (MMA), ethylene glycol dimethylacrylate (EGDMA), 2-butanone, ethyl acetate, cyclohexanone	(Baglioni et al. 2015)
Nanorestore gel	extra dry (MWR), Peggy 5, Peggy 6	Modern painting	TAC, organic solvents, etc.	(Bartoletti et al. 2020a)
	Semi-IPN hydrogel PVP-HEMA, MBA	Linen canvas treated with polymers (Mowilith DM5 and Plexol B500)	EAPC o/w microemulsion; water (73.3 wt%), sodium dodecyl sulfate (3.7 wt%), 1-pentanol (7.0 wt%), propylene carbonate (8.0 wt%) and ethyl acetate (8.0 wt%)	(Domingues et al. 2014b)
	PVA/PVP freeze-thawing	Industrial alkyd paints diluted in turpentine with soiling	-	(Bonelli et al. 2019)
	p(HEMA)/PVP gel	Paper with pressure-sensitive tapes	EAPC system is an oil-in-water microemulsion	(Bonelli et al. 2018)
	Semi-IPN hydrogel PVP-HEMA, MBA	Paper with animal glue and starch paste	α-Amylase enzyme, proteinase K	(Mazzuca et al. 2017)

1.3. Sodium Alginate and Konjac Glucomannan Materials in Cultural Heritage

In this thesis, we are studying two biopolymer materials - sodium alginate and konjac glucomannan - for their potential use in cleaning wooden musical instrument surfaces. These materials have not yet been extensively explored as cleaning systems for fiber materials such as paper, wood, and textiles.

Sodium alginate has been researched in the field of cultural heritage as a hydrogel and film with bioactive components, which can be used as antimicrobial composite coatings and as cleaning systems for stone artworks (Gaggero et al. 2021; Caruso et al. 2023). Researchers have developed an antimicrobial material that uses organic oxidized sodium alginate (OSA), inorganic calcium phosphate oligomers (CPO), and zinc oxide (ZnO) nanoparticles to safeguard historic stone surfaces from microbial biofilms (Li et al. 2021). Moreover, a PVA-borax hydrogel with ZnAl layered double hydroxide (LDH) supported with sodium alginate (SA) was loaded with different antimicrobials in the hydrogel network, including silver nanoparticles (AgNPs), silver nanoparticles-silver chloride (Ag/AgCl), and thyme essential oil (EO). The formulated hydrogels were used for the cleaning test on deteriorated stones (Boccalon et al. 2019, 2021). For a microbicide, alginate hydrogels supported by hypochlorite ions have also been utilized as biocidal agents against microbial colonization (Gabriele et al. 2021, 2022). Apart from stone and inorganic materials, cinnamon essential oils were incorporated into sodium alginate spheres and psyllium-alginate mixture spheres to control the release of the essential oil on the surface of cellulosic material, preventing paper and wood artwork from being damaged by chemical and biological contaminants (Campanella et al. 2021).

Meanwhile, for konjac glucomannan, there have been fewer studies and applications of konjac glucomannan in cultural heritage compared to its abundant research and utilization in cosmetics, foods, and pharmaceuticals. Recently, one of the attempts to use konjac material was to clean the bronze leachates in marble using environmentally friendly chelating agents (Vázquez-de la Fuente et al. 2023).

Chapter 2.

Experimental: Materials, Mock-ups, and Analytical Methods

2.1. Gel Materials

2.1.1. Sodium Alginate Studies

A medium viscosity sodium alginate (SA, Mw ~80,000 - 120,000 g/mol) material with a composition of 61% mannuronic (M) and 39% guluronic (G) acid, M/G ratio of 1.56 was purchased from Sigma Aldrich (Saint Louis, MO, USA). The medium viscosity SA was selected as a material as it is vastly used for the preparation of gels in medical areas (Vicini et al. 2015). For the examination of sodium alginate material, various multivalent cations (Ba^{2+}, Sr^{2+}, Ca^{2+}, $Mg^{2+,}$ and Al^{3+}) were introduced in different concentrations (1%, 2%, 4% w/v, in distilled water) and reaction times (5, 15 and 30 min). Further, the pH of the gels was measured with a paper strip (Carlo Erba, Italy). The results of this section are presented in Chapter 3.

For the preparation of the sodium alginate based-gels, the materials used in sections 3.2.1., 3.3.1., and 3.4.1. were sodium alginate medium viscosity, calcium chloride dihydrate ($CaCl_2 \cdot 2H_2O$, ≥ 99%), 3-glycidoxypropyltrimethoxysilane ($C_9H_{20}O_5Si$, GPTMS, 98%), and imidazole ($C_3H_4N_2$, ≥ 99%), and Deuterium oxide (D_2O, heavy water, 99.9 atom % D) were supplied by Sigma Aldrich, and used without further purification. Water was purified using a Millipore Organex system (R ≥ 18 MΩ.cm). The Pentaerythritol tris[3-(1-aziridinyl)propionate] ($C_{20}H_{33}O_7N_3$, XAMA®7) was generously provided from ICHEMCO srl (Milan, Italy).

2.1.2. Konjac Glucomannan Studies

A konjac glucomannan (KG) material with a purity ≥95%, Mw ~960,000 g/mol was kindly provided by Hubei Yizhi Konjac Co. Ltd (Yichang, China), was used for this study. The examination of konjac material consistency was carried out with a one-pot method using various alkali chemicals NaOH, KOH, $Ca(OH)_2$, and sodium tetraborate decahydrate (CARLO ERBA Reagents, n.d.) with different concentrations of KG (1%, 2%, 4% w/v, in distilled water). The results of this section are presented in Chapter 4.

For the preparation of the konjac glucomannan based-gels, the materials used in sections 4.2.1., 4.3.1., and 4.4.1. were konjac glucomannan, sodium tetraborate decahydrate, poly (vinyl alcohol) (PVA, Mw 146,000-186,000, 99+% hydrolyzed), and polivinilpirrolidone (PVP) were supplied by Sigma Aldrich. Softwood Kraft Lignin (SKL) was provided by Store Enzo (Enzo Chemicals, n.d.) and Omnivin Vitis Vinifera WG tannin (Vv) by OmniChem (OmniChem, n.d.). Water was purified using a Millipore Organex system (R ≥ 18 MΩ.cm).

2.2. Mock-ups and Case Study

2.2.1. East Asian and Western Wooden Mock-ups with Soiling

For representative mock-up preparation, the wooden mock-ups were prepared by considering the most representative East Asian and Western stringed historical musical instruments (Yoshikawa and Waltham 2014; Bucur 2016). On this focus, for East Asian mock-ups (EAM), the hydrophilic nakdong technique (see section 1.1.1.) treated wooden mock-up that can be found in musical instruments such as gayageum in South Korea, koto in Japan, and guzheng in China were prepared. For Western mock-ups (WM), hydrophobic varnish layered (see section 1.1.2.) wooden mock-up that can be found in musical instruments such as violin, viola, and double bass were prepared. A paulownia wood was used for EAM and spruce was used for the WM. The wood samples were cut in 10 cm × 10 cm × 1 cm (longitudinal × radial × tangential direction).

To prepare EAMs, the nakdong technique was applied and the preparation was carried out by the Korean wood master Seongcheol Seo (Wood Working Cooperative, Iksan-si, South Korea) (Figure 4a). A traditional iron tool specifically used for this treatment, customized by a blacksmith, was heated inside the hot kiln stove until it reached up to 1000 °C. After that, the iron tool was pressed with one stroke for 1-3 s along the direction of the wood grain. Lastly, all of each burnt surface was brushed off by brush (Lee et al. 2021).

To prepare WMs, a representative mock-up with glue as a ground layer and oil-colophony varnish was prepared together with professor Claudio Canevari (University of Pavia, Master in Restoration and Conservation of Cultural Heritage, Cremona, Italy) (Figure 4b). A ground layer of rabbit glue (10% w/w water solution) was applied using a brush. After that, two applications of oil-based varnish, composed of linseed oil and colophony (1:1 ratio), were

applied by brush (Invernizzi et al. 2020a). After applying the varnish, all samples were dried under UV light for 30 h.

In the conservation field, there are several adaptations or minimum changes of the mixture based on synthesis dust making from the Wolbers (1992) research. For the contaminant deposition, a dry portion of the synthetic soiling mixture consisted of the following ratios (w/w): iron oxide (burnt sienna pigment, 0.5%), gelatin (10.4%), soluble starch (10.4%), Portland type I cement (20.5%), silica (1.9%), lime (16.7%), kaolin (18.6%), and peat moss (20.8%); it was made by minimally changing the original soiling mixture of Wolbers (Wolbers 1992; Galatis et al. 2012). The wet portion was prepared with mineral oil in chloroform (4.5% v/v). All the soiling components were purchased from Bresciani S.R.L., Milan, Italy (Albano et al. 2020). After, preparing the mixture of the synthetic soiling, 1.1 g of dry portion and 20 mL of wet portion were mixed together. By using an airbrush at a 20 cm distance, the soiling mixture was evenly dispersed on the East Asian (EAM) and Western (WM) mock-up samples.

2.2.2. East Asian and Western Wooden Mock-ups with Sweat

On the representative EAMs and WMs, the synthetic sweat was applied. The synthetic sweat, which mimicked human hand sweat at pH 2.3 according to DIN ISO 9022-12, was purchased from Synthetic Urine e.K. (Eberdingen-Nussdorf, Germany). On all of the WM and EAM samples, synthetic sweat portions were sprayed by repeating the spraying and drying process five times to simulate the contact situation of the instrument user.

2.2.3. Wooden Mock-ups with Restoration Adhesive

In wood manufacture restoration works, commonly protein-based glue is used to attach the splits and to construct the joints. However, an adhesive that lost its functionality is removed and restored again with the new reversible glue. To this concern, an adhesive layer on the wood surface was simulated by following the literature applied to restore bowed string musical instruments, wood frames, and wood panels (H. Weisshaa 1988; A. Pizzi 2003). To do so, mock-ups were prepared using spruce wood (10 cm × 10 cm × 1 cm) with a 200 μm layer of 50% w/w rabbit skin glue (Bresciani Srl, Milan, Italy). Afterward, all samples were

dried for 24 hours at room temperature. To evaluate the cleaning ability of the gel on fresh and aged glue, a mock-up was artificially aged for 14 days (336h) using a custom-made prototype solar box that simulates the solar emission spectrum with a total irradiance of 540 Wm^{-2} at a wavelength of 560 nm (Cazzaniga 2018). The mock-up was placed on a 65 cm diameter rotating holder at a controlled temperature of 45 °C.

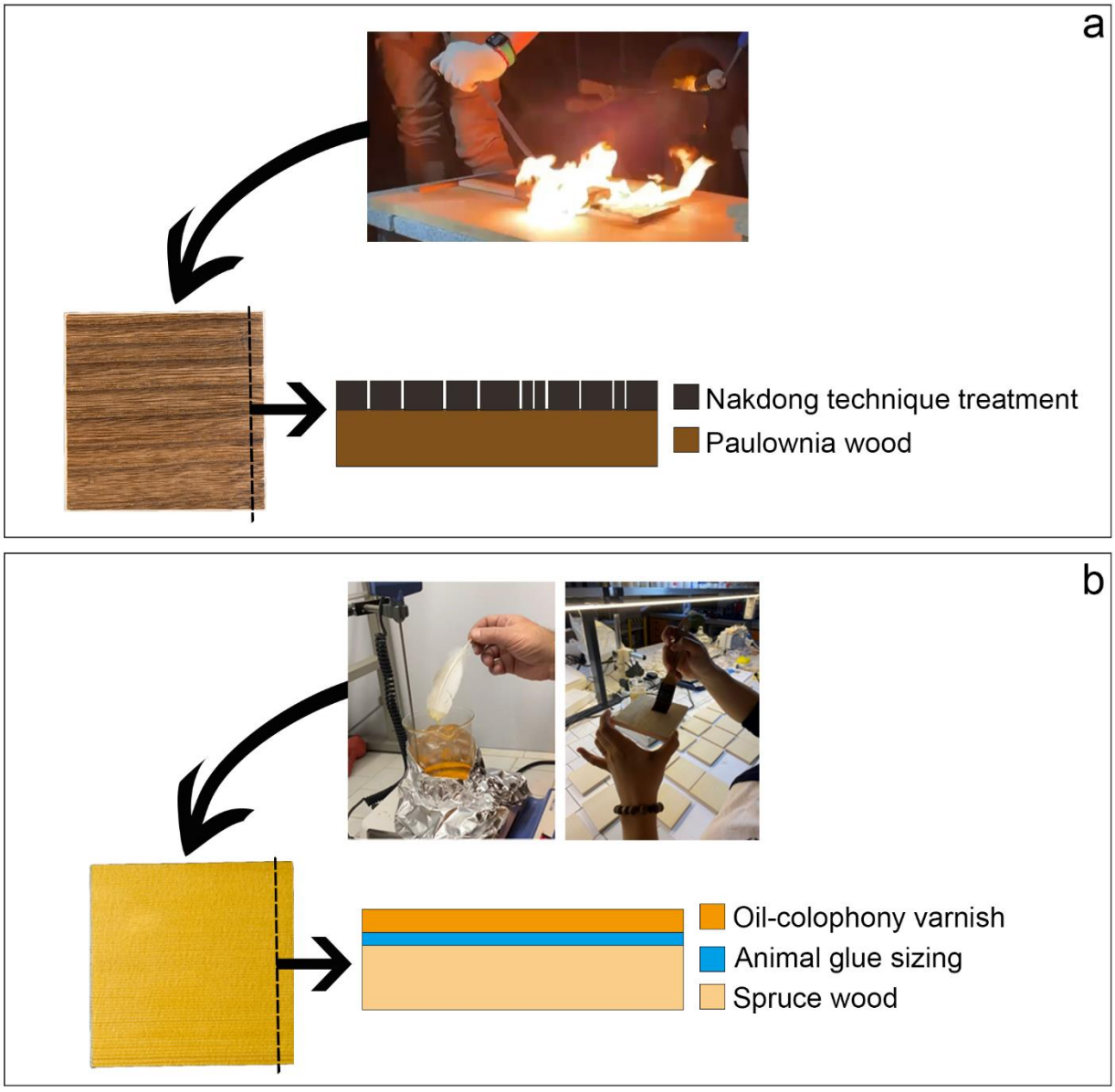

Figure 4. Schematic description of the preparation and reconstruction of wooden mock-ups representative of (a) East Asian and (b) Western musical instrument finishing treatments.

2.2.4. Case Study

A fragment of a historical musical instrument was detached from the front plate of a double bass, which had an extensive residue of naturally aged glue around a wood cleat (Figure 5), possibly related to the past maintenance or restoration procedure. The instrument dates back to 1830 and was made by Leopold Noiriel (1789-1849), a French luthier who worked in Turin for over three decades. As the old glue had lost its functionality, the cleaning test was necessary on the unvarnished side of the fragment, corresponding to the inside of the double bass body.

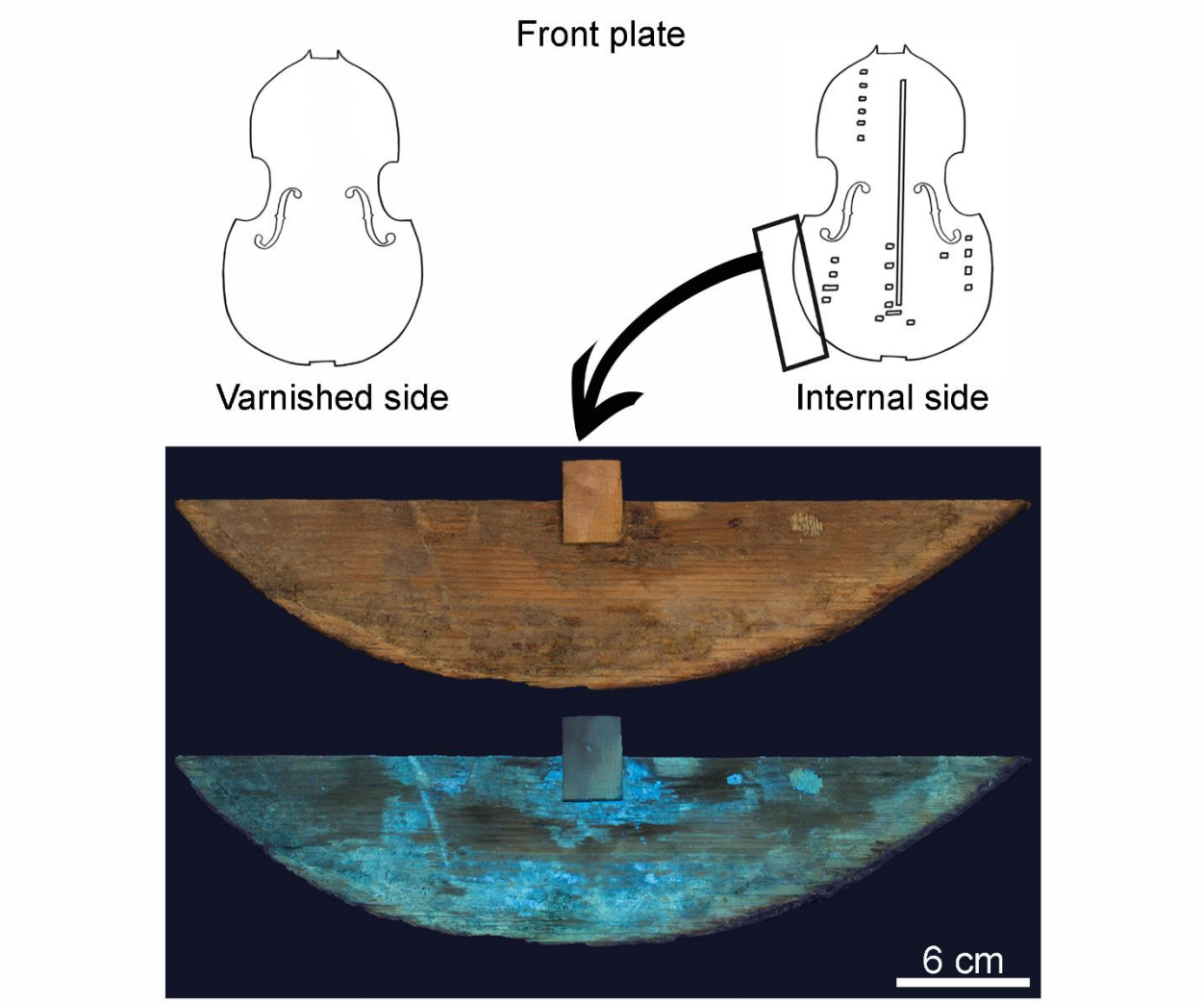

Figure 5. Sketch of the internal side of the double bass front plate and the detached fragment images in VIS (up) and UV (down).

2.3. Analytical Evaluation of the Gel Characteristics

2.3.1. Fourier Transform Infrared Spectroscopy with Attenuated Total Reflection (FTIR-ATR)

Fourier transform infrared spectroscopy with attenuated total reflection (FTIR-ATR) is a widely applied and valuable tool for understanding the chemical composition of hydrogels, such as functional groups and cross-linking with agents (Mansur et al. 2008; Phillips and Williams 2009). Therefore, we used this tool to obtain a chemical composition and its changes due to the cross-linking process. The examination was carried out by means of a PerkinElmer Spectrum 100 Fourier transform infrared spectrometer in the attenuated total reflectance (FTIR-ATR) mode (PerkinElmer, Waltham, MA, USA). The spectra were recorded in 4000-480 cm^{-1} range with 4 cm^{-1} resolution. The gel samples were dried previously to do the measurement, to reduce the effect of band related to water. All spectra were studied by the OPUS software package (ver. 7.2, OPUS, Billerica, MA, USA).

2.3.2. Liquid Nuclear Magnetic Resonance (NMR)

Liquid nuclear magnetic resonance (NMR) spectroscopy is a powerful analytical technique for understanding molecular-level information of hydrogen nuclei (protons, 1H) or carbon nuclei (13C) in organic compounds, capable of characterizing agents, the types of bonds involved, and the arrangement of polymer chains (Spyros 2016; The Nuclear Magnetic Resonance Society of Japan 2018). Given the usefulness of this tool, we used this technique to examine the chemical cross-linking of newly formulated gels prepared based on sodium alginate (SA). Samples were prepared with sodium alginate monomer and reactant in the ratio SA: reactant = 1: 1 in D_2O, then 0.5 ml of the solution diluted with D_2O was placed in a 5 mm diameter NMR tube and analyzed with the Bruker AVNEO 700MHz spectrometer (located at Centro Grandi Strumenti, CGS, University of Pavia) equipped with a TCI cryoprojector. Spectra were acquired at 298K and the reference chemical shift was TSP (sodium salt of 3-(trimethylsilyl)propionic acid-2,2,3).

2.3.3. Thermogravimetric Analysis (TGA)

Thermogravimetric analysis (TGA) and differential scanning calorimetry (DSC) are two thermal analysis techniques that provide information on thermal properties and material stability. DSC also provides information on the crystallinity of the polymer or the presence of cross-linking networks through the thermogram and alteration of thermal behavior (Ebnesajjad 2010).

The thermogravimetric analysis (TGA) was performed with Q5000 equipment (TA Instruments, New Castle, DE, USA) interfaced with a TA5000 data station under nitrogen flow (10 mL min^{-1}) in a platinum plate, heating approximately 3 mg of sample from room temperature to 600 °C (heating rate 10 K min^{-1}). The characteristics of the temperature values for each phase were defined by considering the DTG curve calculated by TA Instruments' Data Analysis software, which also allowed us to obtain the corresponding mass change.

2.3.4. Scanning Electron Microscopy with Energy-dispersive X-ray Spectroscopy (SEM-EDS)

Scanning electron microscopy with energy-dispersive X-ray spectroscopy (SEM-EDS) can provide a high resolution of the morphological characteristics and elemental composition of the material (Phillips and Williams 2009). For this analysis, by the differently featured characteristics of the gel, we used two different SEM instruments.

For the sodium alginate-based gels, prior to the examination, the gel samples were kept in a vacuum desiccator (with a slow vacuum flow) for approximately 24 hours. The samples were coated with graphite using the Cressington Carbon Coater 208 C for 20 seconds. Images were obtained with the Tescan MIRA 3XMU series field emission FE-SEM microscope (TESCAN, Brno, Czech Republic), set up with an accelerating voltage of 5 kV in high vacuum and equipped with a Schottky field emission source, and a Bruker Quantax 200 energy dispersive X-ray spectrometer (Bruker, Billerica, MA, USA). The apparatus is located at Arvedi Laboratory, CISRiC – University of Pavia.

In addition to the examination of the hydrogel, to ensure that no gel residue remained after cleaning, the examination of the gel residue was performed on fresh wood to which the gel was applied for 20 minutes; after the immediate removal of the gel, SEM-EDS analyses were

performed on the surface of the wood under conditions of 20 kV accelerating voltage and low vacuum.

For the konjac glucomannan-based gels, the gel samples were previously freeze-dried to maintain the gel structure. The gold coating was performed to avoid charge effects. Measurements were performed on an SEM Desktop PRO X PHENOM (Thermo Fisher Scientific, Waltham, MA, USA), located at the Department of Materials Science of the University of Milano Bicocca with a standard secondary electron detector with a beam energy between 4.8 and 20.5 kV.

2.3.5. Mechanical Properties

The mechanical properties examination was carried out with texture analysis depending on the shape and form of the gel (either film form or soft form). The thin-form gel was evaluated by stretching (tensile test) and the soft-form gel by compression (compressive test) (Hurler et al. 2012; Mantha et al. 2019; Vigani et al. 2021; Rossi et al. 2022; Said and Sarbon 2022). Furthermore, when conservators carry out cleaning treatments, it is done over a long period; for this reason, we chose a storage period of 60 days as a reasonable length of time to name the aged gels. To study the long-term physical stability of the gels, fresh gels (tested immediately after preparation) and aged gels (stored for 60 days at 4°C) were prepared and tested. (Nussinovitch 2005).

For the tensile test, the films were stretched uniaxially until failure to measure their tensile strength and elongation at break. By means of a TA.XT plus texture analyser (Stable Micro Systems, Godalming, UK), equipped with a 5 kg load cell. Each gel sample, respectively 2 mm thick in film form (1 cm × 3 cm), was clamped onto an A/TG tensile gripping probe and an initial distance of 1 cm was set between the grips. The upper grip was lifted at a constant speed of 2 mm/min for a distance of 50 mm. Prior to the test, the film thickness was measured with a Sicutool 3955G-50 apparatus (Milan, Italy). The tensile strength and elongation at break were calculated; at least three measurements were taken for each film.

The compression test involves the gels being stressed by uniaxial forces perpendicular to the sample surface, which allows the hardness and elasticity of the gel to be studied. The gels were prepared in 30 mm × 30 mm (diameter × height) cylindrical molds and stored at 4 °C prior to the compression measurement. The test was performed with a TA.XT plus texture

analyser equipped with a 5 kg load cell and a P/10 measuring system consisting of a cylindrical probe with a diameter of 10 mm. The probe was lowered with a test speed of 1.00 mm/s to determine a sample deformation of 70%. Compressive stress-strain curves were produced, and the following parameters were considered: (i) hardness as the maximum compressive force (Fmax) per unit area required for deformation of the sample; (ii) Young's modulus (YM) calculated as the slope of the tangent to the first part of the compressive stress-strain curve (<5% of deformation) to study the ability of each gel to withstand changes in length when subjected to compression.

Experimental data were subjected to statistical analysis, carried out through the statistical package Statgraphics 5.0 (Statistical Graphics Corporation, Rockville, Maryland, USA). In particular, a one-way ANOVA was carried out, followed by a Multiple Range Test.

2.3.6. Determination of Moisture Properties of the Gels

The examination of the moisture properties of the gel is important because the prepared gels will be applied to the surface of the wood material. For this purpose, we used the most widely used calculation method to determine the Equilibrium Water Content (EWC) and Swelling Capacity (SC). For determining the Water Release (WR) of the gel, the methodology proposed by Domingues et al. was utilized (Domingues et al. 2014). The mass of the dried gel and that of the initial mixture were weighed using an analytical balance (ACJ 320-4M, KERN, Balingen, Germany).

The EWC is information on the hydrophilicity of polymer networks, and the SC represents the percentage of solvent that can be loaded onto the gel network (Witono et al. 2014; Domingues et al. 2014; Chaudhary et al. 2020). The calculated EWC equation is presented in Equation (2) and SC in Equation (3). Ww is the weight of a sample with absorbed water (g), and Wd is the weight of a gel sample after drying at ambient temperature.

$$Equilibrium\ Water\ Content, EWC\ (\%) = \left[\frac{Ww - Wd}{Ww}\right] \times 100 \quad (2)$$

$$Swelling\ Capacity, SC\ (\%) = \left[\frac{Ww - Wd}{Wd}\right] \times 100 \quad (3)$$

The water release value of the gel provides information on the ability of the gel network to retain the solvent or to disperse it on a porous surface (Domingues et al. 2014; Karoyo and Wilson 2021). The Ws gel was placed on three sheets of filter paper inside a plastic container with a lid to prevent evaporation. The filter paper sheets were weighed before and 30 minutes after gel application. The size and thickness of the gel were 1 × 1 cm^2 and 2 mm, respectively. The WR was calculated using equation (4), where Fd is the initial weight of the filter paper, and Fw is the filter paper's weight with the gel's moisture.

$$Water\ Release, WR\left(^{\mathrm{mg}}/_{cm^2}\right) = [(Fw - Fd)/1] \times 100 \quad (4)$$

2.4. Non-invasive Analytical Setup for the Evaluation of the Cleaning and Removal Efficacy

2.4.1. Imaging

For the documentation of the thesis mock-ups and case-study objects, photos were taken under Ultraviolet (UV) and Visible (VIS) lights. Images were acquired before and after cleaning using a Nikon D4 full-frame digital camera (Minato, Tokyo, Japan) equipped with a 50 mm f/1.4 Nikkor lens. The images were obtained in visible light (f/11 and ISO 100) using an SL-60W LED lamp (GODOX, Shenzhen, China) and UV-induced fluorescence (f/11, ISO 400, and 20 s exposure time) by illuminating with an emission peak at 365 nm.

2.4.2. Stereomicroscopy

A stereo microscope is a microscope capable of providing a three-dimensional view of the sample. We used stereomicroscopy to observe in detail the contaminants (soil and sweat) dispersed on the surfaces of the mock-ups. In addition, for wood with adhesive, to understand the thickness of the glue removed from fresh and aged mock-ups, cross-sections were prepared before and after cleaning by embedding the samples in epoxy resin (Bresciani Srl) and dry polishing with fine silicon carbide sandpaper (800-8000 mesh). The dispersed contaminated samples and the cross-sections were observed in visible and UV light using an Olympus stereomicroscope (SZX10, Olympus, Tokyo, Japan) equipped with an Olympus HD

DP73 camera. Images were captured using PRECiV Capture software (ver. 1.2 Olympus, Tokyo, Japan).

2.4.3. Profilometry

The optical profilometer is a non-contact, interferometry-based method used for the characterization of surface topography and is commonly applied in various fields, from cultural heritage to engineering and medical applications (Courard and Nelis 2003; Rodriguez et al. 2009; Sadowski et al. 2016). In particular, in the case of cultural heritage materials, the profilometer has provided relevant information on smooth surfaces with roughness in the nanometer range to detect cracks and defects (Garbacz et al. 2006). In addition, the optical profilometer provides a wide range of roughness parameters, calculated according to specific ISO standards (De Chiffre et al. 2000; Gadelmawla et al. 2002).

With this metrological technique capable of measuring three-dimensional profiles and obtaining characteristic features, 3D profilometric maps and roughness data were acquired using a Taylor Hobson non-contact 3D profilometer (Taylor Hobson Ltd., PO Box 36, 2 New Star Road, Leicester, LE4 9JQ, UK). Analyses were performed at a magnification of 20× and a working distance of 4.7 mm, covering a surface analysis of 0.8 mm on clean areas. Profilometric measurements were performed on samples with a non-reflective surface to obtain a reliable 3D reconstruction of the surface: soiled-WM, soiled-EAM, and sweat-EAM. Due to the highly reflective surface, profilometric measurements, including 3D maps and calculations of roughness parameters, were not performed on sweat-WM. Five measurements were performed on each cleaned area to obtain an indication of the original surface after the cleaning procedure. Roughness parameters and 3D maps were obtained from the surface analysis and processed with TalyMap Gold 6.2 software.

The roughness parameters obtained from the 3D maps were calculated as defined in ISO 25178. In this study, amplitude parameters were selected to describe the surface of the mock-ups before and after cleaning: arithmetic mean height (Sa), skewness (Ssk), and maximum valley depth (Sv) (Gadelmawla et al. 2002; Sadowski et al. 2016). The mathematical explanation of these parameters can be found in the literature (Bennett 1993; De Chiffre et al. 2000; Garbacz et al. 2006; Feidenhans'l et al. 2015). Sa is the most widely used roughness parameter for quality control. It is defined as the mean of the absolute deviation of roughness

irregularities from the mean line and provides a good general description of height variations, although it is not sensitive to small sample variations. Sv is defined as the maximum depth of the profile below the mean line within the evaluation length. Ssk is used to measure the symmetry of the profile around the mean line, which means that this parameter is sensitive to occasional deep valleys or high peaks. A Symmetrical Height Distribution (number of valleys equal to the number of heights) has zero skewness. Profiles with a majority of valleys have a negative skewness. Profiles with full valleys or high peaks have a positive skewness. The value of Ssk depends on whether the majority of the material sample is above (negative Ssk) or below (positive Ssk) the mean line.

2.4.4. Colorimetry

To standardize and quantify cleaning before and after cleaning, colorimetric measurements were carried out using a portable Konica Minolta spectrophotometer (CM-2600d Konica Minolta, Tokyo, Japan). The acquisition was performed with a 0.8 mm round target accessory after black/zero calibration. The L*, a*, and b* (CIE color space, 1976) values were collected using the SpectraMagic NX software (ver. 3.31., Tokyo, Japan). Since the visual appearance of East Asian and Western mock-up surfaces is different, the average value of the specular component excluded (SCE) mode was used for further calculation. In order to understand the difference between before and after cleaning, $\triangle$E* values were calculated by the following equation (5):

$$Chromatic\ difference, \triangle E^* = \sqrt{[\triangle L^{*2} + \triangle a^{*2} + \triangle b^{*2}]} \quad (5)$$

2.4.5. External Reflection FTIR (ER-FTIR)

The External Reflection FTIR (ER-FTIR) is a highly sensitive technique for analyzing a primary probe of the upper few micrometers of a sample in a non-destructive manner. Due to this characteristic, it has been widely applied in the heritage field for analyzing chemical changes occurring on the surface of materials and identifying materials and surfaces degraded by the environment (Invernizzi et al. 2018a; Cazzaniga et al. 2021; Fiocco et al. 2021a). The analysis was performed with a Bruker Alpha portable spectrometer (Bruker Optics, Billerica, MA, USA). The measurement was taken at a distance of 5 mm through the external

reflectance module consisting of a 23°/23° optical arrangement. Spectra were collected between 7500 and 375 cm^{-1} with a resolution of 4 cm-1 and an acquisition time of 2 minutes. The data were acquired and processed with the OPUS 7.2 software. For an appropriate need, the reflection spectrum was transformed into absorbance spectra using the Kramers-Kronig (KK) algorithm included in the software package (ver. 7.2, OPUS, Billerica, MA, USA).

2.4.6. XRF Spot and Mapping Measurements

X-ray fluorescence (XRF) is the most widely used analytical technique for determining the elemental composition of materials in archaeometry and cultural heritage diagnostics due to its speed, sensitivity, and non-destructive technique (Rovetta et al. 2018; Bezur et al. 2020). XRF measurements were carried out using the energy-dispersive portable XG Lab—Bruker (Bruker Optics, Billerica, MA, USA) ELIO spectrometer with a Rh anode and a 1.2 mm collimator.

The spot analysis was performed by setting a tube voltage of 40 kV, a tube current of 40 μA, and a measurement time of 480 s. Subsequently, the collected values corresponding to the Kα peak net area counts of each element were normalized to the time and average of the entire data set of Rh-Kα peak net area counts at coherent scattering (Invernizzi et al. 2020b). The mean value was calculated over at least three measurements with the corresponding standard deviation.

XRF maps were acquired with a tube voltage of 40 kV and a current of 40 μA, with a measurement time of 3 s and a step size of 1 mm. All data were collected and processed with Elio software (ver. 1.6.0.29, Bruker Optics, Billerica, MA, USA).

To examine the cleaning efficacy from the XRF map, calcium (Ca) was chosen as the marker element for the soiling mixture (containing cement) in soiled-WM and soiled-EAM, and chlorine (Cl) as the marker element for synthetic sweat (containing sodium chloride and ammonium chloride (Zörner et al. 2017) in the sweat-WM and sweat-EAM. The counts per pixel of the marker elements were calculated with pyMCA version 5. 6. 7., ROI imaging tool on 4-pixel areas (2 × 2 in pixels). Subsequently, mean values and standard deviations were calculated with the following equation (6) (Duncan et al. 2021):

$$Cleaning efficacy(\%) = 1 - \left(conts\ per\ pixel\ of\ cleaned\ area \Big/ counts\ per\ pixel\ of\ uncleaned\ area\right) \times 100\% \quad (6)$$

2.5. Cleaning System Evaluation

Evaluations were carried out and compared using star diagrams (Excel radar charts) to assess the cleaning efficiency of the gel systems. This evaluation process was created by modifying the assessment used in previous research (Bartoletti et al. 2020a,b; Bravo 2023) to easily understand different cleaning tools and reflect the conservation decision-making process.

As described in Table 2, five helpful evaluation parameters were established for each cleaning system and rated from 1 (poor/inadequate) to 5 (most appropriate). After the cleaning test, these five criteria were established by evaluating the developed gels. Each parameter signifies the following:

- Durability of gel - This refers to the ability of a cleaning system to withstand strength without breaking. If the gel is not fragile, it could mean that less residue remains after cleaning. Please refer to section 2.3.5 for more details.
- Flexibility of gel - This refers to the ability of a cleaning system to bend easily without breaking. This property might be useful when cleaning particles on irregular surfaces. Please refer to section 2.3.5 for more details.
- Water retentivity of gel - This refers to the ability of a cleaning system to retain water and release less on the surface. This is an important property when applied to hydrophilic surfaces. Please refer to section 2.3.6 for more details.
- Visibility of the underlying surface after cleaning - This parameter refers to the surface observation after cleaning. It is evaluated by detailed observation from magnified images that evaluate the removal of contaminants. Please refer to sections 2.4.2 and 2.4.3 for more details.
- Cleaning Efficacy - This parameter refers to the removal carried out after cleaning. It is analyzed using FTIR (section 2.4.5) and XRF (section 2.4.6).

The documentation tool uses a star rating system to indicate the most promising cleaning systems across all parameters. The systems with the widest stars could be referred to as an effective cleaning tool.

Table 2. Evaluation parameters and corresponding rating scale

Parameter	**Rating**				
	1	**2**	**3**	**4**	**5**
Durability of gel	Fragile, breaks easily	Fairly breakable	Breaks at a certain strength	Fairly hard to break	Durable strength
Flexibility of gel	rigid	Fairly rigid	Moderate texture	Soft and flexible texture	Very flexible texture
Water retentivity of gel	Extreme water release	Moderate water release	Slight amount of water release	Very slight amount of water release	Barely visible water release
Visibility of the underlying surface after cleaning	No visible removal of contaminant	Very Slight removal of contaminant	Slight removal of contaminant	Moderate removal of contaminant	Significant removal of contaminant
Cleaning efficacy	XRF cleaning efficacy over 10 %, no removal examination by FTIR	XRF cleaning efficacy over 40 %	XRF cleaning efficacy over 60 %	XRF cleaning efficacy over 75 %	XRF cleaning efficacy over 90 %, clear removal examination by FTIR

Chapter 3.

Sodium Alginate-based gels[1]

[1] This Chapter are based on:
Lee, C.; Volpi, F.; Fiocco, G.; Weththimuni, M.L.; Licchelli, M.; Malagodi, M. Preliminary Cleaning Approach with Alginate and Konjac Glucomannan Polysaccharide Gel for the Surfaces of East Asian and Western String Musical Instruments. *Materials* **2022**, *15*, 1100. https://doi.org/10.3390/ma15031100
Lee, C.; Di Turo, F.; Vigani, B.; Weththimuni, M.L.; Rossi, S.; Beltram, F.; Pingue, P.; Licchelli, M.; Malagodi, M.; Fiocco, G. Biopolymer Gels as a Cleaning System for Differently Featured Wooden Surfaces. *Polymers* **2023**, *15*, 36. https://doi.org/10.3390/polym15010036

3.1. Sodium Alginate Properties and Applications

Alginates are nature-sourced polysaccharides found mainly as structural components in marine brown algae (*Phaeophyceae*). The water-soluble sodium salt of alginic acid is anionic, biocompatible, and of low toxicity. In addition, it has the characteristic of forming rapid gelation in the presence of divalent cations. It has wide applications in various fields, such as biomedicine, drug carriers, food additives, and cosmetics (G. O. Phillips and P. A. Williams 2009; Abasalizadeh et al. 2020; Fernando et al. 2020; Solberg et al. 2023). The chemical structure of alginate consists of blocks of mannuronic acid (M) units and guluronic acid (G) units that form a binary linear copolymer of β-D-mannuronic acid (M) and α-L-guluronic acid (G) residues (Pawar and Edgar 2012; Pedersen 2018; Solberg et al. 2023). Based on the extracted sources, there are differences in the M and G contents, and due to the high content of L-guluronic acid and G sequences, the gel forms a mechanically robust gel with reduced junctions (Figure 6) (Pedersen 2018; Solberg et al. 2023).

The representative cross-linking of alginate is ionic cross-linking with different cations (e.g., Ca^{2+}, Al^{3+}, Mn^{2+}, Sr^{2+}, Cu^{2+}, and Ba^{2+}), which consists of an ion exchange process with water-soluble alginate (Papageorgiou et al. 2010; Lotfipour et al. 2012; Vicini et al. 2017; Brus et al. 2017). The gelation kinetics and final properties of the gel depend on the presence of the counter ions. The different sequences of MG/MG, GG/GG, and GG/MG junctions determine various gel characteristics. Increasing the egg-box pattern of the GG/GG junction results in stable and rigid gel while increasing long blocks of MG results in greater strength, tightness, and elasticity than the other junction formations (Figure 7) (Draget et al. 2005; Donati et al. 2005; Li et al. 2016; Solberg et al. 2023).

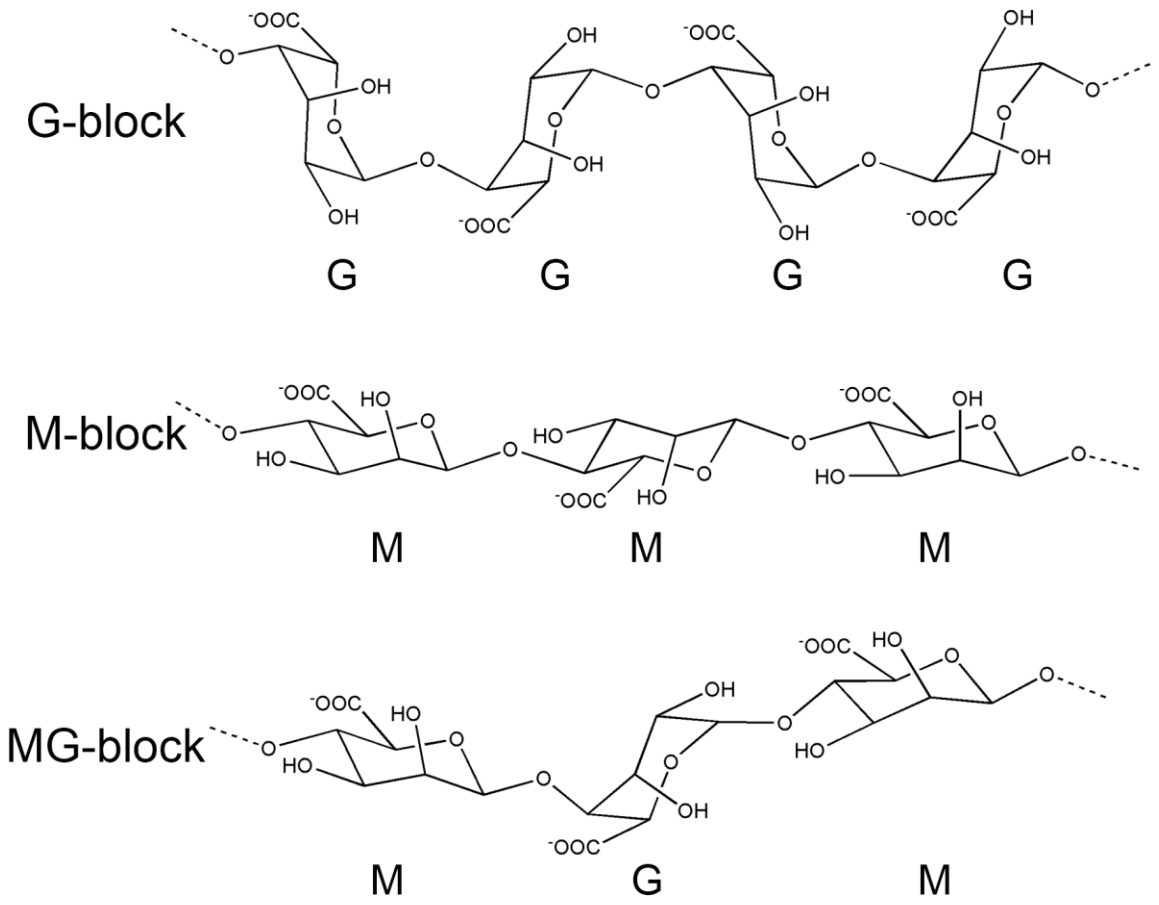

Figure 6. Three different junction zones by calcium ion with alginate. MG/MG, GG/GG, and GG/MG junctions are made up of chains of M-block and G-block (Donati et al. 2005).

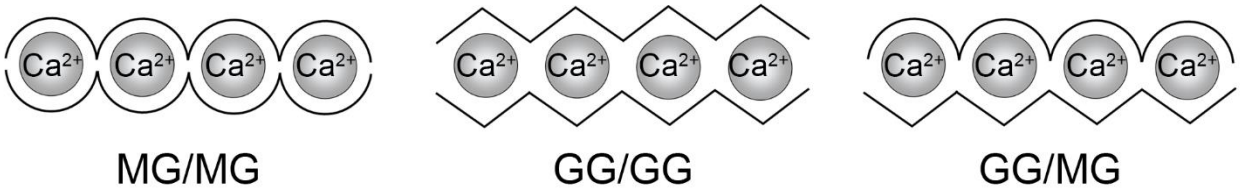

Figure 7. A different block structure in alginate. The M-block represents β-D-mannuronic acid and G-block represents α-L-guluronic acid (G) (Pawar and Edgar 2012).

Furthermore, due to the ionic interaction characteristics of alginate binding to multivalent cations, direct mixing of these two components rarely produces homogeneous gels and most likely results in a gel lump (Haraguchi et al. 2023). Concerning the gelling of alginate by ionic crosslinking, it is essential to control the introduction of the crosslinker. This ionotropic

gelation can be prepared in two different methods: diffusion and internal setting (Figure 8) (Yamauchi 2001; Paques et al. 2014; Gurikov and Smirnova 2018; Solberg et al. 2023). The diffusion method is characterized by the diffusion of a cross-linking ion (e.g., Ca^{2+}, Al^{3+}, Mn^{2+}, Sr^{2+}, Cu^{2+}, and Ba^{2+}) from an external reservoir into the alginate solution, which commonly results into alginate beads and nanoparticles. The internal setting method is prepared by the controlled release of the inert calcium ion source within the alginate solution, which tends to be homogeneous as the calcium source remains evenly distributed during gelation. In this regard, the different consistency of the gels is due to the different sequences of the MG/MG, GG/GG, and GG/MG junctions, the different chemical concentrations, the different cations, and the different preparation methods (Draget et al. 2005; Solberg et al. 2023). For this reason, experimentation was necessary to investigate gels' materials and different handling behaviors by formulating the sodium alginate in different conditions.

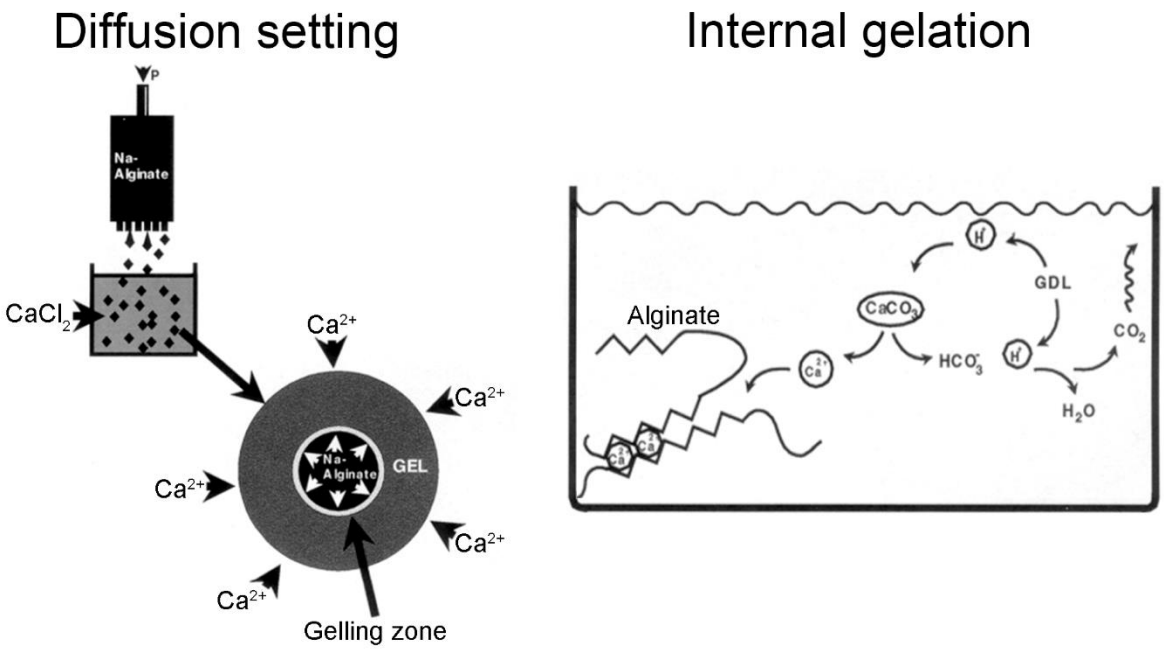

Figure 8. Different gelation methods of diffusion and internal setting methods (Draget et al. 2005).

3.2. Calcium alginate

To investigate the desiring gel texture for the cleaning application, a preliminary examination of the crosslinking of sodium alginate with multivalent cations was conducted. The materials for the investigative study of the sodium alginate are described in section 2.1.1.

The alginate gel prepared by directly introducing the divalent cations commonly created a lump with the solvent and the pH value was 6-7 (Figure 9a). After 15 min, a gradual diffusion of the solvent occurred from the lump form of the gel, leading to leaching problems (Al-Musa et al. 1999; Chuang et al. 2017). However, it was observed that when the gel was prepared in a film-like form with a thickness of 2-3 mm and crosslinked with 2% $CaCl_2$, it exhibited promising strength and flexibility, which are crucial properties for cleaning applications (Figure 9b). While on higher concentrations than 2%, it textured to be rigid, and similar research results are shared when prepared in film form with $CaCl_2$ at high concentrations such as 3% and 6% was not suitable for usage in biomedical applications, while 1.5% was recommended (Li et al. 2016). On the other hand, with the trivalent cation Al^{3+}, a film structure was easily formed, as expected by the three-dimensional bonding structure and the pH value was 4-5 (Figure 9c) (Brus et al. 2017; Nataraj and Reddy 2020). However, the alginate-aluminum gel broke easily and could not be used for the cleaning system. By this overall examination, a 2 % w/v calcium cation solution was selected for crosslinking. The expected reaction between calcium ion and alginate is sketched in Figure 10.

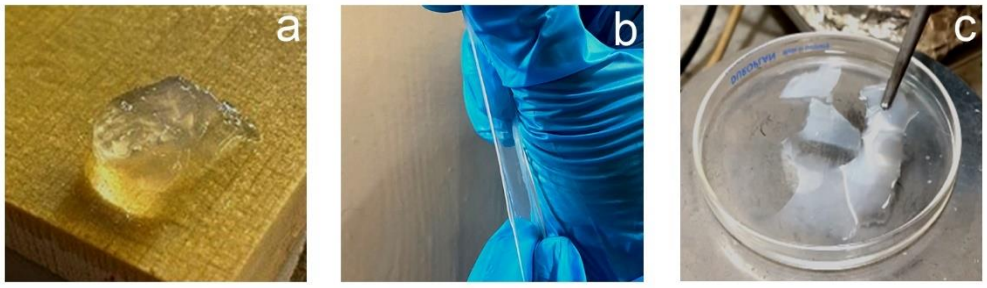

Figure 9. Gelation of alginate with calcium ion formed in egg-shell structure, and after leaving for 10 min on the surface of WM, the solvent diffused (a). Gelation of alginate with calcium ion (b) and with aluminum (c) in thin form gel.

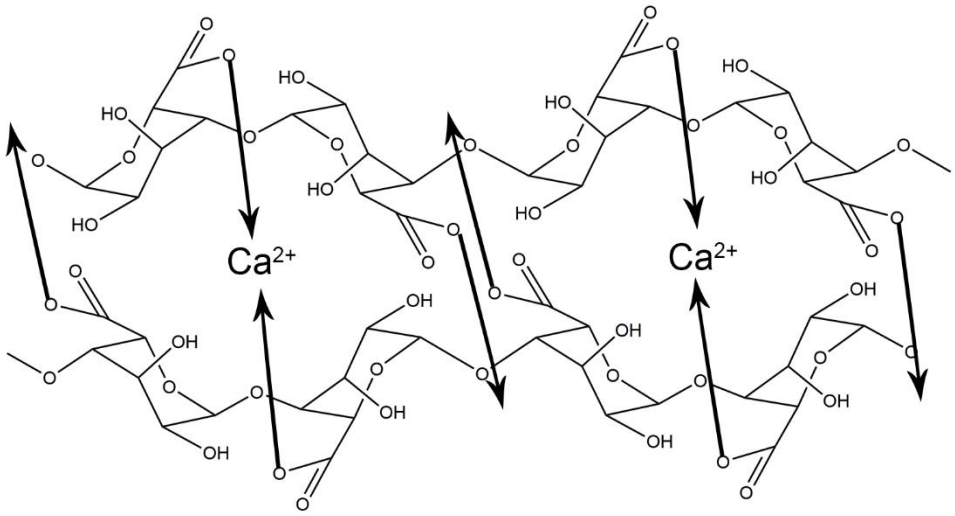

Figure 10. Expected reaction between alginate polymer and calcium ions (Al-Musa et al. 1999).

3.2.1. Gel Preparation

Based on the preliminary examination in section 3.2., the CA gel was prepared. To obtain CA gel, 0.2 g sodium alginate (SA) was added into a beaker containing 10 ml of distilled water, and the solution was stirred at 40 °C until it was completely dispersed. Afterward, in order to prepare it into a film form gel, the SA solution was poured into a petri dish until it reached a 2-3 mm thickness. In the prepared container, $CaCl_2$ 2% (w/v) solution in distilled water was poured to allow cross-linking with calcium ions in a molar ratio of SA: Calcium = 1:900 for 15 min. The formed Ca-alginate (CA) gel was repeatedly washed in deionized water to remove unreacted materials (Figure 11).

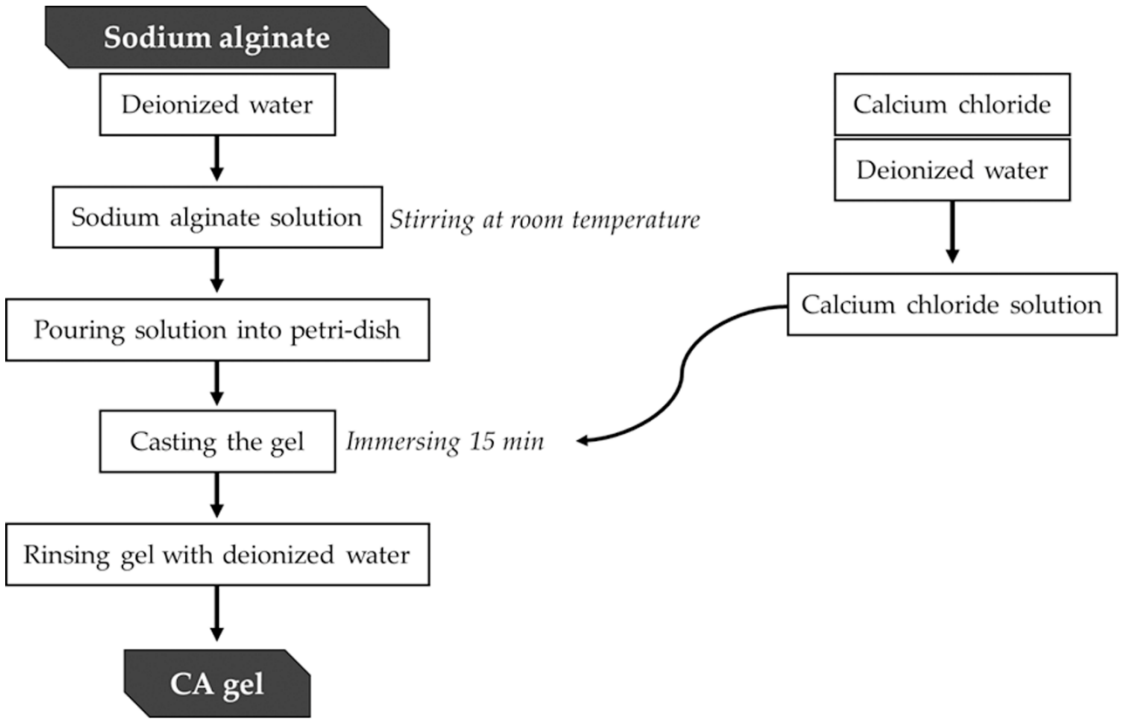

Figure 11. A schematic diagram of steps involved in preparing CA gel.

3.2.2. Gel Characterization

Infrared spectrum (FTIR-ATR) of plain sodium alginate (SA) displays a broad peak between 3600 and 3000 cm^{-1} due to O-H stretching, bands at 1410 and 1600 cm^{-1} ascribed to COO^{-} asymmetric and symmetric stretching, respectively, (Papageorgiou et al. 2010; Li et al. 2016; Badita et al. 2020) (Figure 12a), and a band at 1025 cm^{-1} ascribed to C-O stretching. After

interaction with calcium ions peaks corresponding to symmetric stretching of carboxylate and C-O stretching underwent a shift to a higher wavenumber (from 1406 to 1416 cm^{-1} and from 1025 to 1035 cm^{-1}, respectively) with respect to plain SA, due to electrostatic interactions involving carboxylate groups and calcium ions. The shift of symmetric assignments due to metal-carboxylate groups and peak intensity variations were previously reported and associated to the stabilization of the egg-box structure in alginate derivatives (Papageorgiou et al. 2010; Li et al. 2016; Badita et al. 2020). Additionally, upon examining the gel samples that were dried on a vacuum desiccator (detailed preparation methods are described in section 2.3.4.), it was observed that the surface did not appear to be spherical in shape. Instead, a more elongated structure with an irregular-edged surface was noted (as shown in Figure 12b,c), which was further supported by the information obtained from the SEM image.

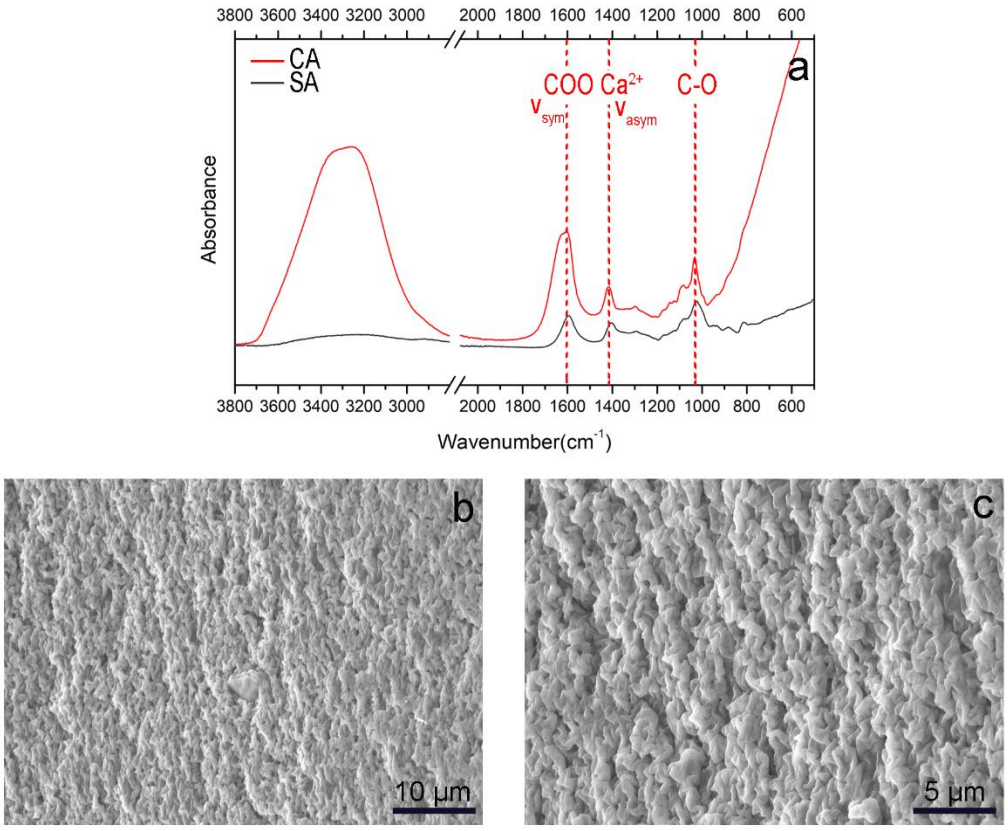

Figure 12. FTIR spectrum of the Ca-alginate formulated gel (CA) and pure sodium alginate (SA) (a). Markers for electrostatic interactions of carboxylate groups and calcium ions (red dotted line). SEM image of CA gel (b) acquired in high vacuum with secondary electrons.

The mechanical properties of the CA gel were measured by comparing it with agar gel as a control. Moreover, fresh and aged CA gel and agar gel were also compared to understand the shelf-life consistency after 60 days.

The CA had statistically significant tensile strength and elongation values at break compared to the agar gel. The agar gel appeared very brittle as it broke easily without elongation; even after 7 days of storage at 4 °C, microorganisms were observed on the agar gel in thin form, and after 60 days, it appeared dry. Consequently, no measurements were performed on the aged agar gel, as this could compromise the accuracy of the test. Comparing fresh and aged CA gels, a significant decrease in elongation at break was observed after 60 days (Table 3). Although the CA gel becomes less mechanically resistant with aging, its mechanical properties are significantly higher than those of the fresh agar gel, offering the possibility of using the CA gel for cleaning even after 60 days.

Table 3. Mechanical properties of gels determined by tensile testing (mean value ± s.d.; n = 3). ANOVA one-way, Multiple Range Test ($p \leq 0.05$): having the different superscript symbols (, **, $^{\#}$, °, §, §§) indicate statistically different data. AUC: Area Under the stress–strain curve.*

Classification		Tensile Strength (kPa)	Elongation at Break (%)	AUC
CA gel	Fresh	328.3 ± 59.3 **	193.7 ± 16.8 $^{\#}$	10029 ± 1751 §
	Aged	239.6 ± 24.3 **	26.7 ± 1.3 $^{\#}$	2396 ± 250 §§
Agar gel	Fresh	13.4 ± 0.1 *	11.8 ± 0.1 °	-
	Aged	measurements were not possible to be taken		

The moisture properties of the CA gel are summarized in Table 4 and were compared to those of agar as a control. The CA gel showed almost half less water uptake than the agar gel, with the result aligned with the equilibrium moisture content (EWC) and swelling capacity (SC). Furthermore, the water release (WR) of agar was six times higher than that of the CA gel, indicating the ability of the CA gel to retain water when subjected to external forces. This result could suggest that CA gel is more efficient in moisture control than agar gel, a traditional hydrogel commonly used for cleaning historical objects.

Table 4. Moisture properties of CA and agar gels used for the cleaning test, namely equilibrium moisture content (EWC), swelling capacity (SC), and water release (WR). The average values and the related standard deviations were determined by repeating the experiment five times. D.W. = distilled water

Gel	EWC (%)	SC (%)	WR (mg/cm^2)
CA	64.0 (± 5.0)	(1.8 ± 0.4) × 10^2	5.4 (± 1.0)
Agar	95.6 (± 0.3)	(2.2 ± 0.2) × 10^3	29.3 (± 2.5)

3.2.3. Cleaning Application and Evaluation of the Efficacy

For the cleaning application, the prepared CA cleaning system was gently rinsed with deionized water and immersed in the 2% of ecosurf^{TM} EH-9 (EH-9, Sigma Aldrich, Saint Louis, MO, USA) solution (v/v, in distilled water) for 24 h. EH-9 is known as a nonionic surfactant that is readily biodegradable and effective in removing oily soils (Keefe and Ormsby 2011; Ormsby et al. 2016). The cleaning was repeated each time for 5 minutes; the gel was applied up to three times (CA_1, CA_2, CA_3) on WM and EAM surfaces, where the synthetic soil and sweat were dispersed, and the preparation of these mock-ups are presented in sections 2.2.1. and 2.2.2.

3.2.3.1. Stereo microscopy and profilometry

For the evaluation of surface topography, macroscopic and microscopic observations were carried out using stereomicroscopy, 3D profilometric maps, and the corresponding roughness parameters, i.e., Sa, Sv, and Ssk, for a comprehensive understanding by adapting the pros and cons of each instrumentation (Rodriguez et al. 2009; Janus et al. 2010). Observing the mock-ups without contamination, the stereo and 3D maps provided information on the different surface roughness of the two mock-ups: the varnish-layered WM appeared to have a smooth and flat surface; in contrast, the EAM showed a distinct surface roughness (Figure 13). After the dispersion of the soil contaminants, a high surface area correlated to the presence of deposits can be observed for soiled-WM and soiled-EAM by stereomicroscopy (Figure 14). With profilometry, the observation of contaminant deposits was more evident (Figure 15), in

line with the results of other research indicating that profilometry can assess polishing quality (Alves et al. 2006; Janus et al. 2010).

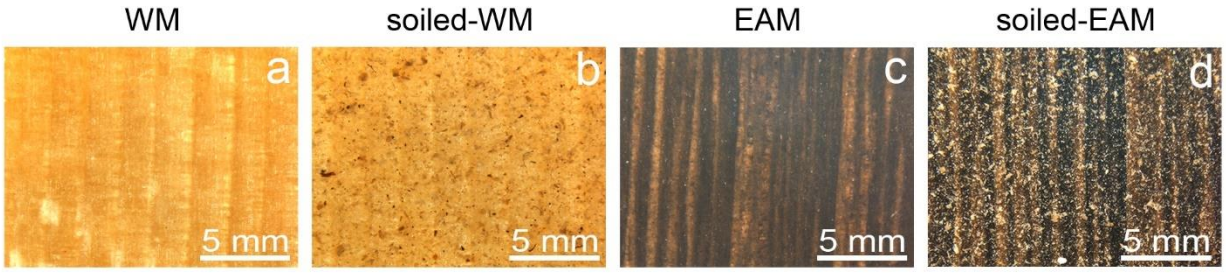

Figure 13. Stereomicroscopy images of WM (a), soiled-WM (b), EAM (c), and soiled-EAM (d) mock-ups.

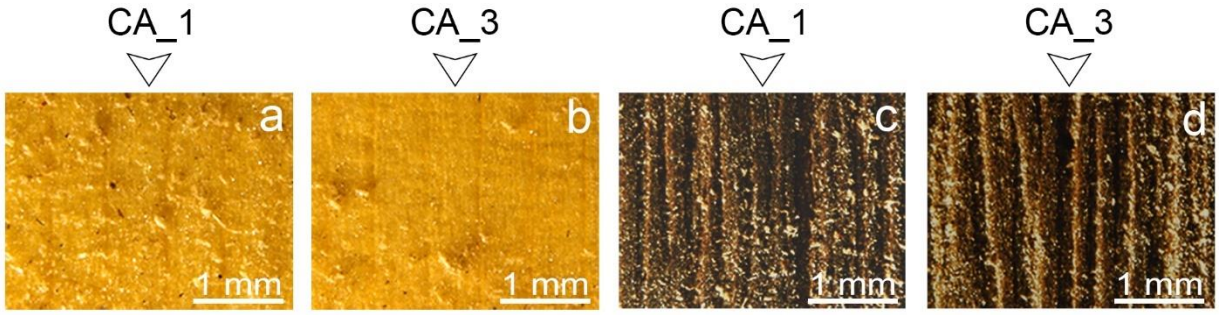

Figure 14. Stereomicroscopy images after the cleaning application on soiled-WM by CA gel at different application times CA_1 (a) and CA_3 (b), and on soiled-EAM by CA_1 (c) and CA_3 (d).

Concerning the cleaning application of CA gel on soiled-WM, no significant soil removal was observed on CA_1 and CA_2 applied areas (Figure 15a,b). After repeating the cleaning on CA_3, some soiling particles were unevenly removed, scarcely providing access to observe the smooth surface of the varnish underneath. Moreover, the roughness parameters obtained by the profilometric measurements confirm a decrease in particle concentration after subsequent applications (Figure 15c,d,e). This trend was also visible in the numerical values of Sa and Ssk parameters, representing a comparable result between the repeated application of CA and agar gel. On the soiled-WM, Sv seems to describe very well the surface roughness reduction through the cleaning applications: both the values related to CA decrease by repeating the applications. The Sv related to agar is displayed here at a slightly lower value.

While the surface of the soiled-EAM appears morphologically inhomogeneous, we considered the micro-scale variations as an indication of the cleaning efficacy (Figure 16a,b). Sa and Ssk parameters appear to have similar trends, with CA from 1 to 3 applications. In contrast, Sv (Figure 16c,d,e) highlighted some differences: the increase in the value of Sv in CA_3 suggests that subsequent applications better removed soiling deposits. Therefore, this could be attributed to the roughness of the EAM and the fact that the removal of soiling deposits within the wood irregularities exposes the original high surface roughness, in contrast to WM, where cleaning exposes the smooth surface.

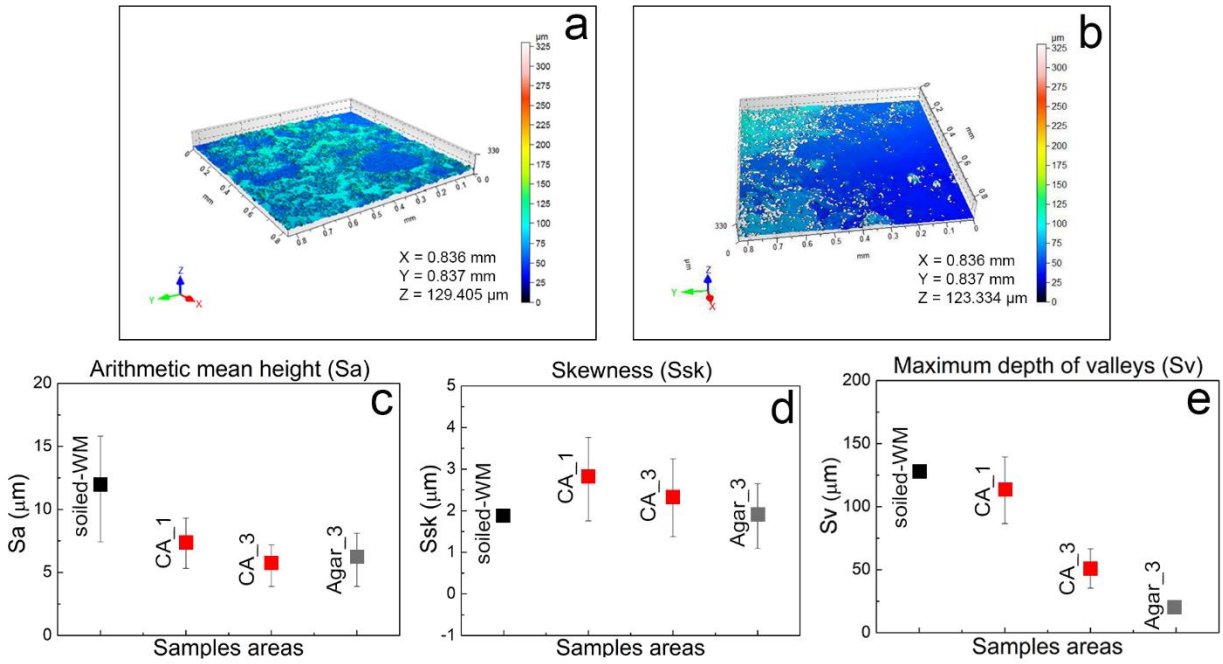

Figure 15. 3D heat maps of soiled-WM (a) cleaned by CA_3 (b). The colour range represents the different heights (in microns) of the details present on the sample surface. Considered roughness values of Sa (d), Ssk (e), and Sv (f) on the different areas of soiled−WM cleaned by different gels and application time CA_1, CA_3, and Agar_3.

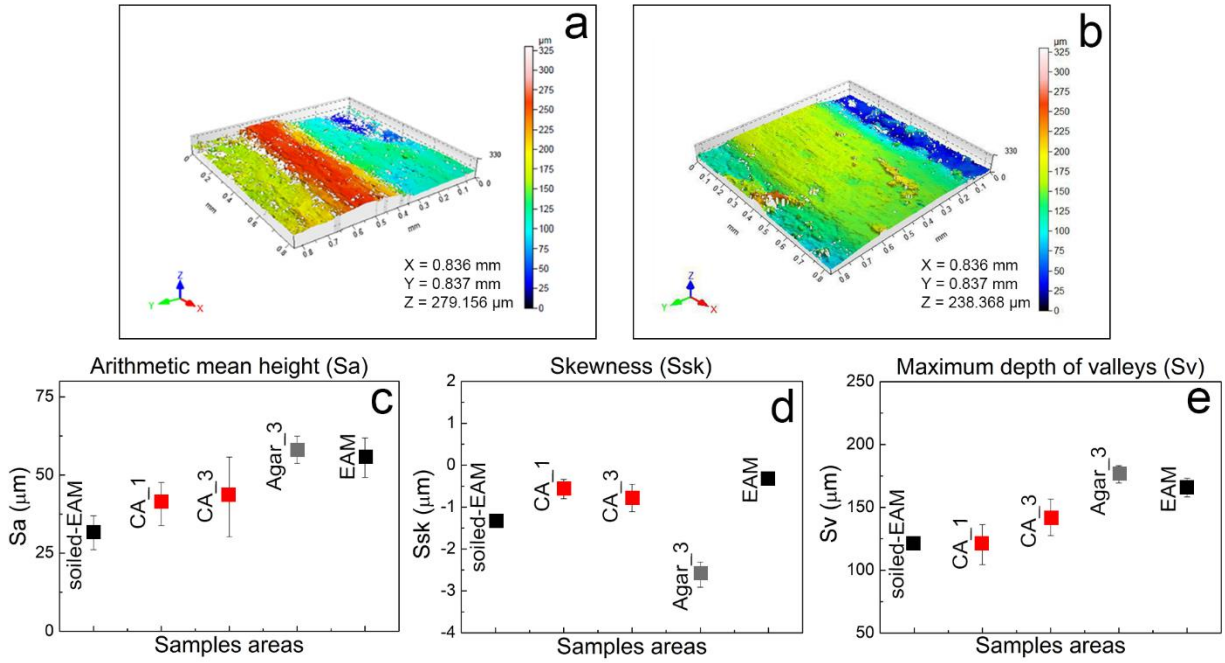

Figure 16. 3D heat maps of soiled-EAM (a) cleaned by CA_3 (b). The colour range represents the different heights (in microns) of the details present on the sample surface. Considered roughness values of Sa (d), Ssk (e), and Sv (f) on the different areas of soiled−EAM cleaned by different gels and application time CA_1, CA_3, and Agar_3.

On the sweat-dispersed mock-ups, traces of sweat were only observed on the surface of the sweat-WM (Figure 17a), whereas on the sweat-EAM (Figure 17b), they were hardly recognized under the stereomicroscope, while profilometry gave minimum differences of changes on the height variations (Figure 17c). This difference could be due to the hydrophobic varnish layer of the WM, which allowed a more superficial crystallization of the dried sweat particles than on the hydrophilic surface of the EAM. In addition, by the reflective surface of the sweat-WM, no profilometric measurements, including 3D maps and roughness parameter calculations, were performed. After the cleaning application on the sweat mock-ups, by repeating the application of CA gel, 1 to 3 applications showed slight value changes (Figure 17d,e). As for the other considered mock-ups, the Sv parameter highlights the greater variations due to successive gel applications (Figure 17f).

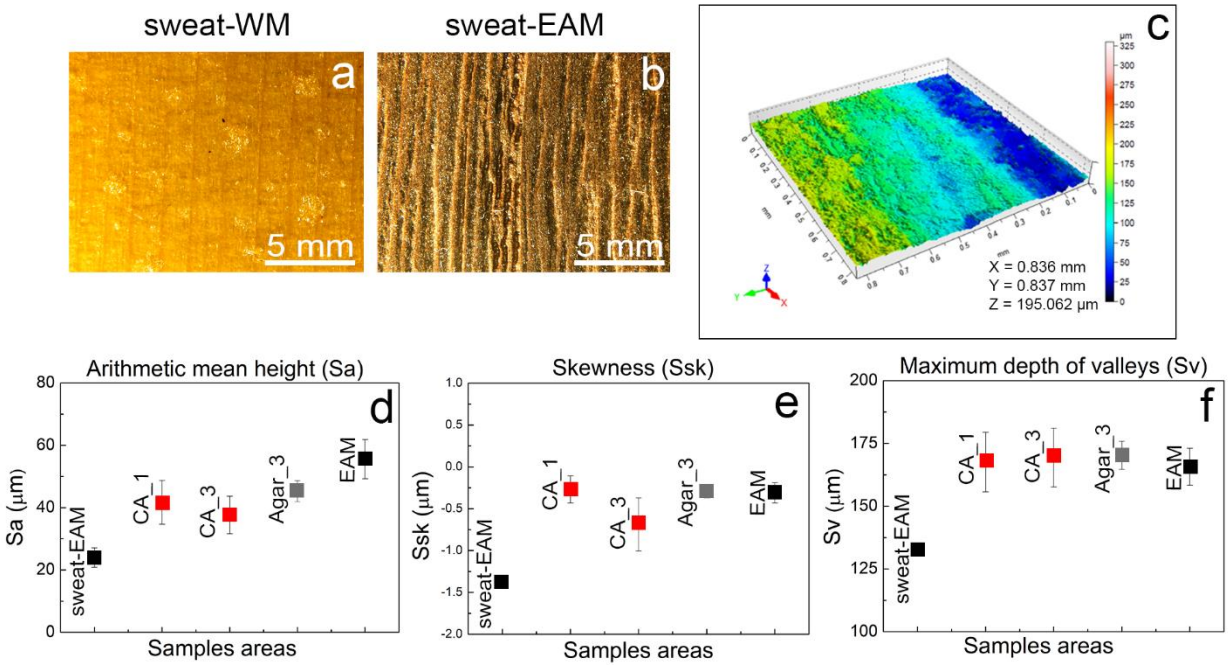

Figure 17. Stereomicroscopy images of sweat-WM (a) and sweat-EAM (b). 3D heat map of sweat-EAM (c). The color range represents the different heights (in microns) of the details present on the sample surface. Considered roughness values of Sa (d), Ssk (e), and Sv (f) on the different areas of sweat−EAM cleaned by different gels and application time CA_1, CA_3, and Agar_3.

3.2.3.2. Colorimetric Measurements

The complete data set with the color coordinates L*, a*, and b* acquired on both WM and EAM, as well as the overall chromatic variation (△E*) result of before and after cleaning is summarized in Table 5.

By comparing the result of WM and soiled-WM, a considerable difference can be observed from L* and b* values collected on the same area before and after cleaning by repeated trials (CA_1, 2, and 3). Indeed, both the brightness and the contribution of the yellow color, respectively indicated by L* and b*, measured on the cleaned areas increase to reach values similar to the bright and yellow surface of the WM surface. Also, the CA_2 application appeared to have the highest △E* value compared to the other applications.

On the EAM areas cleaned by CA_2 and CA_3, it was observed that the related L* values (35.2 ± 1.0 and 35.7 ± 2.2, respectively) are close to the L* value of the area without the

soiling mixture (36.0 ± 0.6), which suggests an effective removal. It is worth noting that L* values on EAM decrease from the soiled to the non-soiled surface due to the bright color of the synthetic soil and the darker wooden surface. This contrast, however, results in an opposing trend for WM. The chromatic variations appeared to be a high variation on the CA_1 while less on CA_2 and CA_3.

Table 5. Color coordinates L, a*, and b* were measured on WM and EAM and with the soiling mixture (soiled-WM and soiled-EAM). After cleaning with CA gel by repeating applications, the average values and the related standard deviations were achieved by repeating the measurement five times. Standard deviation values are given in brackets. The overall chromatic variation (△E*) was calculated between the areas before and after cleaning the soiled-WM and soiled-EAM by repeating cleaning trials using CA gels*

Condition	**L***	**a***	**b***	**△E***
Soiled-WM	75.8 (±0.6)	6.8 (±0.4)	39.7 (±0.7)	-
CA_1	71.6 (±0.6)	7.7 (±0.2)	41.2 (±0.6)	6.3
CA_2	74.2 (±1.0)	6.5 (±0.2)	41.2 (±0.1)	7.8
CA_3	72.0 (±0.7)	7.7 (±0.2)	41.6 (±0.3)	6.9
WM	68.5 (±1.9)	7.4 (±0.3)	35.7 (±0.9)	-
Soiled-EAM	36.0 (±0.6)	4.9 (±0.3)	10.5 (±0.6)	-
CA_1	32.8 (±0.3)	3.8 (±0.3)	7.8 (±0.7)	7.3
CA_2	35.2 (±1.0)	3.5 (±0.1)	7.9 (±0.3)	4.9
CA_3	35.7 (±2.2)	3.9 (±0.2)	8.9 (±1.0)	4.3
EAM	40.0 (±1.4)	3.4 (±0.6)	8.6 (±0.9)	-

3.2.3.3. XRF

The XRF investigation evaluated the effectiveness of the cleaning tests through spot and mapping analysis. In this regard, the elemental composition of synthetic soil, sweat, WM, EAM, and before and after cleaning by CA and agar gel was evaluated.

On WM, the signals of K (Kα = 3.31 keV), Ca (Kα = 3.72 keV), Ti (Kα = 4.52 keV), Cr (Kα = 5.50 keV), Mn (Kα = 5.90 keV), and Zn (Kα = 8.69 keV) were identified as characteristics of the nontreated multilayered coating system. For EAM, signals of K, Ca, Ti, Cr, Mn, and Zn and a weak signal of Fe (Kα = 6.43 keV) were detected. Detected elements, K, Ca, Ti, Cr, Mn, and Zn, on both mock-ups derive mainly from the wood (Pirkkalainen et al. 2012; Fellin et al. 2014), although K and Ca increase in count in WM suggested the contribution from underlying ground and varnish layers (Invernizzi et al. 2020a; Volpi et al. 2021). Regarding the soiling mixture applied on WM and EAM, Si (Kα = 1.74 keV), K, Ca, and Fe were the principal elements detected. These elements may be associated as a source of materials used for the synthetic soil: Ca (kaolin, cement), Fe (cement, burnt sienna pigment), K (peat moss, kaolin), Si (kaolin, silica, cement). In the case of synthetic sweat, only Cl (Kα = 2.64 keV) was detected, likely derived from sodium chloride and ammonium chloride (Zörner et al. 2017).

After cleaning with CA gel, the main compositional changes observed on soiled-WM and soiled-EAM concerned the counts of Ca, Si, K, and Fe. Figure 18 shows the normalized area counts of these peaks before and after cleaning. Compared to soiled-WM and soiled-EAM, the removal of Ca, Si, K, and Fe seemed to increase with the repeated tests from CA_1 to CA_3. This was also evident visually with the XRF map by selecting Ca as a marker.

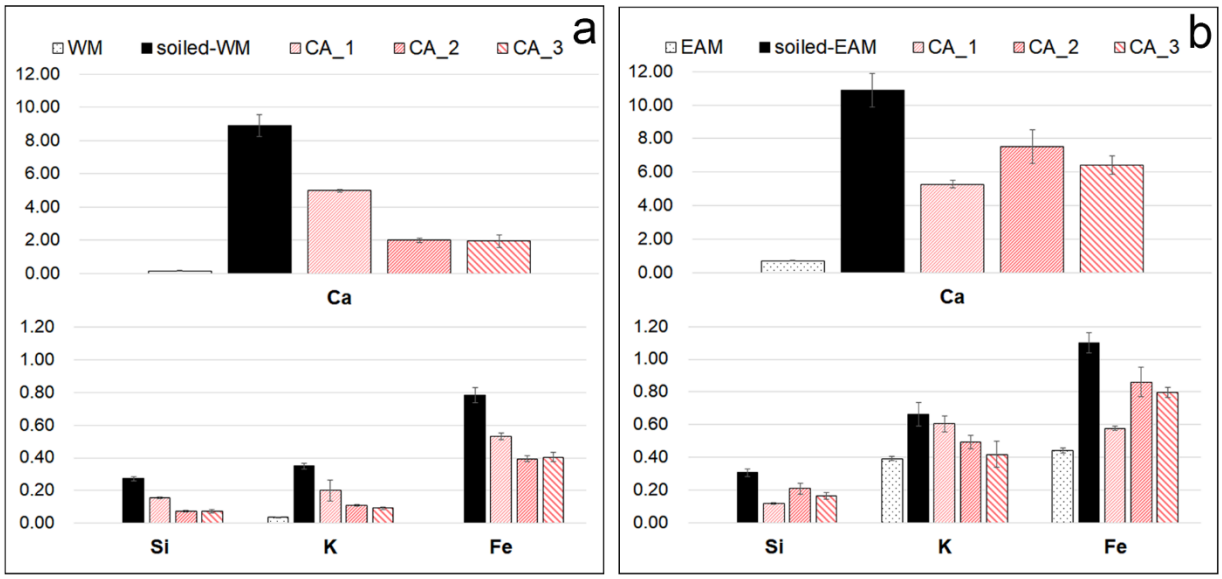

Figure 18. Normalized Ca, Si, K, and Fe counts were detected on (a) WM and (b) EAM. Different bars correspond to plain (WM and EAM) and with soiling deposits treated mock-ups (soiled-WM and soiled-EAM) and after 1, 2, and 3 applications of CA gel (CA_1, CA_2, CA_3). XRF values correspond to the net area counts of the Kα peak of each element normalized to time and the mean of the entire dataset of Rh-Kα peak net area counts, with the related standard deviation.

Including the cleaning efficacy calculated using the XRF mapping data, the cleaning efficacy result aligned with that of the spot analysis presented in Figure 18. On both soiled-WM and soiled-EAM, increasing the application of CA_1 to CA_3 increased the cleaning efficacy (Figure 19). Furthermore, repeated applications with agar showed a cleaning efficacy behavior similar to that of the CA gel. Overall, after three applications on soiled-WM and soiled-EAM, the CA and agar gel showed comparable cleaning efficacy.

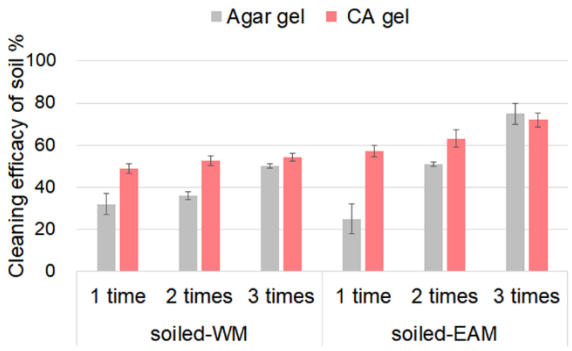

Figure 19. Cleaning efficacy values obtained on soiled-WM, soiled-EAM, and CA gels were applied 1 to 3 times repeatedly. The percentage of cleaning efficacy was calculated based on the counts of calcium markers.

The CA gel significantly removed the sweat component on the sweat-WM, as evidenced by the decrease in Cl counts in Table 6. On the sweat-EAM, the Cl counts decreased with increasing cleaning trials, suggesting satisfactory sweat removal efficiency. Interestingly, the Cl value on the sweat-WM control is higher than the corresponding sweat-EAM value (11.94 and 3.35, respectively). This result was considered with the stereomicroscope examinations, which showed traces of dried sweat (as crystallized droplets in section 3.2.2.1.) on the sweat-WM, whereas on the sweat-EAM, the sweat drops were hardly visible. It is possible that the hydrophilic and porous structured paulownia wood (EAM mock-up) adsorbed the sweat, while the hydrophobic surface of the WM did not.

Table 6. Normalized Cl (Kα) counts on sweat-WM and sweat-EAM, before (control) and after different cleaning applications with SA and KG.

Mock-Up	Control	CA_1	CA_2	CA_3
Sweat-WM	11.94	0.11	0.09	0.09
Sweat-EAM	3.35	2.50	1.50	0.52

In all tests with CA gel on sweat-WM, the cleaning efficacy was over 90%, whereas sweat-EAM showed a lower cleaning efficacy (Figure 20). Agar gel also provided excellent cleaning efficacy after a single application, which also occurred in the second and third repetitions of cleaning. Overall, the results recommended repeated cleaning trials when gel cleaning is performed on hydrophilic surfaces contaminated with sweat, such as sweat-EAM. Conversely,

on hydrophobic surfaces such as varnished WM with sweat, a single application may be sufficient to achieve satisfactory removal efficiency.

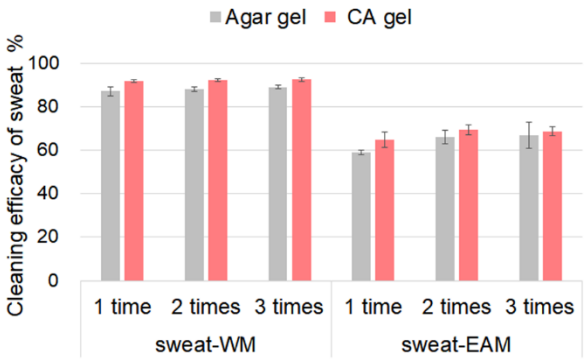

Figure 20. Cleaning efficacy values obtained on sweat-WM and sweat-EAM and CA gels were applied 1 to 3 times repeatedly. The percentage of cleaning efficacy was calculated based on the counts of chloride markers.

3.2.3.4. ER-FTIR

Alongside the XRF analysis, an investigation was carried out to evaluate cleaning by spectroscopic features of ER-FTIR. For this purpose, pseudo-absorbance and KKT spectra were investigated to identify significant bands on synthetic soil, sweat, WM, EAM, and before and after cleaning with CA and agar gel, summarized in Table 7.

On WM, the KK transformed spectra displayed the spectral profile of the oil–colophony varnish with characteristic bands around 3000 and 2800 cm^{-1} (νCH_3 and νCH_2), 1735 cm^{-1} ($\nu C=O$), at 1460 and 1380 cm^{-1} ($\delta C-H$), and 1250 cm^{-1} and 1170 cm^{-1} ($\nu C-O$) (Figure 21) (Weththimuni et al. 2016; Invernizzi et al. 2018b; Cazzaniga et al. 2021). As with EAM, the bands were all studied and interpreted in the pseudo-absorbance spectra. Since the nakdong technique resulted in a high surface roughness, as already confirmed in section 3.2.2.1, this feature led to a predominant presence of the diffuse contribution. (Invernizzi et al. 2022). EAM surface displayed the bands related to wood around 1740 cm^{-1} ($\nu C=O$, hemicellulose) and at 1595, 1510, 1460, and 1240 cm^{-1} (lignin-related bands) (Figure 22) (Liu et al. 2016; Fiocco et al. 2021b; Kolya and Kang 2021).

The soiled-WM and soiled-EAM in pseudo-absorbance spectra featured characteristic bands of kaolin at 1020–1000 cm^{-1} and 915 cm^{-1} (Galatis et al. 2012; Tironi et al. 2012; Bartoletti et al. 2020b; Cazzaniga et al. 2021) and calcium carbonate around 1420 cm^{-1} and at 875 cm^{-}

[1], probably derived from the cement (Galatis et al. 2012; Cazzaniga et al. 2021). In addition, organic components, such as gelatin, starch, and peat moss, contributed to the bands around 2900 cm^{-1} (Heller et al. 2015; Invernizzi et al. 2018b; Cazzaniga et al. 2021). For sweat, the inverted band (Reststrahlen) at 1420 cm^{-1} (νC-N) in the pseudo-absorbance spectra and the bands at 3170 and 3060 cm^{-1} (νC-H and νN-H) in the KK transformed spectra appeared, which are assumed as the body fluid composition of the mixture of DIN ISO 9022-12 (Manivannan and Rajendran 2011; Oliver et al. 2016; Takamura et al. 2018; Zhuang et al. 2020).

After the application of the cleaning agent, the characteristic bands of WM and EAM gradually appeared, while a marginal reduction in the intensity of the bands corresponding to the contaminants was observed. This could mean that some soiling mixture or sweat components were removed. On soiled-WM, after cleaning with CA gel, the bands attributed to kaolin at 1040, 1000, and 915 cm^{-1} and to calcium carbonate at 875 cm^{-1} decreased in intensity (Figure 21a), while the oil-colophony varnish contributing band was recognized (Figure 21b). Similar results were achieved on the surface of the soil-EAM, and the cleaning test with Agar_3 also showed comparable removal to that achieved with CA_3 (Figure 22). By observing each spectrum of repeated cleaning trials, the CA gel and agar gel had to be applied three times to obtain detectable spectral changes.

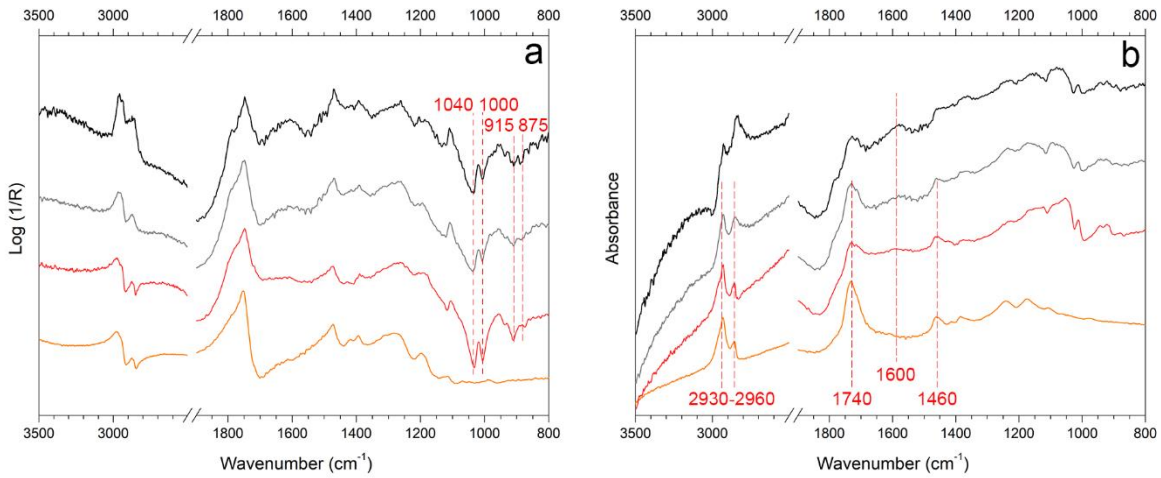

Figure 21. ER-FTIR spectra in (a) pseudo-absorbance and (b) after Kramers-Kronig transform of soiled-WM (black), area cleaned with Agar_3 (grey), CA_3 (red) and, a reference of WM (orange). The marker bands selected for identifying the soiling mixture are reported.

Table 7. Reflection FTIR band assignment in the range 4000-800 cm^{-1} identified on EAM and WM and on the soiling mixture and sweat dispersed on the mock-ups. For the derivative bands marked with an asterisk (*), the value refers to the maximum of the band after the application of KK transformations. Inv. = inverted band (Restrahlen) in the pseudo-absorbance spectra

Attribution	Band assignment	Wavenumber (cm^{-1})
WM (without depositions)	$\nu_{as}CH_3$, ν_sCH_3	2930-2860*
	C=O	1740-1730*
	δ_sCH_2, $\delta_{as}CH_3$, δ_sCH_3	1460*, 1380*
	νC-O	1250*, 1170*
EAM (without depositions)	νC=O hemicellulose	1740
	νC=O lignin	1595
	aromatic skeletal vibration of lignin	1510
	aromatic CH deformation and $\nu_{as}CH_3$ in lignin	1460
	νC–O in lignin and xylan, syringyl ring	1240
Kaolin	νO-H	3620
	δSi-O	1040-1000
	νO-H	915
Calcium carbonate	νC-O by calcium carbonation	1420, 875
Organic components	νC-H	2950-2825*
	νC=O	1650-1600*
Sweat	νC-H and νN-H	3200-3000*
	νC-N	1470-1410 (inv.)

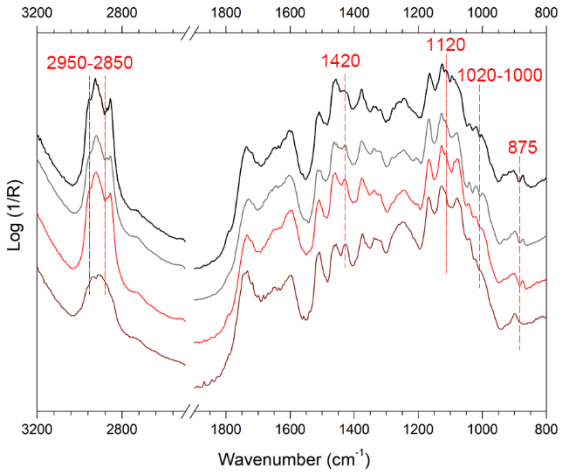

Figure 22. ER-FTIR spectra in pseudo-absorbance were acquired on soiled-EAM (black), area cleaned with Agar_3 (grey), CA_3 (red), and a reference of EAM (brown). The marker bands selected for identifying the soiling mixture are reported.

On sweat-WM, all cleaning systems, regardless of gel or repeated application time, clearly induced the disappearance of sweat-related bands (Figure 23). On the other hand, detecting representative sweat peaks on the sweat-EAM was difficult. As already mentioned for the stereomicroscope and XRF results in sections 3.2.2.1. and 3.2.2.2., it was assumed that the sweat deposit may have been absorbed by the rough surface of the EAM, making its detection difficult.

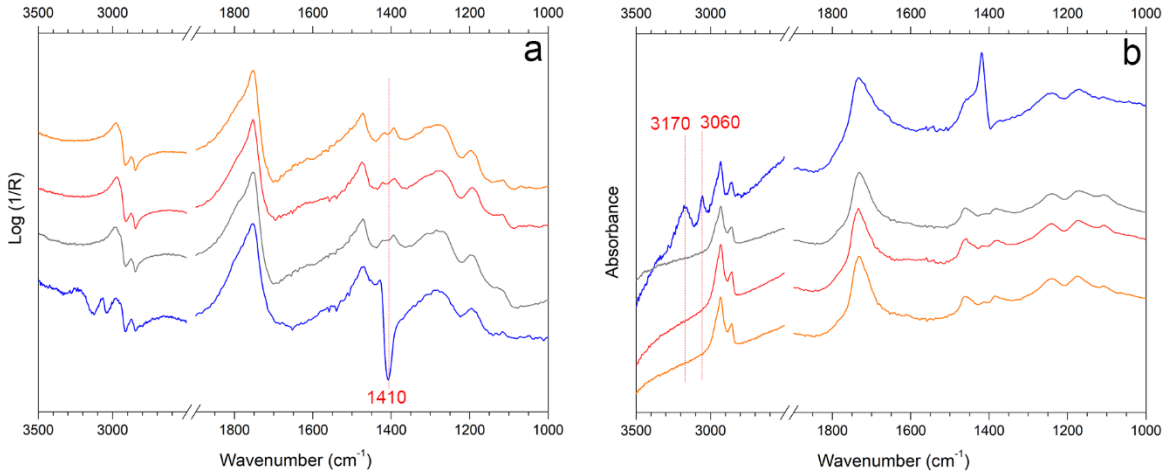

Figure 23. Reflection FTIR spectra in (a) pseudo-absorbance and (b) after Kramers-Kronig transform of WM (orange) and sweat-WM (blue) cleaned with Agar_3 (grey) and CA_3 (red). The marker bands selected for identifying synthetic sweat components are reported.

3.3. CA-GPTMS

This gel was developed with the specific objective of chemically modifying the carboxyl groups in alginate. As documented in other research, the functionalization of alginate improves moisture retention and mechanical properties (Zaman and Beg 2013; Vueva et al. 2018; Szabó et al. 2020; Rosiak et al. 2021).

In this study, we utilized the bifunctional silane 3-glycidoxypropyltrimethoxysilane (GPTMS) to obtain the functionalization of calcium alginate (CA) gel. GPTMS is characterized by the presence of a reactive organic epoxide and a hydrolysable methoxysilane group, which makes it suitable for the functionalization of various chemical compounds (Reyes-Peces et al. 2020; Tran et al. 2020; Weththimuni et al. 2021).

The carboxylic groups present in alginate polymer are expected to react with GPTMS by the opening of the epoxide ring, while methoxysilane groups of GPTMS can react with each other by providing an auto-crosslinked network (Vueva et al. 2018). As a result, it is possible to expect a desirable mechanical strength and improvement in durability, reproducibility, tenability, and absorbency. Moreover, the investigated chemical modification allows the preparation of thin films from the obtained gel material, which can be used as an appropriate cleaning tool for wooden artworks.

Our hypothesis centers on the covalent ester bonding that is expected to occur between the carboxylic groups of the alginate polymer and the epoxy ring of GPTMS, as presented in Figure 24.

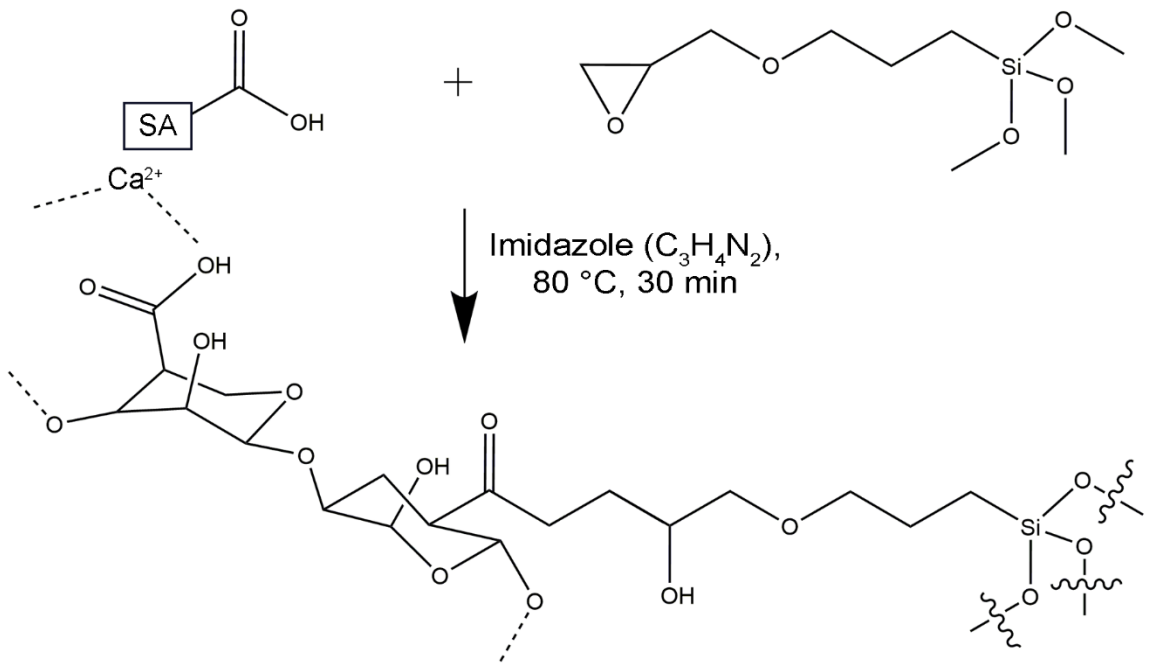

Figure 24. Expected reaction between alginate polymer and GPTMS and calcium ion.

3.3.1. Gel Preparation

The steps for the preparation of CA-GPTMS gel are presented in Figure 25, 0.2 g sodium alginate (SA) was added into a beaker containing 10 ml of distilled water and the solution was stirred and slightly heated at 40 °C until it completely dissolved. Then, 3-glycidoxypropyl trimethoxysilane was added dropwise into the alginate solution (three different amounts of GPTMS were added into the SA by keeping the sodium alginate monomer and GPTMS molar ratios respectively in SA: GPTMS = 1: 1, 2, and 4) and finally, 1% (w/w, respect to the reactants) imidazole was added as a catalyst into the reaction mixture with continuous magnetic stirring in an oil bath at 80 °C for 30 minutes for the reaction. In order to prepare it into a film-form gel, SA solutions were poured into Petri dishes with a thickness of about 2-3 mm. After that, 2% (w/v) $CaCl_2$ solution was slowly poured into the prepared Petri dishes, and the reactions were maintained for 15 minutes to allow the cross-linking process with calcium ions and finalized the gel formulations, and they were named as CA-GPTMS_1, CA-GPTMS_2, and CA-GPTMS_4 according to their molar ratios as mentioned before. After forming CA-GPTMS, the gel was repeatedly washed in deionized water to remove unreacted materials as well as the catalyst.

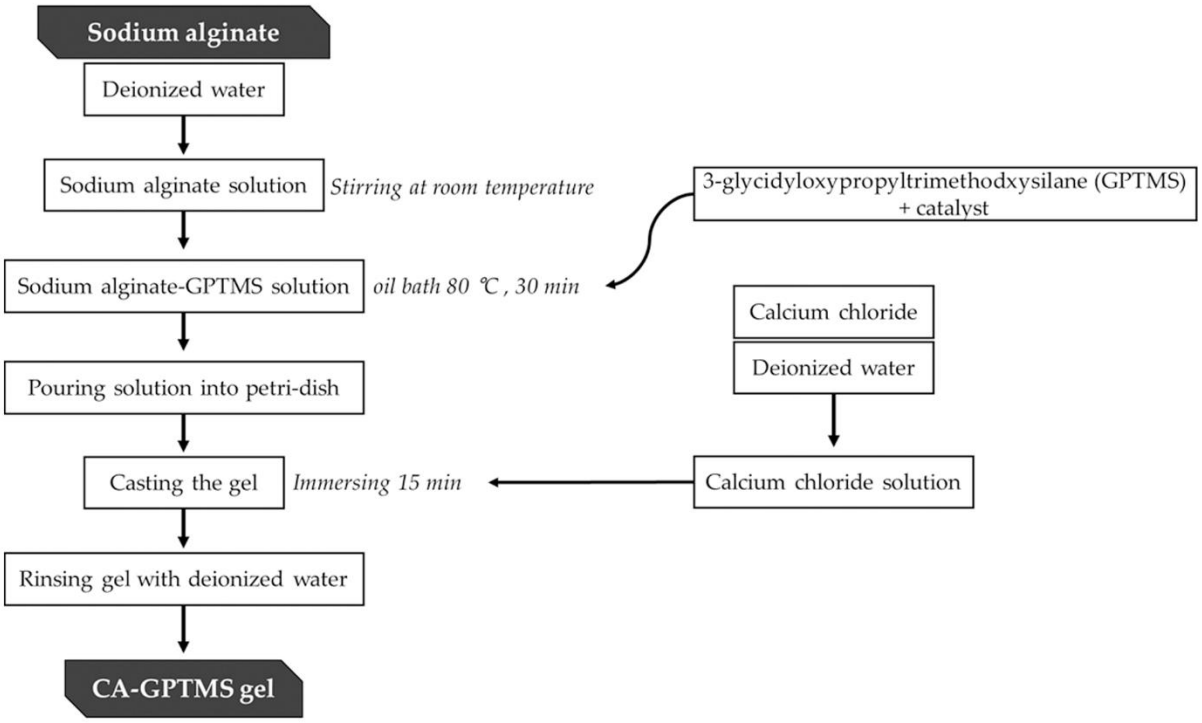

Figure 25. A schematic diagram of steps involved in preparing CA-GPTMS gel.

3.3.2. Gel Characterization

The functionalization of alginate and GPTMS epoxy ring opening and formation of ester group occurrence can be demonstrated by the ^{1}H-NMR and 2D-HSQC (Figure 26 and Figure 27). The methoxy silane group (δ 1H 3.36 ppm) and functionalized proton *e'* of the epoxy ring can be observed (δ 1H 3.37 ppm) by ^{1}H-NMR (Gabrielli et al. 2013). The correlation signals at epoxy ring-opening and reaction allocation with carboxylic groups were highlighted by HSQC: (δ ^{1}H 3.65, 3.57 ppm, δ ^{13}C 62.9 ppm) (Gabrielli et al. 2014; Connell et al. 2017; Vueva et al. 2018).

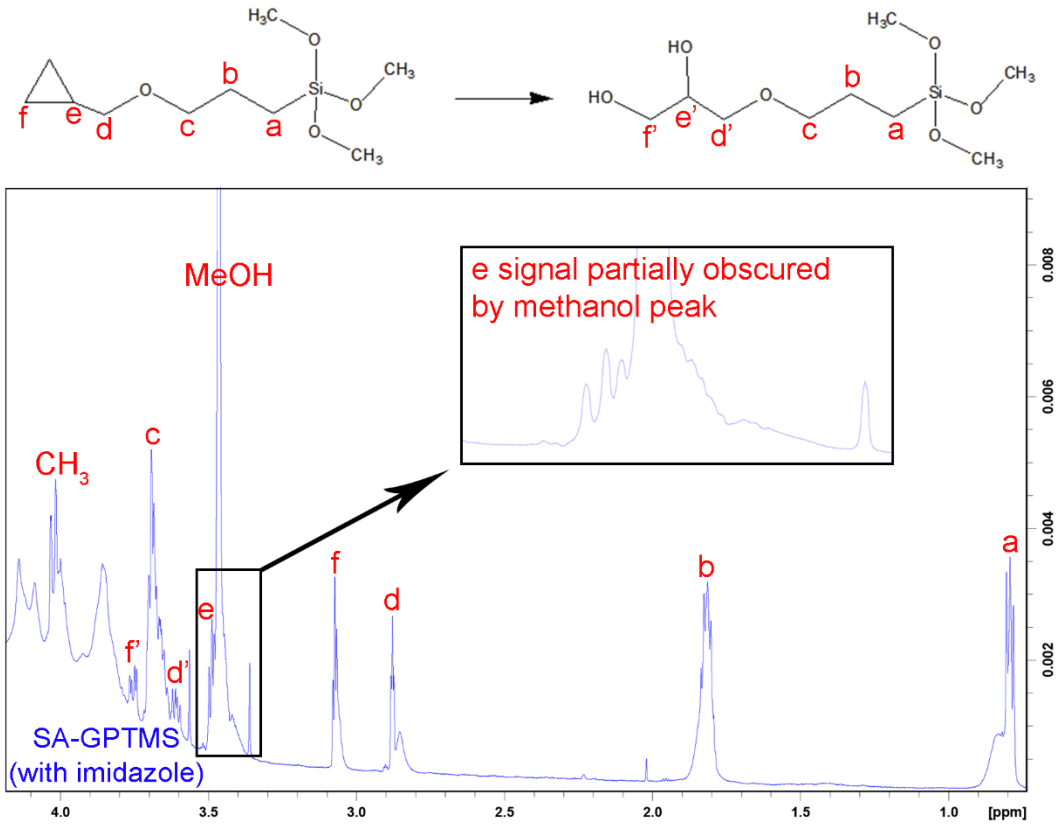

Figure 26. Liquid state [1]H-NMR of sodium alginate and GPTMS (SA-GPTMS).

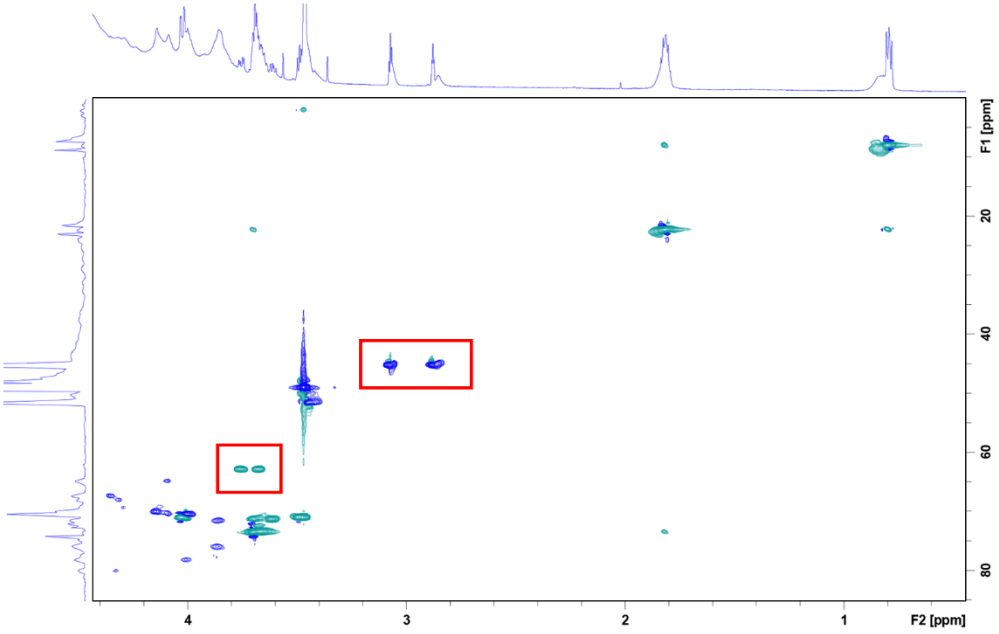

Figure 27.HSQC NMR spectrum of sodium alginate functionalized with GPTMS.

After NMR confirmed that the reaction between alginate and GPTMS had taken place, the gel produced after adding calcium ions was studied by FTIR-ATR and SEM-EDS (Figure 28). The FTIR spectrum of CA-GPTMS_2 showed some differences compared to plain alginate (SA) (Figure 28a). The peak ascribed to COO^{-} asymmetric and symmetric bands underwent a shift and intensity variations, confirming the electrostatic interactions of carboxylate groups and calcium ions (Papageorgiou et al. 2010; Li et al. 2016; Badita et al. 2020). Absorptions at 2945 and 2840 cm^{-1}, ascribed to stretching of CH_3 and CH_2 in the GPTMS side chain appeared, while signals at 1210, 910, and 855 cm^{-1}, attributable to oxirane derivatives decreased their intensity or disappeared in the spectra of the silane-modified gels. Moreover, bands at 1085 and 870 cm^{-1} can be assigned to Si-O-Si and Si-O, respectively (Li et al. 2020; Weththimuni et al. 2021). Above all, the results may indicate that CA-GPTMS gel is a chemical gel functionalized by ester bonding with the carboxylic group of the alginate as well as by ionic interaction with calcium.

Moreover, the morphological features of CA-GPTMS and plain CA have been investigated by SEM experiments (Figure 28b). Spherical particles entangled on the elongated and uniform network of alginate polymer were observed in the modified gel. It can be assumed that such different morphology may be caused by silane-induced cross-linking, as also suggested by EDS analysis (Figure 28c) that shows the presence of Si, in addition to C, O, and Ca, within the spherical particles.

The mechanical properties of the CA-GPTMS gel were measured by comparing it with agar gel as a control, physically crosslinked CA gel, and with chemically crosslinked CA-GPTMS Gels (CA-GPTMS_1, CA-GPTMS_2, and CA-GPTMS_4) (Figure 29).

All newly formulated gels of CA-GPTMS significantly improved tensile strength, except CA-GPTMS_1, compared to the physical CA gel (Figure 29a). It is assumed that the higher concentration of GPTMS shows higher elongation, as also reported in the literature (Reyes-Peces et al. 2020; Li et al. 2020). With regard to elongation at break, it showed a lower value than CA, which represents CA-GPTMS as a firmer structure (Figure 29b). In addition, the linear portion of the high values of the stress-strain curve from CA-GPTMS_2 confirmed the material's elastic and stretching-resistant texture (Figure 29c).

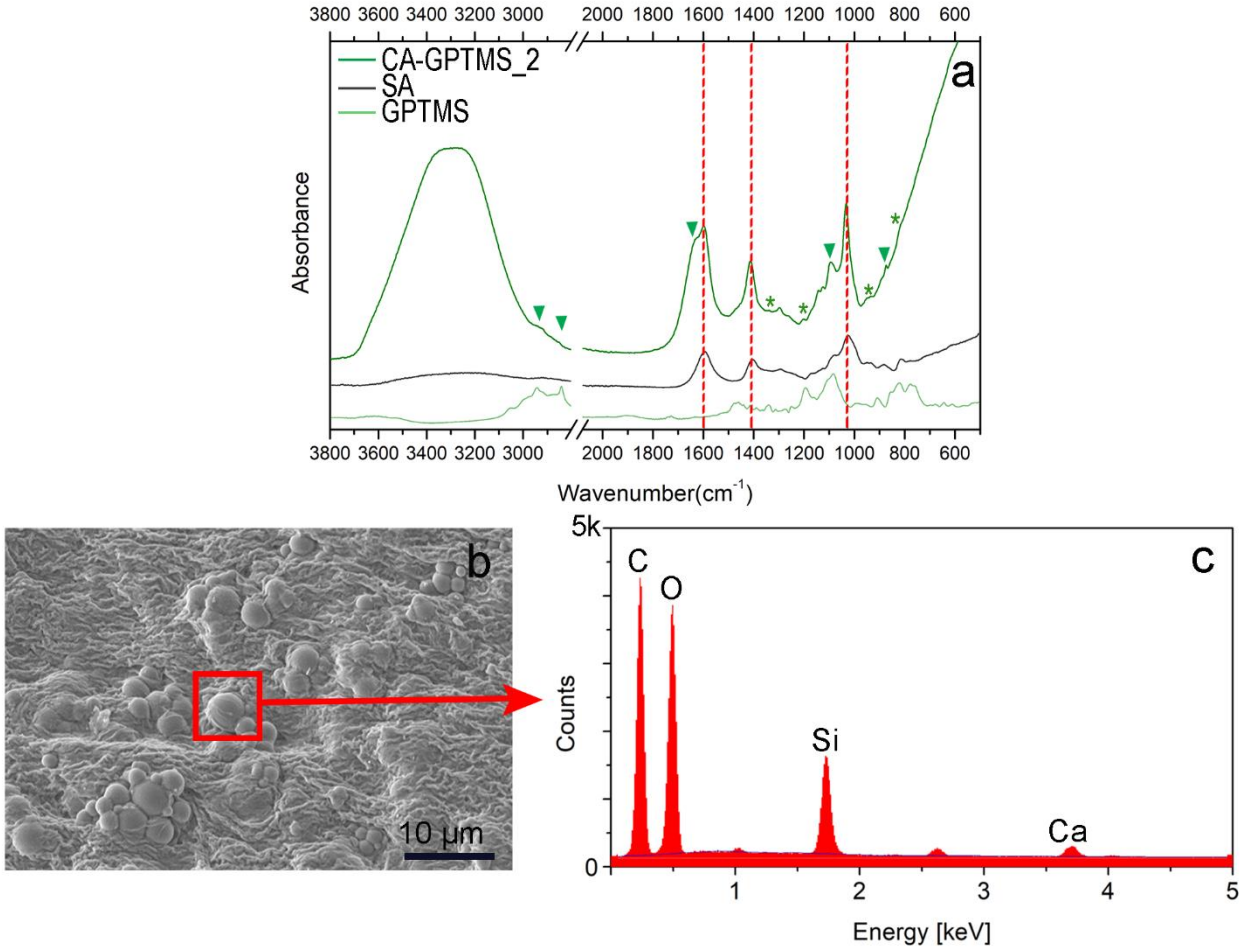

Figure 28. FTIR spectrum of the Ca-alginate-GPTMS gel formulated in sodium alginate monomer and GPTMS molar ratios respectively in SA: GPTMS = 1: 2 (CA-GPTMS_2), pure sodium alginate (SA) and GPTMS reactants (a). Markers for electrostatic interactions of carboxylate groups and calcium ions (red dotted line), siloxane groups (triangle), and epoxy groups of GPTMS (asterisk) are displayed. SEM image of CA-GPTMS_2 gel film acquired in high vacuum with secondary electrons (b) and its EDS spectrum (c).

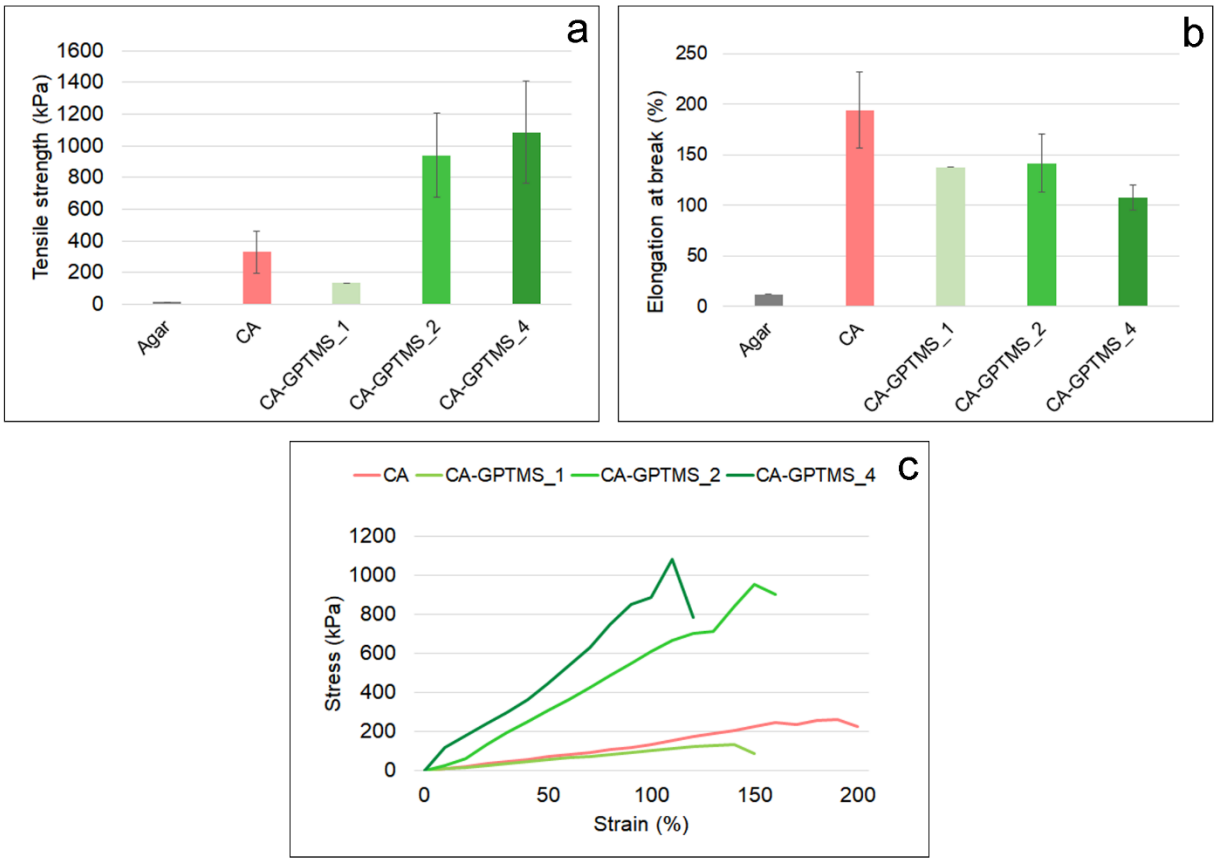

Figure 29. Mechanical properties determined by tensile test (mean value ± s.d.; n = 5): tensile strength (a) and elongation at break (b). Stress-strain curves of CA, CA-GPTMS_1, _2 and _4 gels.

The moisture-related properties of CA-GPTMS gels, namely CA-GPTMS_1, CA-GPTMS_2, and CA-GPTMS_4 are summarized in Table 8 for comparative purposes alongside conventional CA and agar gels.

Newly formulated chemical CA-GPTMS gels showed a significant reduction of the hydrophilicity and water loading, demonstrated by lowered equilibrium water content (EWC) and solvent capacity (SC) values when compared to physical CA and agar gels (Table 8). This decrease in hydrophilicity can refer to the hydrophobic chains coming from the GPTMS (glycidoxypropyltrimethoxysilane) component within the CA-GPTMS gels (Li et al. 2020). It was also observed that EWC and SC gradually increased by increasing the amount of crosslinker in CA-GPTMS. In terms of water release (WR), CA-GPTMS gels proved to be six times more retentive than agar, while no significant difference was found with CA physical gel. The water dispersion tests, as shown in Figure 30, have confirmed that CA-

GPTMS_2 gel has a higher retentive power compared to CA and agar. This is due to the localised release of solvent (aqueous fluorescein solution) only at the point where the CA-GPMS_2 was in contact. These moisture properties describe CA-GPTMS_2 as a safe material for hydrophilic and porous surfaces. The material has a lower tendency for water to diffuse through the chemical network, making it ideal for use on such surfaces.

Table 8. Moisture properties of CA-GPTMS gels, CA, and agar: equilibrium moisture content (EWC), swelling capacity (SC), and water release (WR). Mean values and standard deviations were calculated on five repetitions

Gel	EWC (%)	SC (%)	WR (mg/cm^2)
CA-GPTMS_1	41.5 (± 8.5)	(7.4 ± 2.9) × 10	6.9 (± 0.9)
CA-GPTMS_2	41.9 (± 6.5)	(7.4 ± 2.4) × 10	4.4 (± 1.8)
CA-GPTMS_4	43.7 (± 8.3)	(8.1 ± 2.6) × 10	4.3 (± 1.5)
CA	64.0 (± 5.0)	(1.8 ± 0.4) × 10^2	5.4 (± 1.0)
Agar	95.6 (± 0.3)	(2.2 ± 0.2) × 10^3	29.3 (± 2.5)

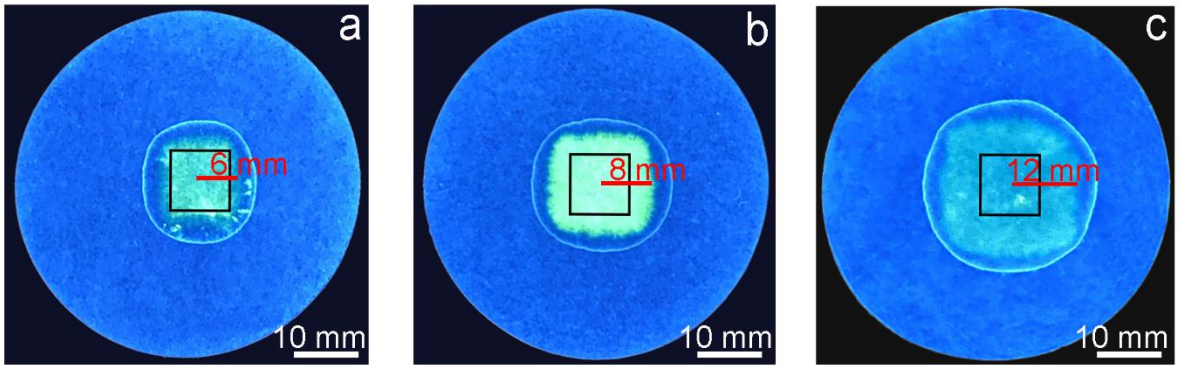

Figure 30. Water dispersion tests after CA-GPTMS (a), CA (b), and agar (c) gel loaded with 2,7-dichlorofluorescein solution and applied on the filter paper. The black square represents the area of the applied gel (1x1 cm), while the red line qualitatively indicates the water dispersion.

Altogether, the results of gel characteristics showed that CA-GPTMS_2 gel is the best choice for use in cleaning applications, as it has high elasticity and strength compared with physical CA and agar gel. At the same time, the moisture properties of CA-GPTMS_2 gel exhibited strong retentive ability compared with CA and agar gel.

3.3.3. Cleaning Application and Evaluation of the Efficacy

The chemical gel CA-GPTMS_2 was applied for the glue removal test on fresh and aged mock-ups, in comparison with the agar gel used as a reference cleaning system. The gels were kept in contact with the glue layer for 20 minutes with mylar cover to prevent excessive evaporation during application. After cleaning the gel, the remains of the swollen glue were gently removed with a swab and scalpel. The same application was carried out in the case study on the double bass fragment (described in section 2.2.4.), where the old glue required cleaning.

3.3.3.1. Gel residue examination

Before applying the CA-GPTMS_2 gel, we examined whether the CA-GPTMS_2 gel left any gel residue on the wood surface after the gel cleaning application. In this regard, an SEM-EDS analysis was performed on the wood sample before and after the application of the CA-GPMTS_2 gel. The results demonstrated that no unwanted materials were present on the wood surface and that the morphology of the wood structure was visible as before the cleaning applications (Figure 31a,b). Furthermore, EDS analysis revealed that the wood surface had the same elemental composition before and after cleaning. Only C and O elements were detected on the CA-GPTMS gel and not Si, indicating the absence of any possible gel residues on the cleaned wood surface (Figure 31c). It is believed that the new chemical bonding system, which involves the bonding of alginate with GPTMS and its cross-linking process, prevented the release of any gel residues. As a result, this study suggests that the CA-GPTMS_2 gel is residue-free and can be safely used for cleaning purposes, even on delicate and porous surfaces like those found on wooden artifacts.

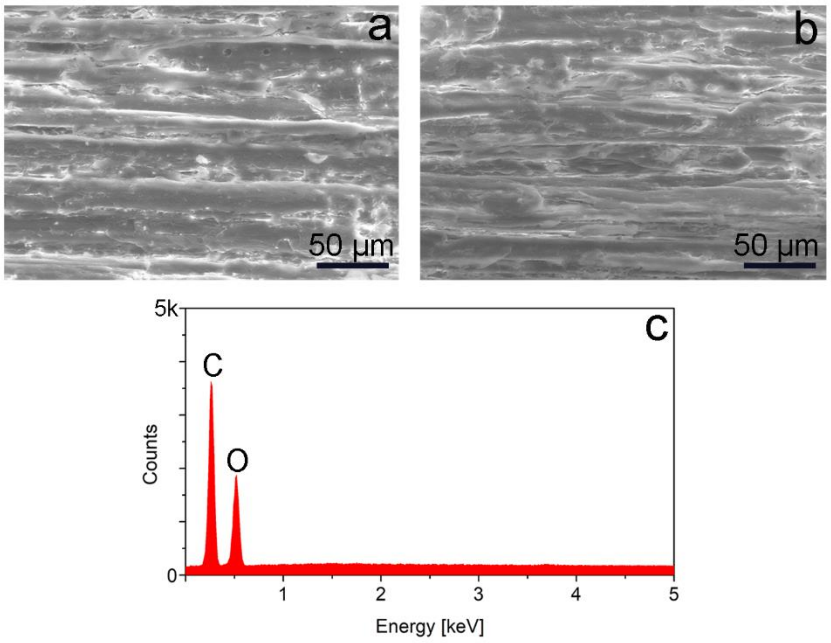

Figure 31. SEM-EDS acquired in low vacuum by secondary electrons Tescan detector on wood surface before (a), and after CA-GPTMS_2 gel application (b), and corresponding elemental analysis after cleaning (c).

3.3.3.2. Cross-section

After applying CA-GPTMS_2 and agar gel, the cross-section observation of the cleaned area demonstrated that both gels have similar efficacy, as shown in Figure 32. The fresh and aged mock-ups had an average animal glue layer of 200 µm. However, following the cleaning application, the glue layer was visibly reduced to 20-30 µm on fresh mock-ups using both CA-GPTMS_2 and agar gel. On the aged mock-ups, the reduction was to 40-60 µm. When removing glue, it is believed that water molecules cause collagen to swell and undergo hydrolysis. This process partially breaks down the helical structure of collagen that binds in interchain bonds, ultimately resulting in the softening of the glue and making it easier to remove (Schellmann 2007; Adams 2021). In the case of aged glue, the loss of protein hydrogen bonds, such as peptide bonds, carboxyl, and amine groups, reduces hydrophilicity, which may slow down the swelling process (Schellmann 2007).

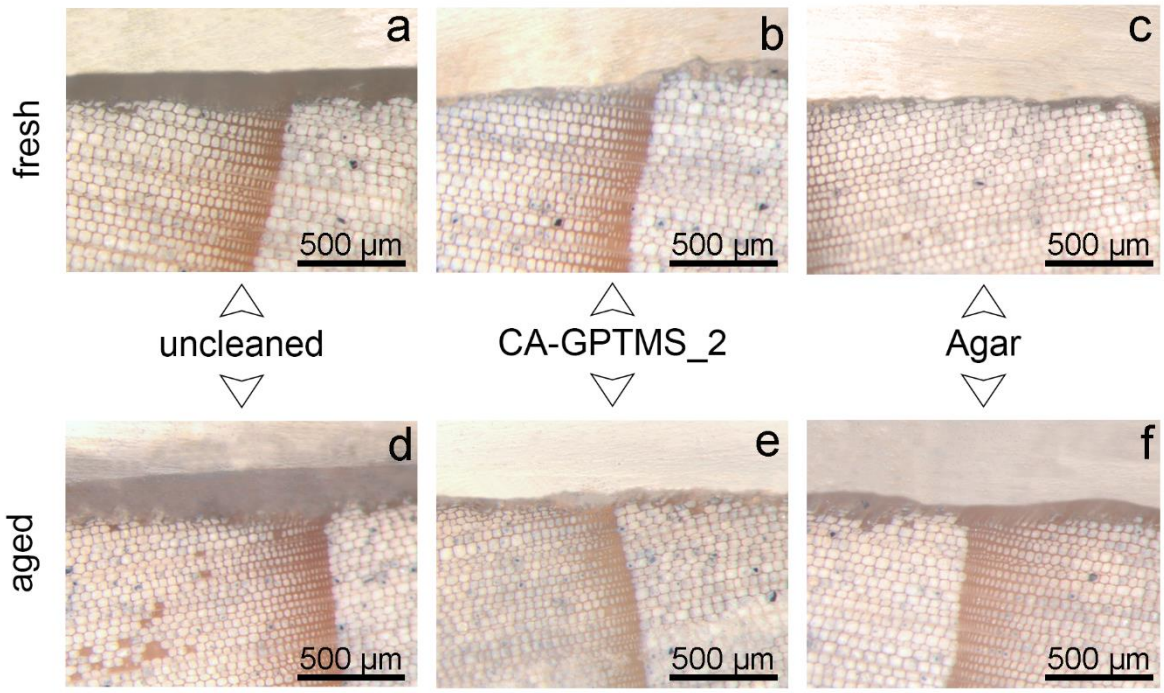

Figure 32. Observation of the cross-sections of the fresh mock-up (a) by stereomicroscope: before cleaning process: the average surface area of 200 µm, after cleaning with CA-GPTMS_2 (b): the average surface area of 25 µm, after cleaning with agar (c): the average surface area of 25 µm. Observation of the cross-section of the aged mock-up (d) by stereomicroscope: before cleaning process: the average surface area of 200 µm, after cleaning with CA-GPTMS_2 (e): the average surface area of 45 µm, after cleaning with agar: the average surface area of 60 µm (f).

3.3.3.3. ER-FTIR

The ER-FTIR transformed KKT spectra analysis of the cross-section revealed that a partial glue residue was still present after the cleaning procedure, as shown in Figure 33. Both fresh and aged mock-ups presented peaks at 1660 cm^{-1} and 1550 cm^{-1}, which were attributable to protein amide I and amide II (Pellegrini et al. 2016; Invernizzi et al. 2018b; Fiocco et al. 2021b; Baglioni and Chelazzi 2013). Additionally, a shoulder around 1720 cm^{-1} was observed in the clean areas due to the carbonyl groups of the wood substrate (Chaudhary et al. 2020; Albano et al. 2022). While the cleaning process effectively removed some glue residue, it was less successful on the aged mock-ups than the fresh ones. However, this result can still be useful depending on the restorer's objectives. The cleaning process can be repeated either to

remove all the glue or to leave the surface glue that is directly in contact with the wood, which may contain other treatments applied to the wood surface (Albano et al. 2022).

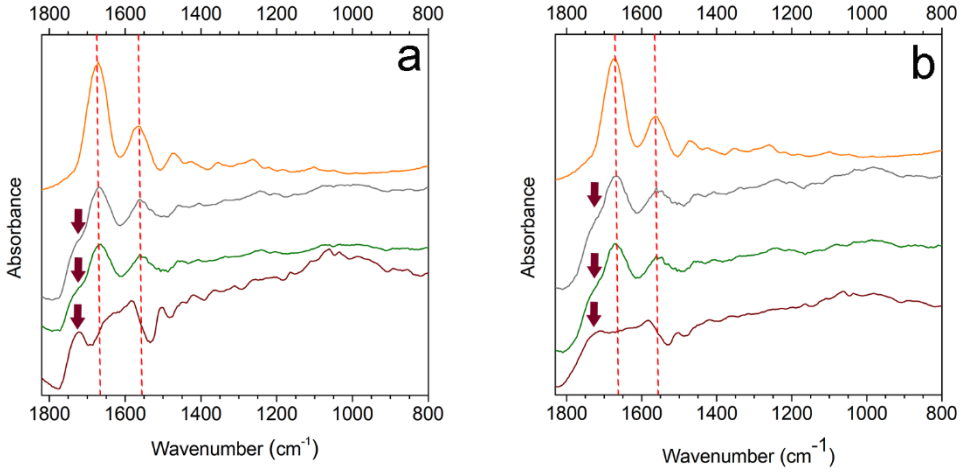

Figure 33. The ER-FTIR spectra of after Kramers-Kronig transform of fresh (a) and aged (b) wood-animal glue mock-up (orange), cleaned with agar (grey) and CA-GPTMS_2 (green), and wood (brown). The marker bands of animal glue are represented in a dotted red line while those of wood are represented with brown arrows.

3.3.3.4. Case study

CA-GPTMS_2 was successfully applied to remove the residues of aged glue present on the internal part of the detached fragment of the double bass during the past restoration procedures (Figure 34). Observing the UV image of before and after cleaned area (Figure 34a,d), the glue layer was significantly removed, letting the underneath wood surface uncovered, as it can be clearly observed by ER-FTIR analysis (Figure 34e). Also, the naturally aged glue was partially removed, representing the feature signal of amide I and amide II, but the intensity decreased significantly in the cleaned area. Moreover, just after 20 minutes of application, it was clearly visible that only the area where the CA-GPTMS_2 had been applied was selectively swelling with water, while no water leaching occurred on the unapplied part (Figure 33c). This confirms the result discussed above: high fluid retention capacity displayed by CA-GPTMS_2 reduces the possible dispersion of water in the non-contacted area (in this case, wood).

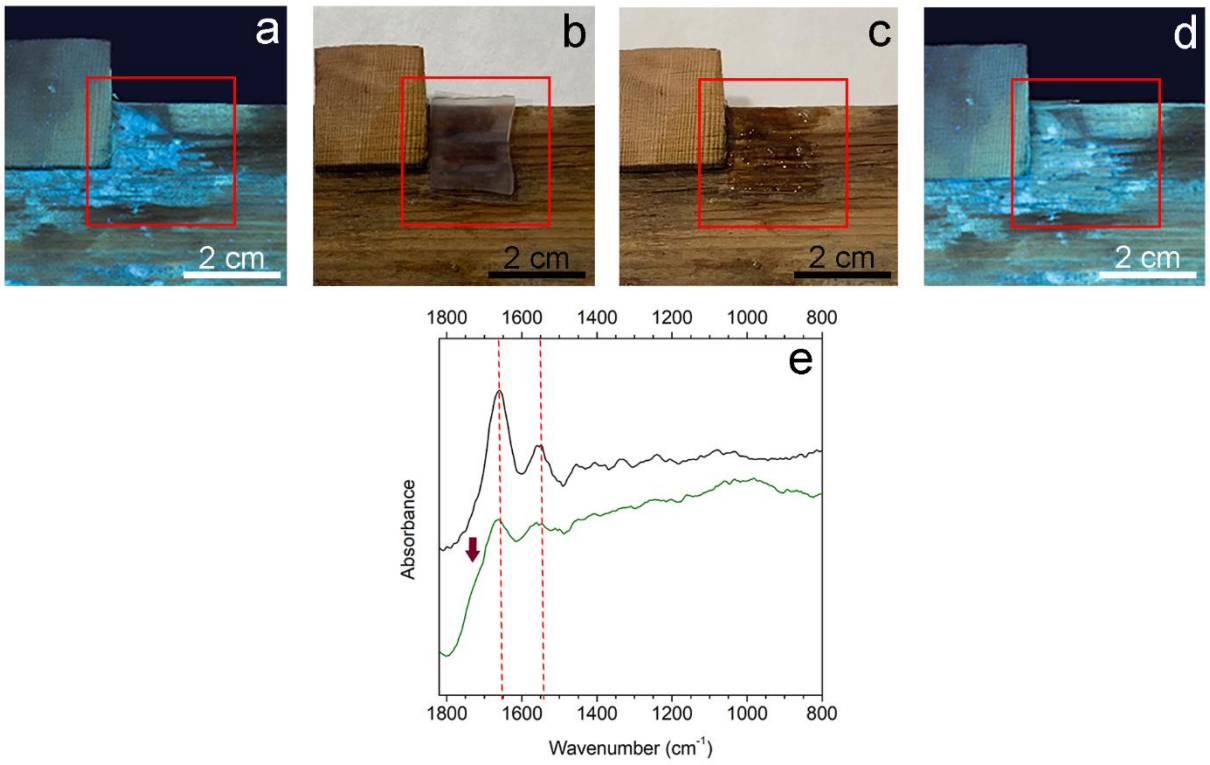

Figure 34. Images of the wooden fragment plate of the double bass, area before cleaning (a), during cleaning with the CA-GPTMS_2 (b), right after the 20 min application (c), after cleaning (d), and ER-FTIR spectra after Kramers-Kronig transform acquired before (black) and after (green) cleaning area with CA-GPTMS_2 (e). The marker bands of the animal glue are represented in a dotted red line and the wood is represented in brown arrows.

3.4. CA-XAMA7

This gel formulation was also developed with the same objective as the CA-GPTMS gel, in order to associate improvements in moisture retention and mechanical properties through the functionalization of carboxyl groups in the alginate (Zaman and Beg 2013; Vueva et al. 2018; Szabó et al. 2020; Rosiak et al. 2021; Naga et al. 2022).

Therefore, in this study, the Pentaerythritol tris[3-(1-aziridinyl)propionate], commonly referred to as XAMA®7, was employed to functionalize alginate gel. Trisaziridine consists of a pentaerythritol core with three attached 1-aziridinylpropionate functional groups. It is widely utilized as a crosslinking agent and modifier in diverse fields, such as adhesive and coating, to improve strength, flexibility, hardness, and to be resistant to such solvents (Chen et al. 2007; Licchelli et al. 2011, 2013; Jang et al. 2015; Naga et al. 2022).

The presence of carboxylic groups in alginate polymer allows for the expectation of reactions with the aziridine rings in XAMA®7. These reactions lead to the formation of covalently crosslinked networks within the alginate polymer. This cross-linking process is expected to improve the mechanical and chemical properties of the resulting material. The hypothesis of this study is based on the covalent ester bonding between the alginate polymer's carboxyl groups and the aziridine rings of XAMA®7, as presented in Figure 35.

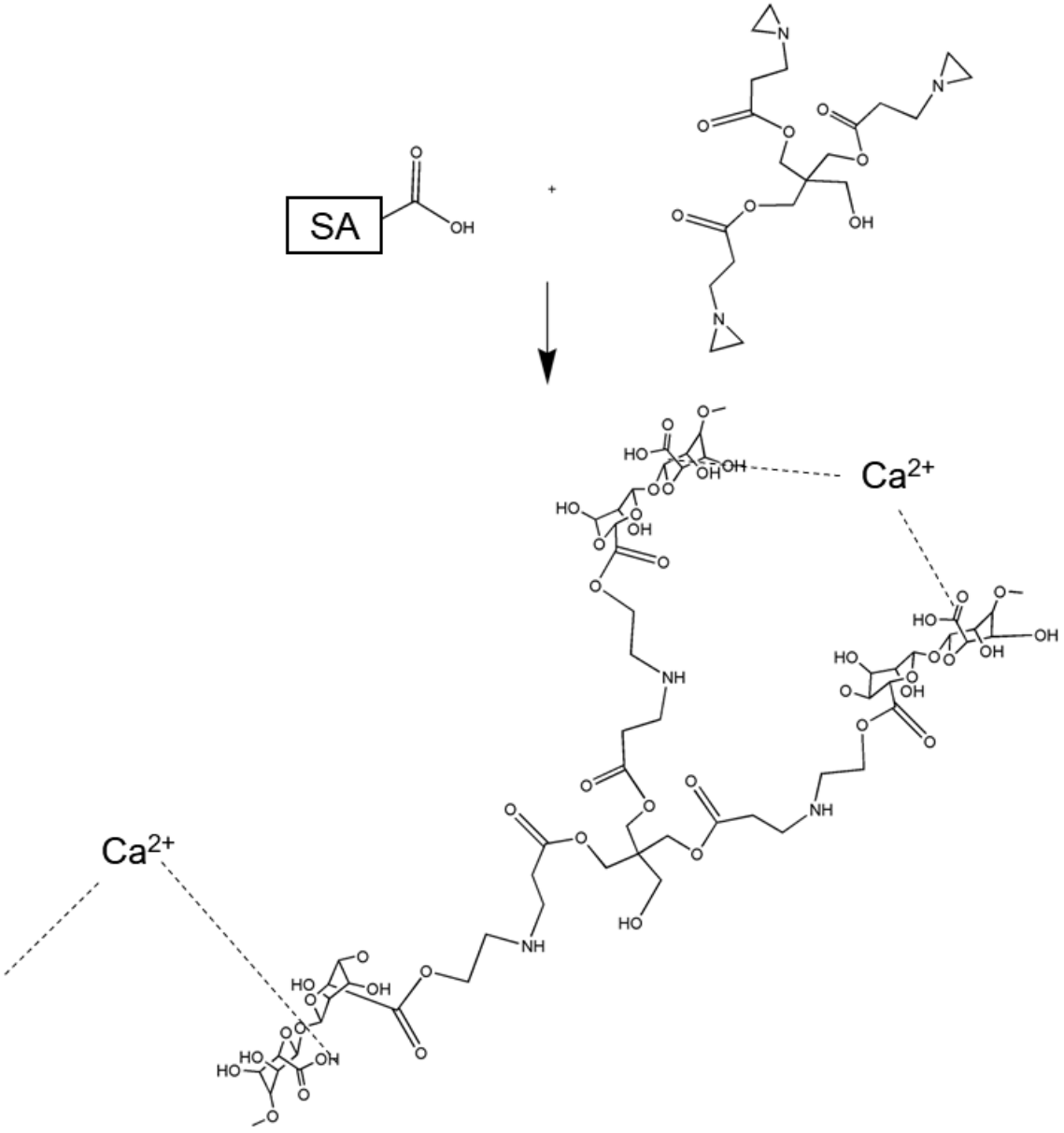

Figure 35. Expected reaction between alginate polymer, XAMA 7 and calcium ion.

3.4.1. Gel Preparation

The preparation steps of CA-XAMA7 are described in Figure 36. For CA-XAMA7, 0.2 g sodium alginate (SA) was added into a beaker containing 10 ml of distilled water, and the solution was stirred and slightly heated at 40 °C until it was completely dissolved. Then, XAMA®7 was added dropwise into the alginate solution (three different amounts of XAMA®7 were added into the SA by keeping the sodium alginate monomer and XAMA®7 molar ratios respectively in SA: XAMA®7 = 1: 0.5, 1, and 2) and stirred with a magnetic bar at 50 °C for 30 minutes for the reaction. In order to prepare it into a film-forming gel, SA solutions were poured into Petri dishes, keeping the thickness of about 2-3 mm. After that, 2% (w/v) $CaCl_2$ solution was slowly poured into the prepared Petri dishes, and the reactions were maintained for 15 minutes to allow the cross-linking process with calcium ions and finalized the gel formulations, they were named as CA-XAMA7_0.5, CA-XAMA7_1, and CA-XAMA7_2 according to their molar ratios as mentioned before. After forming CA-XAMA7, the gel was repeatedly washed in deionized water to remove unreacted materials.

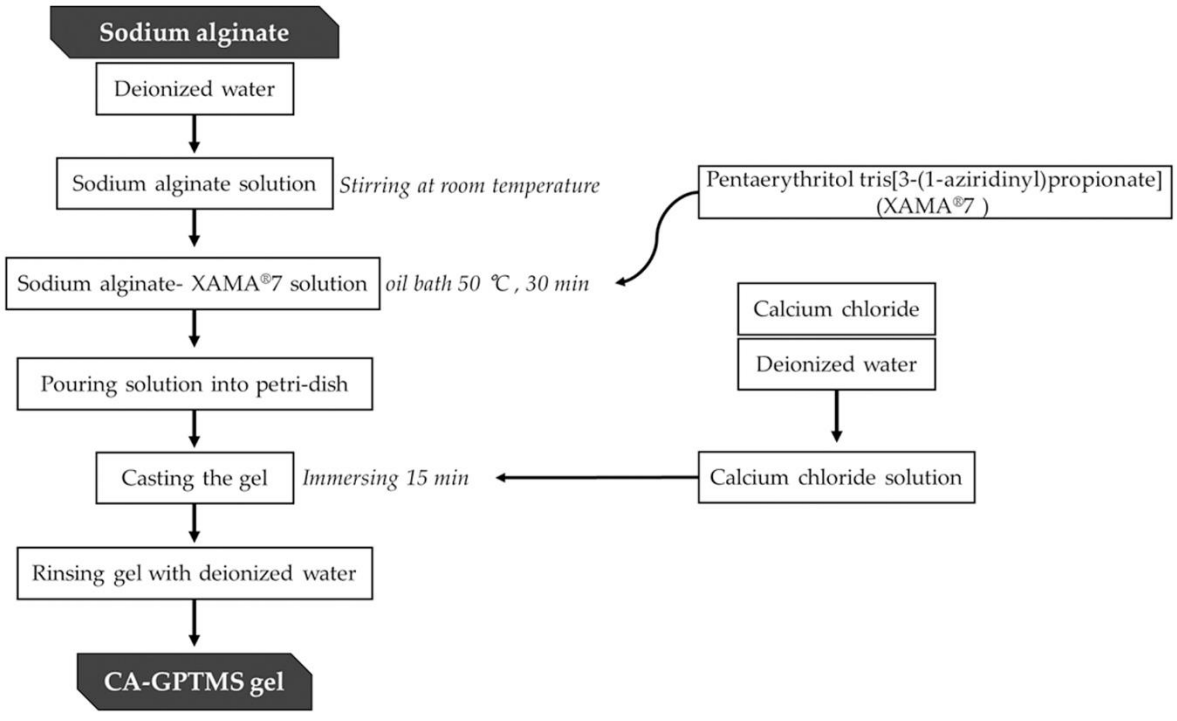

Figure 36. A schematic diagram of steps involved in preparing CA-XAMA7 gel.

3.4.2. Gel Characterization

The functionalization of alginate and XAMA®7 aziridine ring opening and formation of ester group occurrence can be demonstrated by the ^{1}H-NMR and 2D-COSY (Figure 37 and Figure 38). On the ^{1}H-NMR spectra, two sets of peaks at 1.73 and 1.33 ppm of XAMA®7 indicate the proton signals of the aziridine ring (Ishizone et al. 2003; Chen et al. 2007; Chen et al. 2015), which are no longer present in the spectrum of functionalized alginate SA-XAMA7 (Figure 37). In this regard, 2D-COSY confirmed the aziridine ring opening and suggested connectivity of protons of the SA-XAMA7 (Chen et al. 2007; Chen et al. 2015; Vilas-Boas et al. 2020) by the correlations of the protons b, d and e, f (Figure 38). The TGA revealed that the thermal stability improval when the ratio of XAMA®7 increased in the formulation of CA-XAMA7 (Figure 39) (Vueva et al. 2018; Jiang et al. 2019).

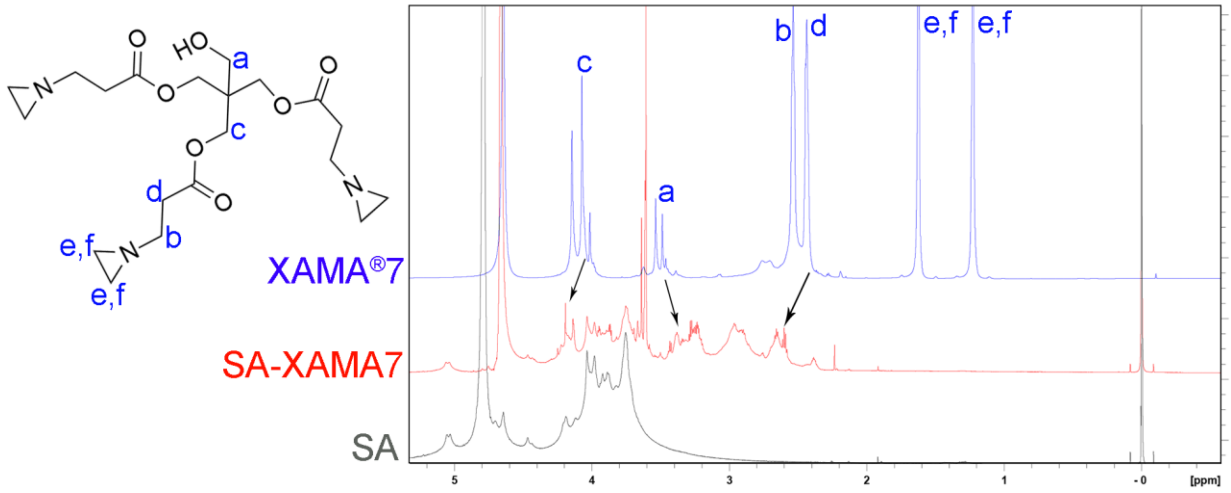

Figure 37. Liquid state ^{1}H-NMR of sodium alginate (SA), XAMA®7, and sodium alginate functionalized with XAMA®7 (SA-XAMA7).

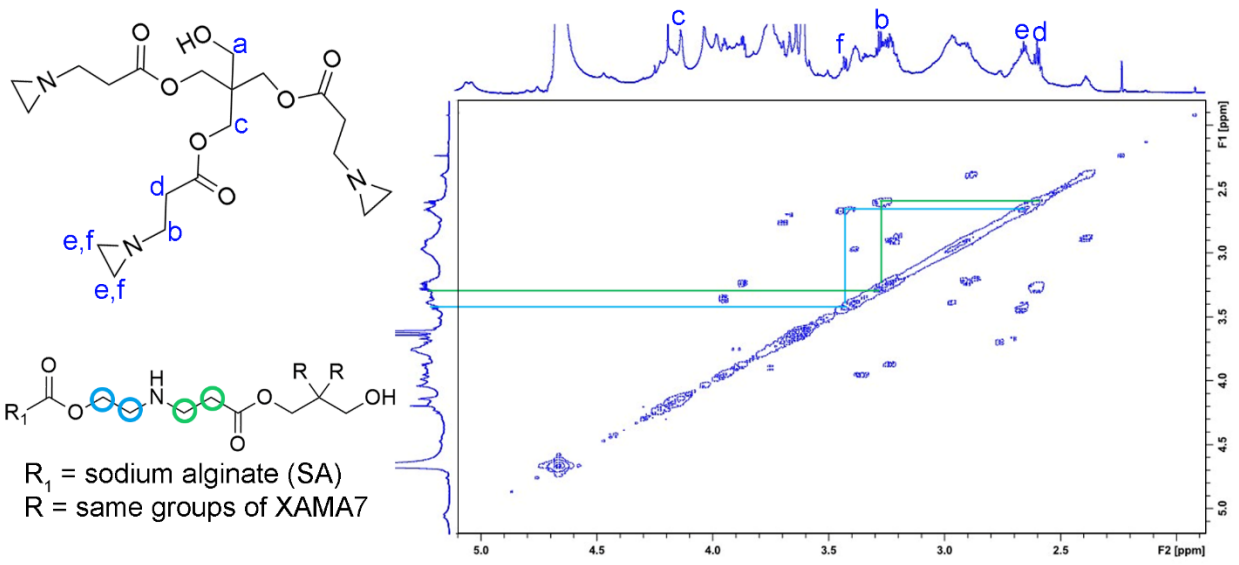

Figure 38. 2D-COSY NMR spectrum of sodium alginate functionalized with XAMA®7 (SA-XAMA7). Blue and green lines, respectively point out the connections between protons b, d, e, and f.

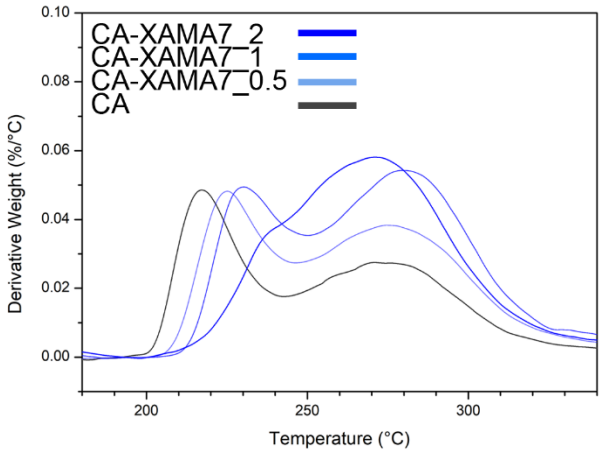

Figure 39. Thermogravimetric analysis (TGA) (a) curves of CA and CA-XAMA7 gels in different ratios.

After confirming by NMR and TGA analysis that the reaction between alginate and trisaziridine occurred, the gel produced after adding calcium ions was studied by FTIR-ATR and SEM (Figure 40). The FTIR spectrum of CA-XAMA7_1 showed some differences compared to simple alginate (SA). The peak attributed to asymmetric and symmetric COO^- bands shifted and changed in intensity, confirming the electrostatic interactions of carboxylate groups and calcium ions

(Papageorgiou et al. 2010; Li et al. 2016; Badita et al. 2020). With the reaction with trisaziridine, the ester bands of C=O stretching (1725 cm^{-1}) and C-O stretching (1120 cm^{-1}) appeared (Chen et al. 2007; Chen et al. 2015; Licchelli et al. 2011, 2013; Vilas-Boas et al. 2020). Most importantly, the result may indicate that the CA-XAMA7 gel is a chemical gel functionalized by ester bonding with the carboxyl group of alginate and ionic bonding with calcium. Furthermore, the SEM image provided information on the CA-XAMA 7_1 gel as a compact and homogeneous surface compared to the CA (in section 3.2.2.) and CA-GPTMS gel.

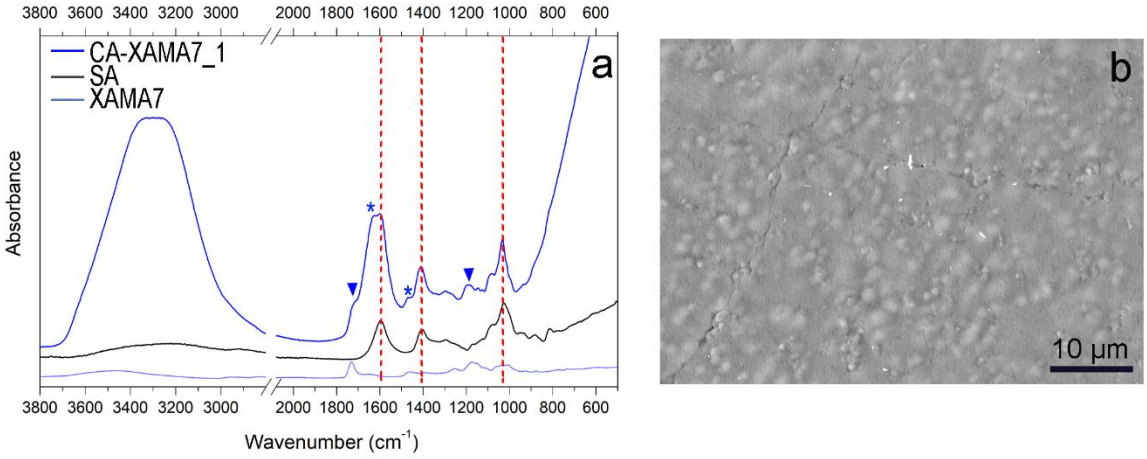

Figure 40. FTIR spectrum of the Ca-alginate-XAMA7 formulated gel in sodium alginate monomer and XAMA®7 molar ratios respectively in SA: XAMA®7 = 1: 1(CA-XAMA7_1), pure sodium alginate (SA) and XAMA®7 reactants. Markers for electrostatic interactions of carboxylate groups and calcium ions (red dotted line), ester groups (triangle), and methylene derivation from XAMA®7 (asterisk) are displayed. SEM image of CA-XAMA7_1 gel film acquired in high vacuum with secondary electrons (b).

The mechanical properties of the gels were measured by comparing them with physically crosslinked CA gel and with chemically crosslinked gels of CA-XAMA7 (CA-XAMA7_0.5, CA-XAMA7_1, and CA-XAMA7_2). Furthermore, the most promising gel to be used for cleaning applications, Ca-XAMA7_1 was compared in fresh and aged gels to understand shelf-life consistency after 60 days (Figure 41).

All the newly formulated CA-XAMA7 gels significantly improved tensile strength compared with physical CA and agar gels, showing increased stretching strength and stiff texture (Figure 41a,b). In addition, based on these results, it is implied that exceeding a certain amount of XAMA®7, CA-XAMA7 becomes strongly elastic but at the same time rigid,

presenting a more plastic consistency, being probably referable to CA-XAMA7_1 the highest value in tensile strength, while decreasing the value from CA-XAMA7_2. This was an expected result as XAMA®7 is applied widely to improve the strength and flexibility of the polymers (Chen et al. 2007; Licchelli et al. 2011, 2013; Jang et al. 2015; Naga et al. 2022). Upon aging in CA gels, the mechanical properties of CA-XAMA7_1 were significantly higher, implying that the gel texture of CA-XAMA 7_1 can be maintained even after 60 days (Figure 41c,d).

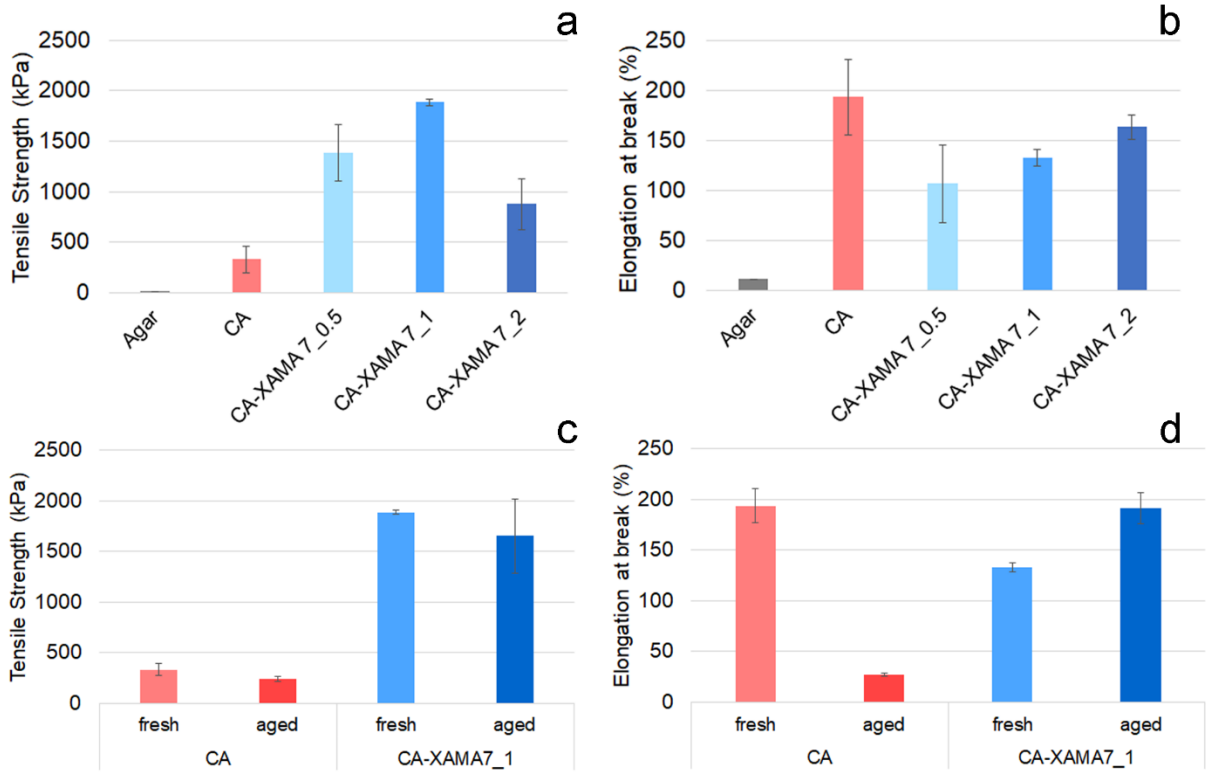

Figure 41. Mechanical properties determined by tensile test (mean value ± s.d.; n = 5): tensile strength (a) and elongation at break (b). fresh and aged gel of CA and CA-XAMA7_1 tensile strength (c) and Elongation at break (d).

The moisture properties of CA-XAMA7 gels are summarized in Table 9 for comparison with conventional CA and agar gels. The newly formulated CA-XAMA7 chemical gels showed a significant reduction in hydrophilicity and water loading, demonstrated by the decrease in Equilibrium Water Content (EWC) and Solvent Capacity (SC) values compared to the physical CA and agar gels (Table 9). In addition, it was also observed that EWC and SC gradually increase with the increase of CA-XAMA7 ratio, which might be the promoted result

by the hydroxyl groups in trisaziridine. Regarding Water Release (WR), CA-XAMA7 gels demonstrated six times more retention than agar, while no significant difference was noted with CA physical gel.

Table 9. Moisture properties of CA-XAMA7 gels, CA, and agar: equilibrium moisture content (EWC), swelling capacity (SC), and water release (WR). Mean values and standard deviations were calculated on five iterations

Gel	EWC (%)	SC (%)	WR (mg/cm^2)
CA-XAMA7_0.5	24.8 (± 4.7)	33.3 (± 8.3)	3.7 (± 0.3)
CA-XAMA7_1	35.4 (± 2.4)	54.9 (± 5.9)	4.0 (± 1.8)
CA-XAMA7_2	37.8 (± 4.2)	61.4 (± 10.7)	4.2 (± 0.8)
CA	64.0 (± 5.0)	$(1.8 \pm 0.4) \times 10^2$	5.4 (± 1.0)
Agar	95.6 (± 0.3)	$(2.2 \pm 0.2) \times 10^3$	29.3 (± 2.5)

Overall, the results of gel characteristics showed that CA-XAMA7_1 gel is the best choice for use in cleaning applications, as it has elasticity and durability even when the gel is aged, compared with physical CA and agar gel. At the same time, the moisture properties of CA-XAMA7_1 gel showed optimal water-loading and controlling properties.

3.4.3. Cleaning Application and Evaluation of the Efficacy

Based on the previous study in section 3.2.2., the CA gel performed very well in cleaning the surface of the sweat-WM after the single application. For this reason, a preliminary cleaning examination of CA-XAMA7_1, sweat-WM was used for the application test and in order to obtain incidental and representative data, we used XRF mapping and calculated cleaning efficacy to evaluate the cleaning. The prepared CA-XAMA7_1 cleaning system was immersed separately in the 2% v/v solution of ecosurf™ EH-9 and 2% and tween® 20 (v/v, in distilled water) for 24 hours to make it ready for use. Cleaning was performed for a single application in 5 minutes.

3.4.3.1. XRF mapping

XRF mapping provided a clear view of the sweat droplets, and on the areas cleaned by the CA-XAMA7_1 gel loaded with the different surfactant tween® 20 and ecosurf™ EH-9, the removal of sweat droplets was demonstrated (Figure 42).

The result of cleaning efficacy was 96% with d.w., 95% with tween 20®, and 95% with ecosurf™ EH-9, demonstrating good cleaning efficacy of removing sweat composition containing chlorine. This result was also evident in section 3.2.2.3, where a single application significantly removed the hydrophobic WM surface when cleaning with CA gel.

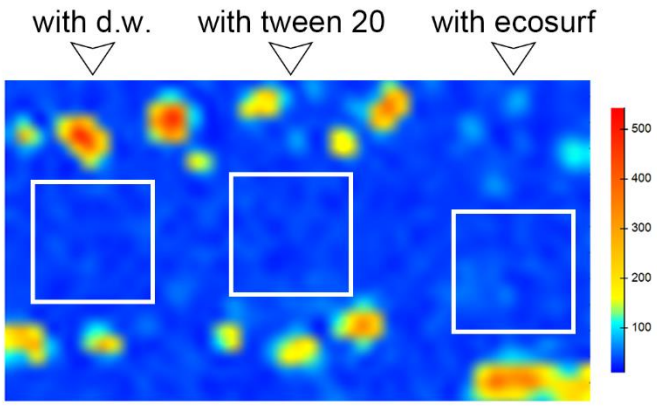

Figure 42. XRF heat maps on sweat-WM after cleaning with CA-XAMA7_1 with deionized water and with different surfactants tween® 20 and ecosurf™ EH-9 The color range represents high to low counts of chlorine marker.

3.5. Evaluation and Optimisation of Alginate-based Gels

The alginate-based gels studied in this study (Sections 3.1., 3.2., and 3.4.) were evaluated using the rating scale described in Section 2.5. Subsequently, the characteristics of the alginate-based gels and the cleaning results of each gel after cleaning soiled and sweat mockups were evaluated (section 3.3. CA-GPTMS gel is excluded in this study as it was not used to clean these mockups), as presented in Figure 43.

Ionically cross-linked CA gels showed less hydrophilicity than the physically cross-linked agar gel, which conservators widely use. However, the newly formulated CA-XAMA 7 gel proved to be a hydrophobic and highly retentive gel due to the reduction of hydrogen bonds through ester linkage. Furthermore, it is important to consider that conventional rigid agar gels are brittle and literature reports that they can leave gel residue on the surface (Scott 2012; Jan van den Berg et al. 2019). Meanwhile, CA and CA-XAMA7 gels have shown significantly greater strength and pliability than agar gels.

After cleaning soiled mockups (Figure 43a,b), the cleaning efficacy agar and CA gel showed a similar result on both the WM and EAM surfaces. At the same time, also after cleaning sweat mockups (Figure 43c,d), no difference in the cleaning efficacy of the gel was found between the agar, CA, or CA-XAMA7 gel, but a better removal was shown when cleaning the hydrophobic sweat-WM surface than on the hydrophilic sweat-EAM surface.

Overall, there was not much difference in the cleaning behavior, but rather an improvement in the texture of the CA and CA-XAMA7 gels, with a wider star diagram than the agar gel.

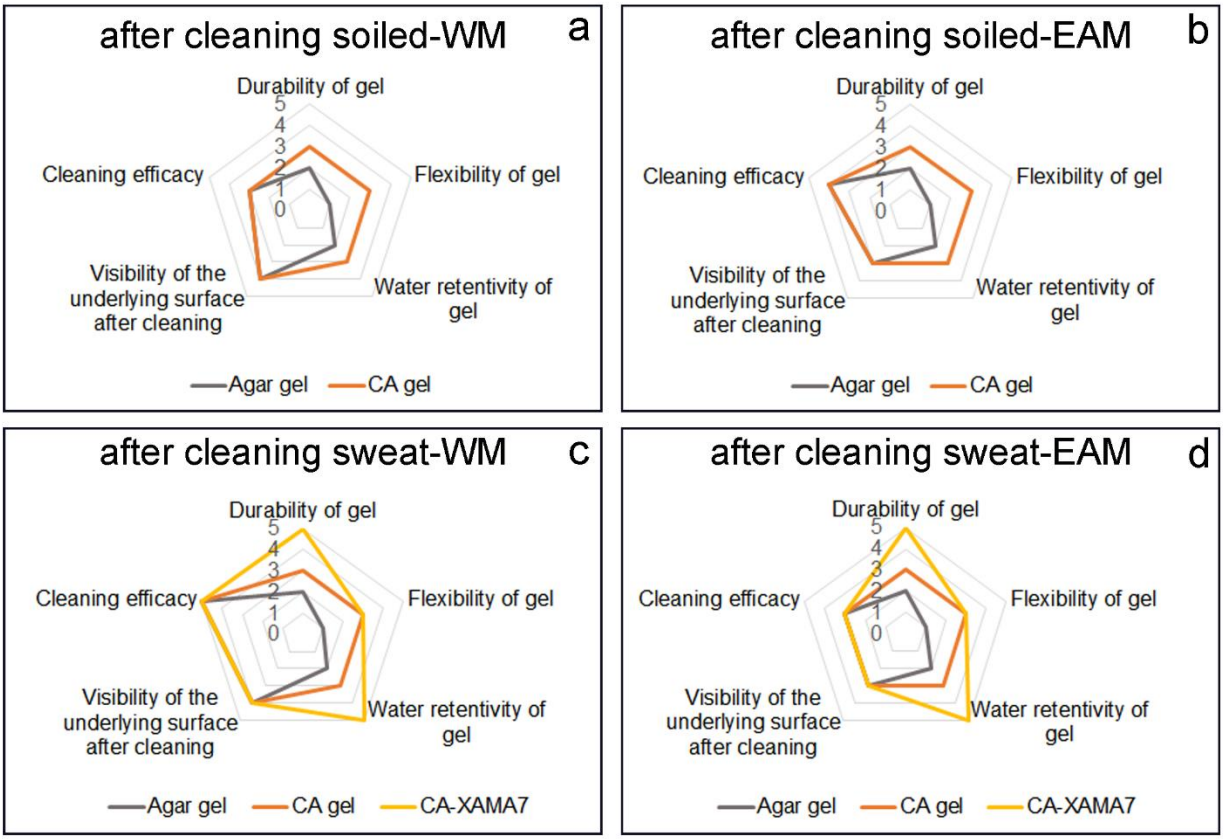

Figure 43. Star diagrams comparing the results of agar and CA gel characteristics and cleaning evaluation after cleaning soiled-WM (a) and -EAM (b) and agar, CA gel, and CA-XAMA7 gel characteristics and cleaning evaluation after cleaning sweat-WM (c) and -EAM (d).

Chapter 4.

Konjac Glucomannan-based gels[2]

[2] This Chapter are based on:
Lee, C.; Volpi, F.; Fiocco, G.; Weththimuni, M.L.; Licchelli, M.; Malagodi, M. Preliminary Cleaning Approach with Alginate and Konjac Glucomannan Polysaccharide Gel for the Surfaces of East Asian and Western String Musical Instruments. *Materials* **2022**, *15*, 1100. https://doi.org/10.3390/ma15031100
Lee, C.; Di Turo, F.; Vigani, B.; Weththimuni, M.L.; Rossi, S.; Beltram, F.; Pingue, P.; Licchelli, M.; Malagodi, M.; Fiocco, G. Biopolymer Gels as a Cleaning System for Differently Featured Wooden Surfaces. *Polymers* **2023**, *15*, 36. https://doi.org/10.3390/polym15010036

4.1. Konjac Glucomannan Properties and Applications

Konjac glucomannan is a natural polysaccharide derived from the tuber of *Lasioideae Amorphophallus*, a perennial Araceae plant. The chemical structure of heteropolysaccharide konjac consists of D-mannose and D-glucose monomers linked by β-1,4 bonds and has a short side branch at the C-3 position of mannose (Figure 44) (Williams et al. 2000; Phillips and Williams 2009). It has been widely used in China, Korea, and Japan as a traditional medicine in the treatment of asthma, skin disorders, and dietary fiber to control diabetes and obesity (Alonso-Sande et al. 2009; Chua et al. 2010).

Representative cross-linking of konjac is an alkaline process. The mannan of konjac contains very small amounts of acetyl groups, and with this chemical structure, deacetylation with alkaline treatment is used to form a gel (Li et al. 2015; Huang et al. 2015; Zhou et al. 2018; Ma et al. 2019). The formation of alkali-treated konjac gel is the most widely used as it has been long used for oriental foods. Other than this, borate crosslinking is used by forming a gel with two *cis*-diol pairs of different konjac molecules by connecting with the borate ion to form an interchain crosslink (Gao et al. 2008a, b; Song et al. 2019).

Thanks to this chemical structural feature, konjac exhibits compatibility with other polymers, biodegradability, absorption, and water retention. These features allow it to be used for thickening, gelling and texturizing foods, pharmaceutical products, and oriental cosmetics (Alonso-Sande et al. 2009; Impaprasert et al. 2017; Yang et al. 2017; Ma et al. 2019; Wang et al. 2019).

4.2. Konjac Borax

To investigate the desiring gel texture for the cleaning application, a preliminary examination was carried out to understand which crosslinker would be appropriate for konjac to have an adequate consistency. The material and the investigative study of konjac glucomannan material are described in section 2.1.2.

The konjac prepared with the alkali chemicals NaOH, KOH, and $Ca(OH)_2$ showed a good gel-like texture (Zhang et al. 2021). However, all the alkaline konjac gel appeared as a white gel with a pH of 10-13, which is not appropriate for the cultural heritage field as this gel could be applied on delicate surfaces (Figure 45a). For the one crosslinked with sodium tetraborate decahydrate (borax), flexibility was enhanced as the concentration of borax and konjac increased (Gao et al. 2008a, b). This feature was recognizable as the konjac-borax hydrogels are also reported to have a good self-healing and flexible texture, as the intermolecular bonds and bonds involving $B(OH)^{4-}$ and hydroxy groups of konjac chains are dynamically reversible (Song et al. 2019; Chen et al. 2019). At the same time, the konjac-borax gel was colorless and transparent (Figure 45b). By this preliminary examination, sodium tetraborate decahydrate was selected for the crosslinking, and Figure 46 shows the expected reaction between konjac and borate ions.

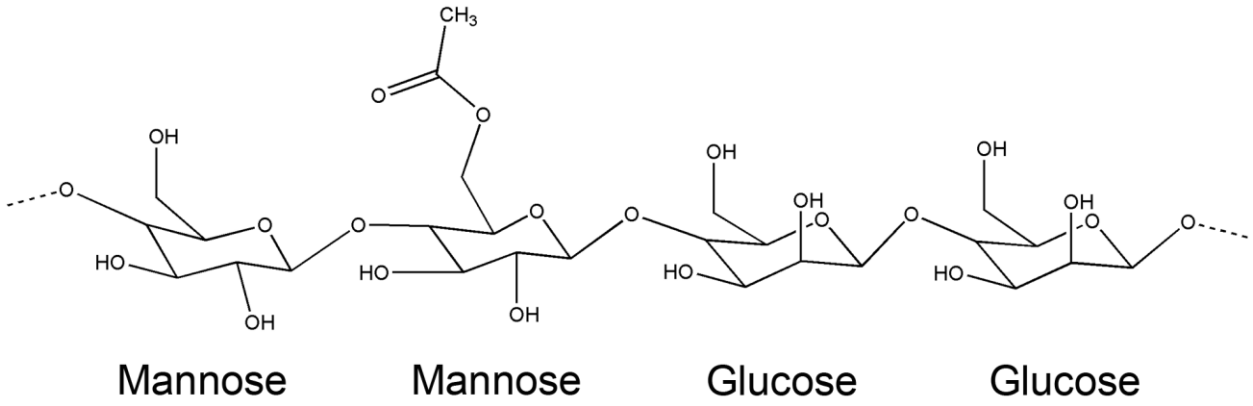

Figure 44. The structure of β-1,4-linked D-glucose and D-mannose repeating units in konjac glucomannan (Williams et al. 2000).

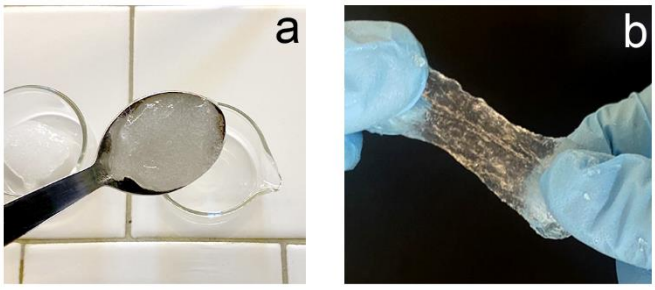

Figure 45. Image of alkaline konjac gel (a) and konjac-borax gel.

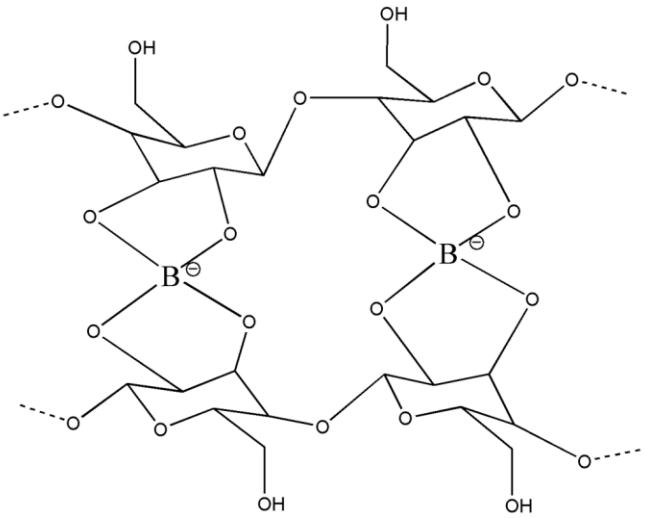

Figure 46. Expected reaction between konjac polymer and borate ions (Song et al. 2019).

4.2.1. Gel Preparation

Based on the preliminary examination described in section 4.2., konjac glucomannan (KG)-borax (B) gel was prepared at 50 °C, and while stirring, 0.1 g of sodium tetraborate decahydrate (borax) was added in 10 mL KG solution (Molar ratio 1:6250) (Figure 47). The KG solution was left at room temperature for 30 min to stabilize the mixture. The stabilized mixture was then placed in bulk form in deionized water, maintaining the temperature at 90 ± 10 °C for 20 min. The immersed KGB gel was taken out, cooled, and dried at room temperature until the water on the surface dried.

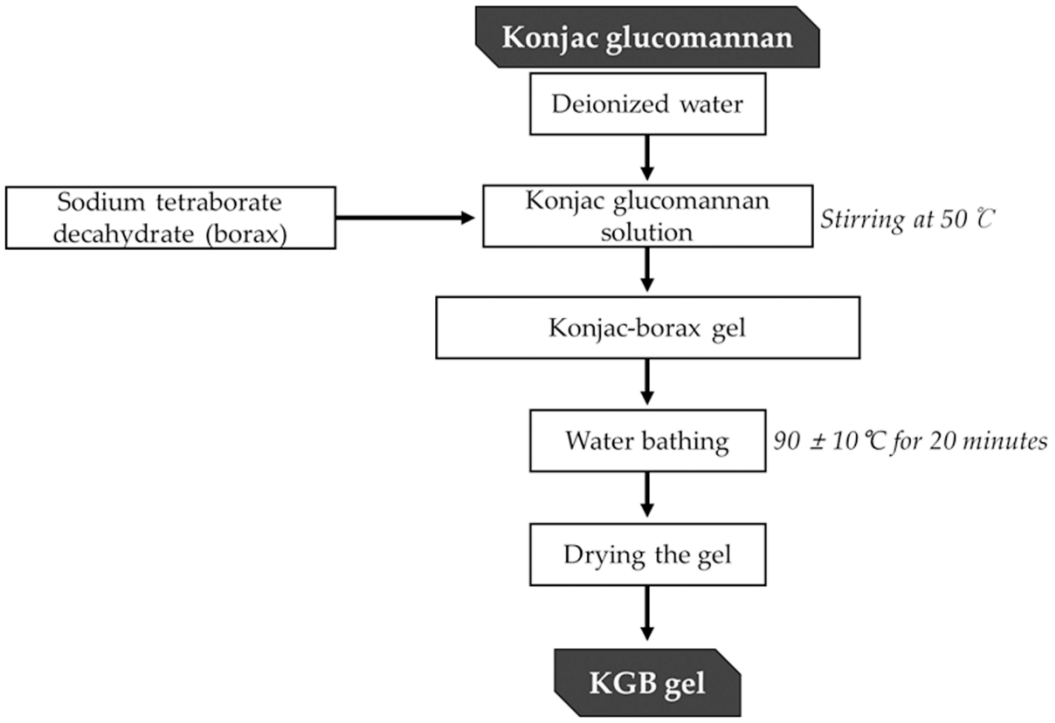

Figure 47. A schematic diagram of steps involved in preparing KGB gel.

4.2.2. Gel Characterization

By FTIR-ATR, plain konjac powder showed a broad band centered at 3315 cm^{-1} corresponding to O-H stretching groups and the bands at about 2900 cm^{-1} ascribed to C-H stretching vibrations in the $–CH_2$ or $–CH_3$ groups (Figure 48a). Also, the vibration of the carbonyl at 1725 cm^{-1} corresponds to the acetyl groups of KGM molecules (G. O. Phillips and P. A. Williams 2009; Song et al. 2019; Wang et al. 2020). As for other konjac characteristic peaks appeared at 1640 cm^{-1} (the bending vibration of -OH groups), 1020 cm^{-1} (C-O-C vibrations), and 880 cm^{-1} and 800 cm^{-1} corresponded to the stretching vibrations of mannose units (Song et al. 2019; Wang et al. 2020).

After the crosslinking, on the range of 1500-1200 cm^{-1}, there appeared a band at 1420 cm^{-1}, which might be attributed to the signal of the asymmetric stretching relaxation of B-O-C after crosslinking the hydroxyl groups and the borate ions (Spoljaric et al. 2014; Song et al. 2019).

The surface morphology of the hydrogel appeared as a complex three-dimensional conjugated feature with apertures (Figure 48b).

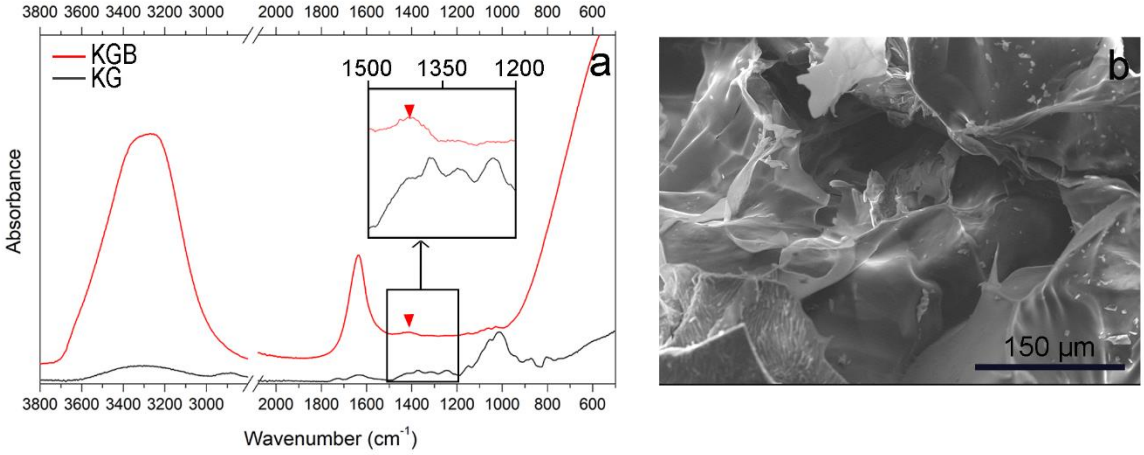

Figure 48. FTIR spectrum of the konjac glucomannan-borax formulated gel (KGB) and pure konjac glucomannan (KG) (a). Markers for interactions of hydroxyl groups and borate ions (triangle) are displayed. SEM image of KGB gel acquired in standard secondary electrons (b).

The formulated KGB gel appeared as a soft gel, which was evaluated with the compression test to examine the mechanical properties. The KGB gel was measured by comparing it with the agar gel as a control, and to understand the shelf-life consistency after 60 days, fresh and aged KGB gel and agar gel were compared.

When comparing the fresh-KGB gel with the fresh-agar gel, the agar gel showed significantly higher hardness and Young's modulus than the KGB gel (Table 10). These results of the agar gel are in agreement with other studies that have described agar as a stiff and rigid gel (Scott 2012; Kanth et al. 2018; Cremonesi 2019). High hardness values and Young's modulus correspond to a high gel stiffness, while low values correspond to a higher elasticity and softness. Therefore, lower hardness values and Young's modulus suggest that KGB gel can change shape more flexibly than agar gel, which might suggest that it is more suitable for cleaning rough surfaces. Furthermore, the stress-strain curve confirmed that the KGB gel had a linear, elastic texture due to steadily increasing stress-strain values, whereas the agar gel had passed the yield point, meaning that it had broken and the strain was not recoverable (Figure 49).

Table 10. Mechanical properties of gels determined by compressive test (mean value ± s.d.; n = 3). ANOVA one-way ($p < 0.05$), Multiple Range Test: having the different superscript symbol (, **, °, #, §, §§) indicate statistically different data. AUC: Area Under the stress–strain curve.*

Classification		Hardness (kPa)	Young's Modulus (kPa)	AUC
Agar gel	Fresh	47.0 ± 2.5 *	556.4 ± 47.2 °	2361 ± 202 §
	Aged	52.3 ± 1.9 *	464.2 ± 96.0 °	2179 ± 194 §
KGB gel	Fresh	30.0 ± 3.3 **	46.9± 0.1 #	766 ± 15 §§
	Aged	40.4 ± 12.8 **	30.2 ± 2.5 #	868 ± 264 §§

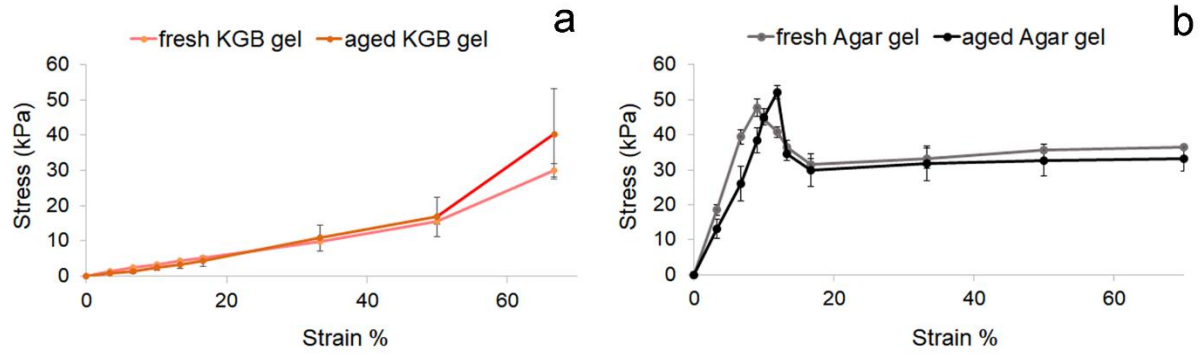

Figure 49. Stress–strain curves of fresh and aged KGB gel (a) and agar gel (b).

The moisture properties of the KGB gel are summarized in Table 11 and were compared to those of agar as a control. The KGB gel showed slightly lower water uptake than the agar gel, with a result in line with the equilibrium moisture content (EWC) and swelling capacity (SC), signifying a high hydrophilicity of the gel. Interestingly, the water release (WR) was less than half that of the agar control, meaning that it is able to retain a high amount of solvent in its network while avoiding excessive solvent release and diffusion after cleaning. This is important because it is directly related to the risk of causing long-term degradation of the cleaned surface.

Table 11. Moisture properties of SA and KG gels used for the cleaning test, namely equilibrium moisture content (EWC), swelling capacity (SC), and water release (WR). The average values and the related standard deviations were determined by repeating the experiment five times. D.W. = distilled water.

Gel	EWC (%)	SC (%)	WR (mg/cm^2)
KGB	93.9 (±1.4)	$(1.5 \pm 0.3) \times 10^3$	14.2 (±1.0)
Agar	95.6 (± 0.3)	$(2.2 \pm 0.2) \times 10^3$	29.3 (± 2.5)

4.2.3 Cleaning Application and Evaluation of the Efficacy

For the cleaning application, the prepared KGB cleaning system was immersed in 2% of ecosurf^{TM} EH-9 solution (v/v, in distilled water) for 5 h and was then ready for use. The cleaning was repeated each time for 5 minutes; the gel was applied up to three times (KGB_1, KGB_2, KGB_3) on WM and EAM surfaces, where the synthetic soil and sweat were dispersed (see the preparation of mock-ups in section 2.2.1. and 2.2.2).

4.2.3.1. Stereo Microscopy and Profilometry

A representative description of the microscopic characteristics of WM, EAM, synthetic soil and sweat is given in Section 3.2.2.1.

After cleaning the soiled-WM with KGB gel, a significant difference emerged when observing the stereomicroscopy and 3D profilometry map (Figures 50a,b and Figure 51a,b). Furthermore, with the repetition of the cleaning from KGB_1 to KGB_3, the soiling particles decreased, reaching the smooth surface of the WM and were obviously observed by stereomicroscopy, 3D map and roughness parameter. This trend was clearly visible from the roughness value Sv, which reduced the height depth by repeating the cleaning (Figure 51c,d,e). Even when comparing the result of the roughness parameter of the Agar_3, KGB_3 achieved a comparable cleaning result.

For the soiled-EAM surface after cleaning with the KGB gel, the investigation of the surface morphology could not fully reveal the different cleaning efficiencies obtained with the KGB

gel and agar due to the pronounced roughness, especially with stereomicroscopy (Figure 50c,d and Figure 52a,b). However, some relevant information can be obtained through the surface roughness parameters. The values of Sa and Ssk increase with the repetition of cleaning (Figure 52c,d). Interestingly, the values of Sv show the effectiveness of cleaning, such as removing soiling deposits from the irregular surface area (Figure 52e). This may be explained by the ability of the KGB gel to remove soiling particles from rough areas, perhaps related to its softness and elasticity, which is confirmed in section 4.2.1.

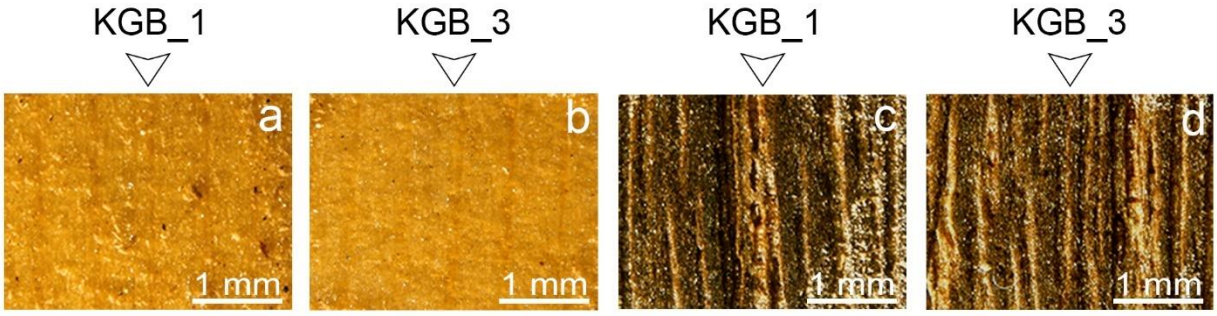

Figure 50. Stereomicroscopy images after the cleaning application on soiled-WM by KGB gel at different application times KGB_1 (a) and KGB_3 (b), and on soiled-EAM by KGB_1 (c) and KGB_3 (d).

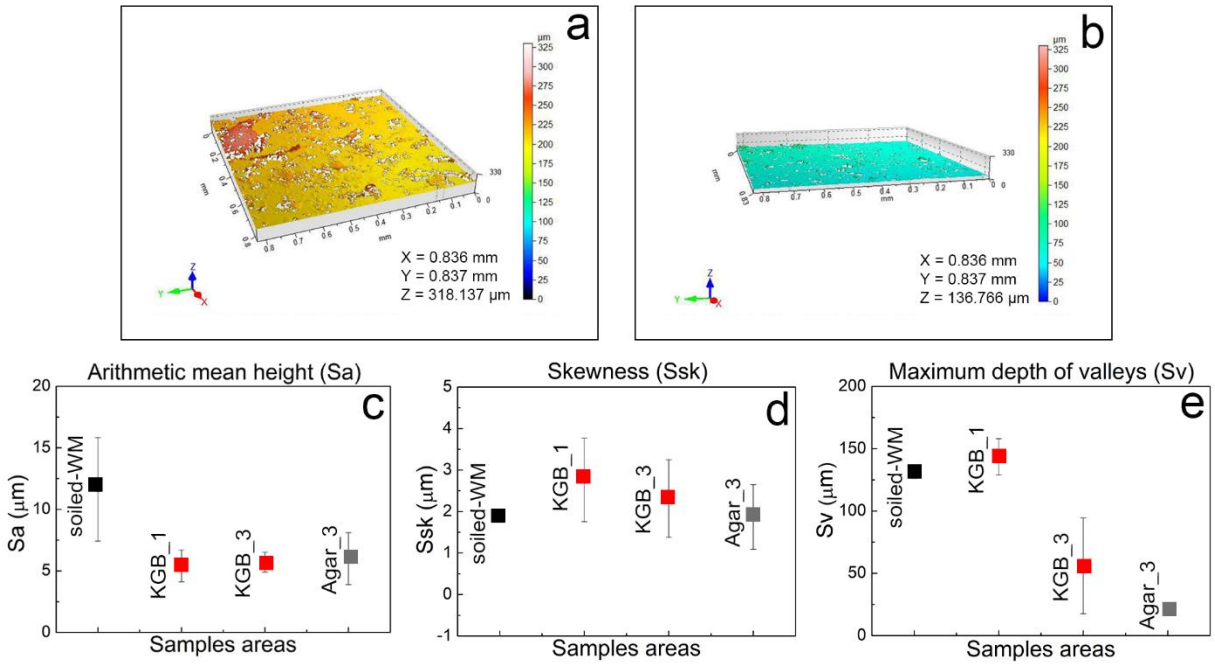

Figure 51. 3D heat maps of soiled-WM cleaned by KGB_1 (a) and KGB_3 (b). The color range represents the different heights (in microns) of the details present on the sample surface.

Considered roughness values of Sa (c), Ssk (d), and Sv (e) on the different areas of soiled−WM cleaned by different gels and application time KGB_1, KGB_3, and Agar_3.

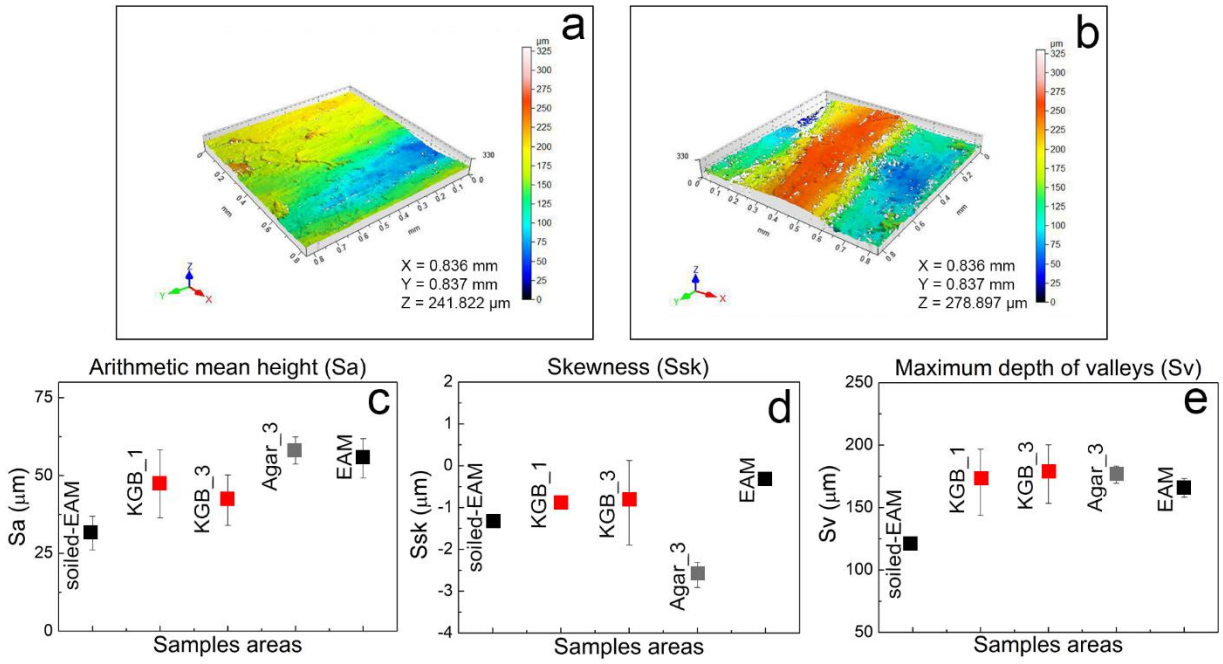

Figure 52. 3D heat maps of soiled-EAM cleaned by KGB_1 (a) and KGB_3 (b). The color range represents the different heights (in microns) of the details present on the sample surface. Considered roughness values of Sa (c), Ssk (d), and Sv (e) on the different areas of soiled−WM cleaned by different gels and application time KGB_1, KGB_3, and Agar_3.

As explained in section 2.3.3., due to the reflective surface of the sweat-WM, no profilometric measurements were performed, including 3D maps and examination of roughness parameters. While on the sweat-EAM, the sweats were hardly recognizable under the stereomicroscope (see Figure 17 in section 3.2.3.1.). In this respect, profilometry provided minimal differences in height variations, showing some differences after cleaning with KGB gel. After the cleaning application was repeated 1 to 3 times, the application gave a recognizable difference in the roughness parameter (Figure 53). Repeating the application up to 3 times increased the Sa, Ssk and Sv values, meaning the uneven and rough surface clearly appeared. Furthermore, KGB_3 and Agar_3 gave comparable results in all parameters Sa, Ssk and Sv.

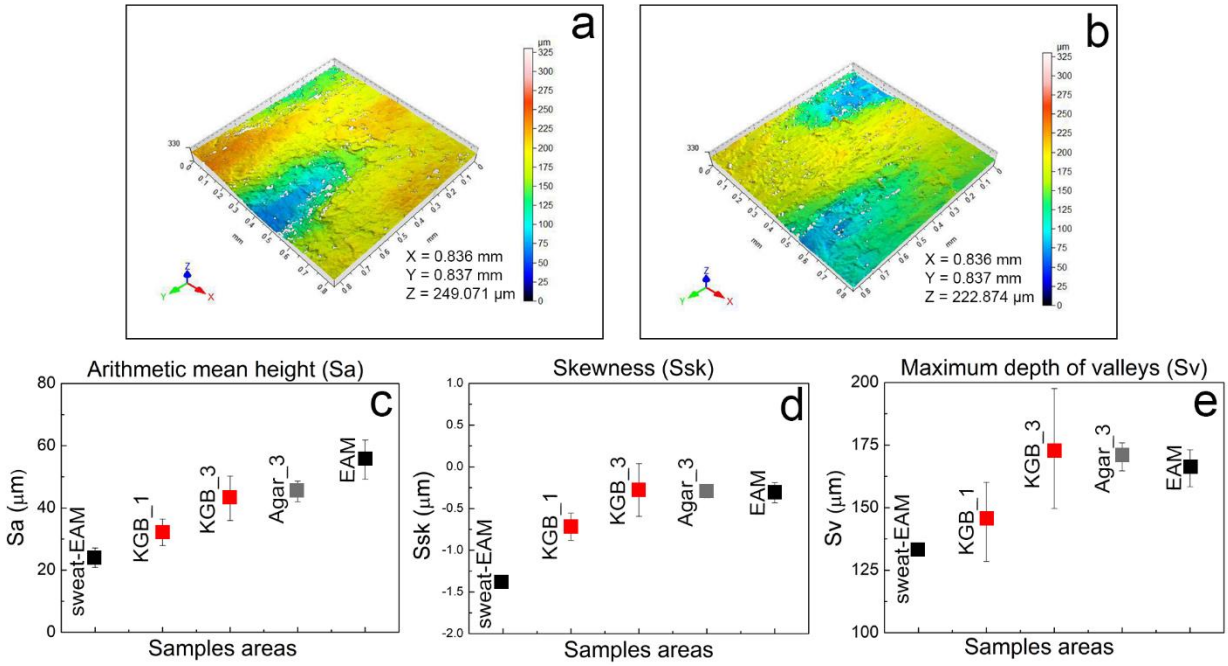

Figure 53. 3D heat maps of sweat-EAM cleaned by KGB_1 (a) and KGB_3 (b). The color range represents the different heights (in microns) of the details present on the sample surface. Considered roughness values of Sa (c), Ssk (d), and Sv (e) on the different areas of soiled−WM cleaned by different gels and application time KGB_1, KGB_3, and Agar_3.

4.2.3.2. Colorimetric Measurements

The complete data set with the color coordinates L*, a*, and b* acquired on both WM and EAM, as well as the overall chromatic variation (△E*) result of before and after cleaning, is summarized in Table 12.

After the application of the KGB gel for repeated trials (KGB_1, 2 and 3), both the brightness and the yellow contribution, respectively indicated by L* and b*, measured on the cleaned areas, increased to values similar to the bright, yellow WM surface. Furthermore, with the KGB_2 application, the △E* value appeared higher compared to the other applications.

On the EAM areas from the single application of KGB gel, a high decrease in L* values and an increase in a* values were observed, signifying that the bright-colored soiling deposits were removed, while the redness of the dark wood EAM surface was revealed. In addition, by increasing the repetition of the cleaning tests, the △E* value increased.

Table 12. Color coordinates L, a*, and b* were measured on WM and EAM and with the soiling mixture (soiled-WM and soiled-EAM). After cleaning with KGB gel by repeating applications, the average values and the related standard deviations were achieved by repeating the measurement five times. Standard deviation values are given in brackets. The overall chromatic variation (△E*) was calculated between the areas before and after cleaning the soiled-WM and soiled-EAM by repeating cleaning trials using KGB gels.*

Condition	L^*	a^*	b^*	△E*
Soiled-WM	75.8 (±0.6)	6.8 (±0.4)	39.7 (±0.7)	-
KGB_1	72.6 (±0.2)	7.4 (±0.2)	41.5 (±0.1)	7.1
KGB_2	74.0 (±0.3)	6.9 (±0.1)	41.4 (±0.1)	7.9
KGB_3	73.5 (±0.1)	7.2 (±0.0)	41.5 (±0.1)	7.7
WM	68.5 (±1.9)	7.4 (±0.3)	35.7 (±0.9)	-
Soiled-EAM	36.0 (±0.6)	4.9 (±0.3)	10.5 (±0.6)	-
KGB_1	33.1 (±2.5)	5.2 (±0.2)	9.9 (±0.9)	7.2
KGB_2	32.3 (±0.3)	5.1 (±0.3)	9.7 (±0.3)	8.0
KGB_3	32.0 (±2.3)	5.7 (±0.8)	10.2 (±1.7)	8.5
EAM	40.0 (±1.4)	3.4 (±0.6)	8.6 (±0.9)	-

4.2.3.3. XRF

A description of the elemental composition of WM, EAM, synthetic soil and sweat is given in Section 3.2.2.3.

After cleaning with KGB gel, the main compositional changes observed on soiled-WM and soiled-EAM were the Ca, Si, K and Fe counts. Figure 54 shows the normalized area counts of these peaks before and after cleaning. Interestingly, with a single application of KGB_1, Ca, Si, K, and Fe showed a high-count reduction. In particular, the soiled-EAM surface showed a higher calcium count reduction than the cleaned soiled-WM surface. Regarding this result, a Ca marker was selected to examine the XRF map, and the cleaning efficiency was evaluated using the calculation described in section 2.3.6. (Figure 55).

The cleaning efficacy results shown in Figure 55 were in line with those of the spot analysis presented in Figure 54. The single application of the KGB gel showed high efficacy, especially on the soiled-EAM surface. This could be due to the high hydrophilicity of the KGB gel and its characteristic as a flexible gel, which may facilitate access to the uneven surface of the EAM, impacting adhesion in crevices, and other reasons, such as chemical interactions with functional groups on the surface of the EAM. On the other hand, agar gel, which is a rigid gel, showed good cleaning efficacy upon repeated cleaning.

A single trial of KGB gel application on the sweat-WM surface showed significant removal of the sweat component, as evidenced by the decrease in Cl counts in Table 13. On the sweat-EAM, Cl counts decreased with increasing cleaning trials, suggesting satisfactory sweat removal efficiency. As explained in Sections 3.2.2.1. and 3.2.2.2., this may be due to the different surface characteristics, as WM is a hydrophobic surface and EAM a hydrophilic surface. By the result shown in Figure 56, after the single application of KGB gel, the evaluation of the cleaning efficacy showed almost 90% removal of sweat components from sweat-WM and 60% removal from sweat-EAM. The agar gel also provided excellent cleaning efficacy after a single application, which also occurred in the second and third repetition of the cleaning.

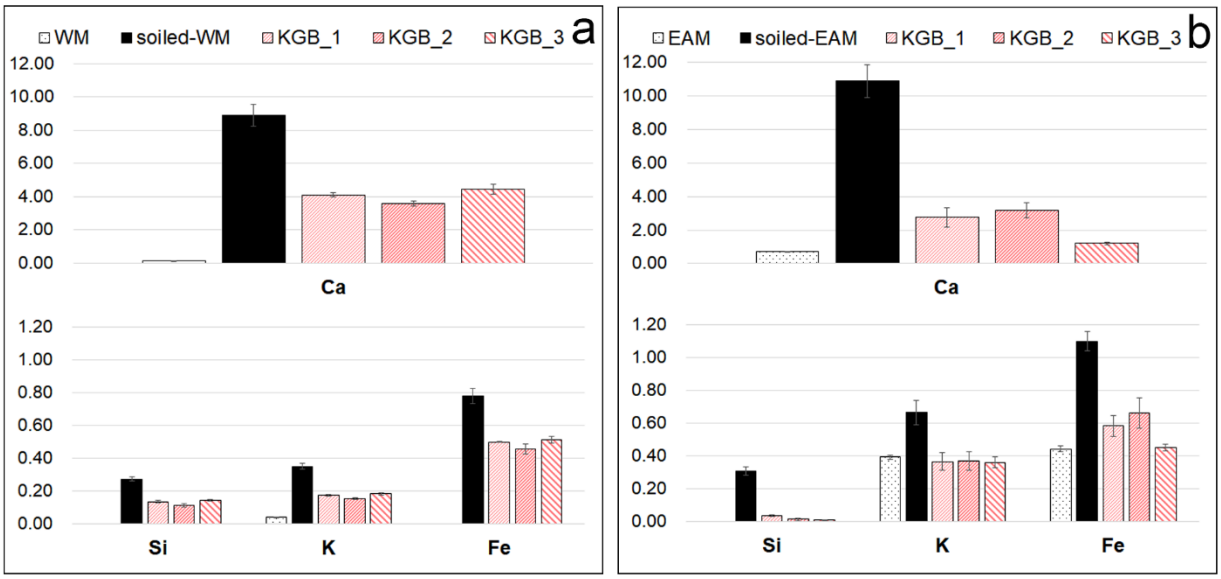

Figure 54. Normalized Ca, Si, K, and Fe counts were detected on (a) WM and (b) EAM. Different bars correspond to plain (WM and EAM) and with soiling deposits treated mock-ups (soiled-WM and soiled-EAM) and after 1, 2, and 3 applications of KGB gel (KGB_1, KGB_2, KGB_3). XRF values correspond to the net area counts of the Kα peak of each element normalized to time and the mean of the entire dataset of Rh-Kα peak net area counts, with the related standard deviation.

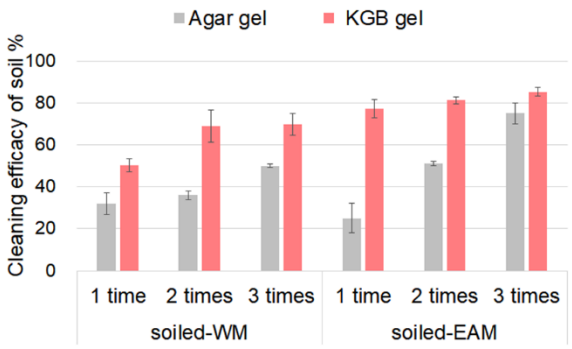

Figure 55. Cleaning efficacy values obtained on soiled-WM and soiled-EAM and KGB gels were applied 1 to 3 times repeatedly. The percentage of cleaning efficacy was calculated based on the counts of calcium markers.

Table 13 Normalized Cl (Kα) counts on sweat-WM and sweat-EAM, before (control) and after different cleaning applications with KGB gel

Mock-Up	Control	KGB_1	KGB_2	KGB_3
Sweat-WM	11.94	0.10	0.12	0.12
Sweat-EAM	3.35	1.90	1.12	0.49

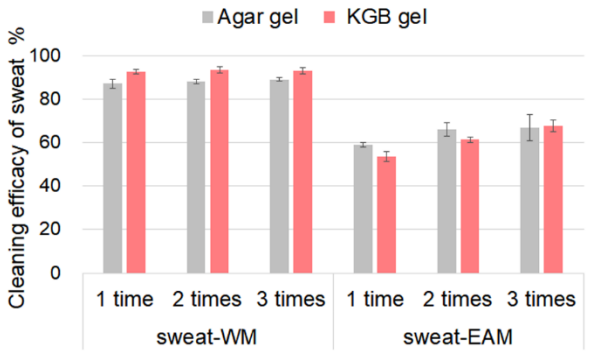

Figure 56. Cleaning efficacy values obtained on sweat-WM, sweat-EAM, and KGB gels were applied 1 to 3 times repeatedly. The percentage of cleaning efficacy was calculated based on the counts of chloride markers.

4.2.3.4. ER-FTIR

A description of the significant bands of WM and EAM, synthetic soil components and sweat is given in section 3.2.2.4.

Comparing the pseudo-absorbance spectra before and after cleaning with KGB_3 on soiled-WM, there is a marginal decrease in the intensity of the bands attributed to kaolin at 1040, 1000 and 915 cm^{-1} and calcium carbonate at 875 cm^{-1} (Figure 57a). On the transformed KKT spectra, the organic material at 1600 cm^{-1} decreased in intensity and the band contributing to oil-varnish was more clearly recognizable (Figure 57b). Comparable results were obtained on the surface of the soil-EAM, and the cleaning test with Agar_3 also showed similar removal to that obtained with KGB_3 (Figure 58). It is also considered that at least three cleaning applications are required to detect a recognizable spectral change.

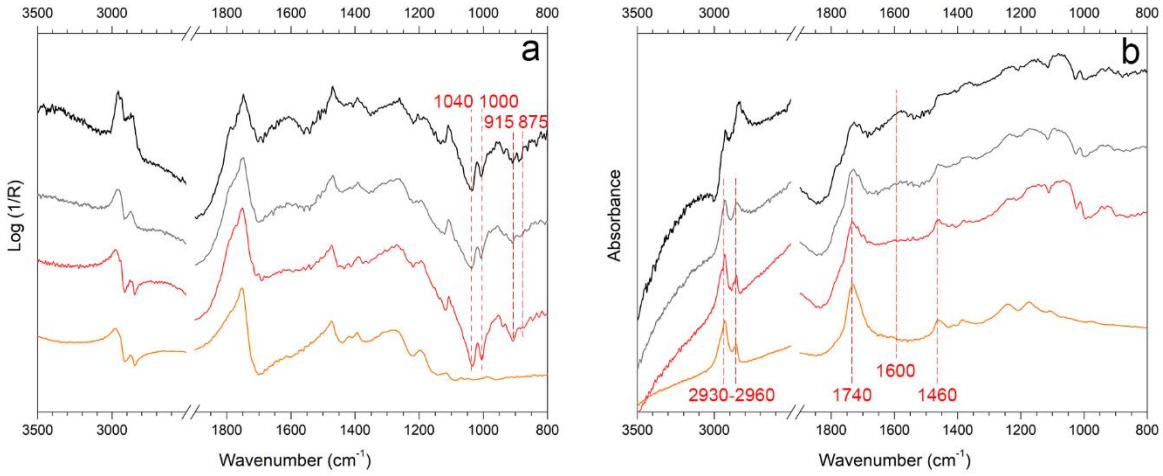

Figure 57. ER-FTIR spectra in (a) pseudo-absorbance and (b) after Kramers-Kronig transform of soiled-EAM (black), area cleaned with Agar_3 (grey), KGB_3 (red) and, a reference of WM (orange). The marker bands selected for identifying the soiling mixture are reported.

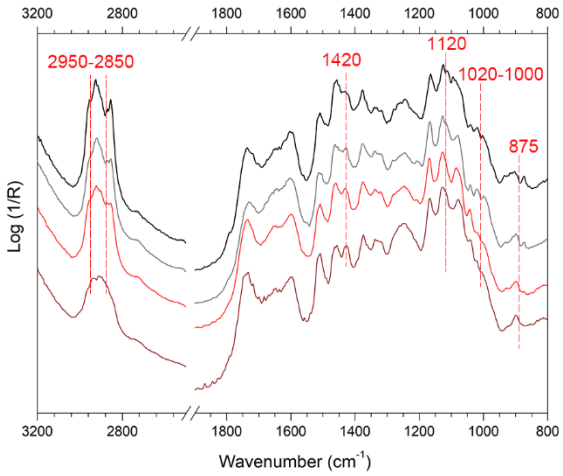

Figure 58. ER-FTIR spectra in pseudo-absorbance acquired on soiled-EAM (black), area cleaned with Agar_3 (grey), KGB_3 (red), and a reference of EAM (brown). The marker bands selected for identifying the soiling mixture are reported.

After cleaning with KGB gel on the sweat-WM, no matter the repeated gel application, the disappearance of sweat-related bands was clearly detected (Figure 59). Conversely, the detection of representative sweat peaks on the sweat-EAM was difficult. As previously mentioned for the stereomicroscope and XRF results, it was assumed that the sweat deposit

might have been absorbed by the hydrophilic surface of the EAM, making its detection difficult.

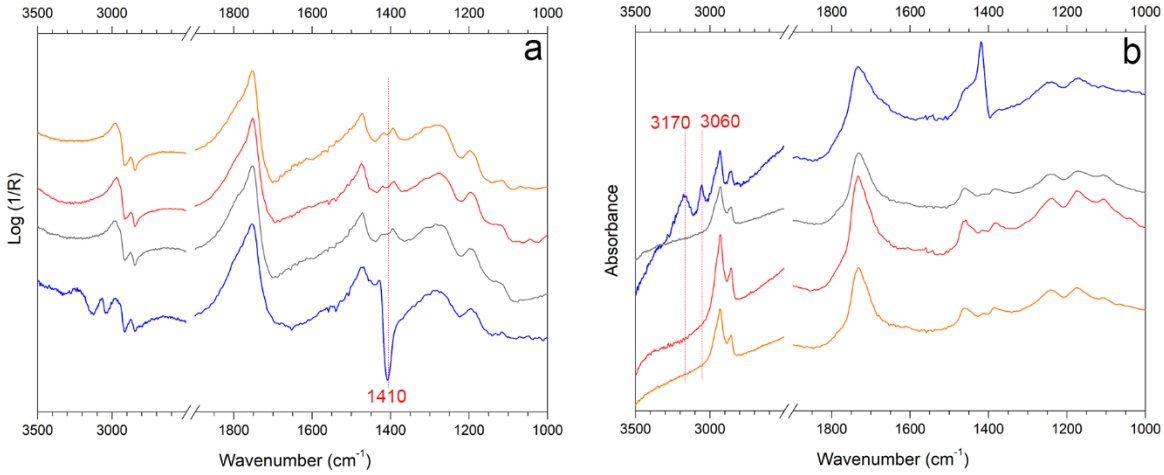

Figure 59. Reflection FTIR spectra in (a) pseudo-absorbance and (b) after Kramers-Kronig transform of WM (orange) and sweat-WM (blue) cleaned with Agar_3 (grey) and KGB_3 (red). The marker bands selected for identifying synthetic sweat components are reported.

4.3. Konjac borax-PVA-PVP

This gel was developed with the intention of forming a hydrogel that is somewhat more pliant than the konjac-sodium tetraborate decahydrate (borax) gel (KGB). As documented in other research, the design of a hydrogel to achieve high elasticity, high strength and long durability can be performed through double-network (DN) hydrogels (Huang et al. 2017; Ai et al. 2021) and interpenetrating polymer network (IPN) hydrogels (Chen et al. 2019; Mastrangelo et al. 2020). These methods can improve previously brittle hydrogels for high tensile strength, extensibility, and toughness.

For this purpose, we have chosen polyvinyl alcohol (PVA), a chemical representative of self-healing and biocompatible properties. PVA contains many hydroxyl groups, providing excellent water retention (Li et al. 2015; Al-Emam et al. 2019, 2020; Rosciardi et al. 2022). PVA hydrogels are prepared with a physical cross-linking network through hydrogen bonding and reversible *diol*-borate ester. However, studies have reported that PVA-sodium tetraborate decahydrate gels have limitations in dimensional stability and low mechanical strength (Al-Emam et al. 2019, 2020; Ai et al. 2021; Stagno et al. 2021). To overcome this problem, we

added polyvinylpyrrolidone (PVP) and sodium tetraborate decahydrate to the PVA system to strengthen the network structure by forming the interchain hydrogen bond. Due to its chemical structure containing vinyl and vinylpyrrolidone groups, PVP is known for its water-solubility, hydrophilicity, water-absorbing capacity, and material featuring as biocompatible and non-toxic (Huang et al. 2017; Ni et al. 2019).

Our hypothesis centers on interpenetrating polymer network (IPN) by combining konjac, PVA, PVP polymers and sodium tetraborate decahydrate (borax). Also, the physically crosslinked hydrogel was further formed using the freeze-thawing method to tailor the mechanical properties for the cleaning application. The expected crosslinked hydrogel is depicted in Figure 60.

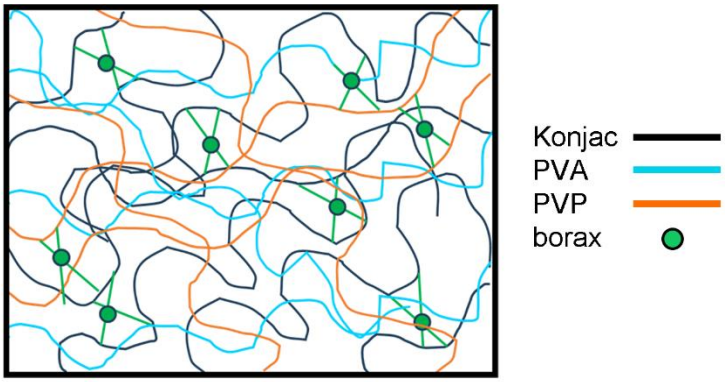

Figure 60. Expected reaction between konjac glucomannan, polyvinyl alcohol (PVA), polyvinylpyrrolidone (PVP), and sodium tetraborate decahydrate (borax).

4.3.1. Gel Preparation

The steps of the preparation of KGPPB gel are presented in Figure 61. 0.2 g of KG and 0.1 g of PVP were mixed and dissolved in 10 ml of deionized water at 50 °C to prepare the KG-PVP solution. Also, the PVA solution was prepared by 0.3g of PVA in 2 ml of deionized water at 90 °C. After on KG-PVP, the PVA solution was mixed together at 90 °C with constant magnetic stir (Molar ratio KG: PVA: PVP = 1: 1: 0.1) at 90 ± 10 °C for 30 minutes. Afterwards, 0.05g of sodium tetraborate decahydrate (borax) was added, and the gel mixture was mixed very well to react with the borax with the remaining hydroxyl groups of konjac. The prepared KGPPB gel was taken out, cooled at room temperature, and placed in the mould. Finally, the KGPPB gel was fabricated by freezing-thawing (FT), keeping the mould for at -

18 °C 16 h (freezing cycle) and for 8 h at ambient temperature (thawing cycle). The FT cycle was repeated up to three cycles (FT0, FT1, FT2, FT3).

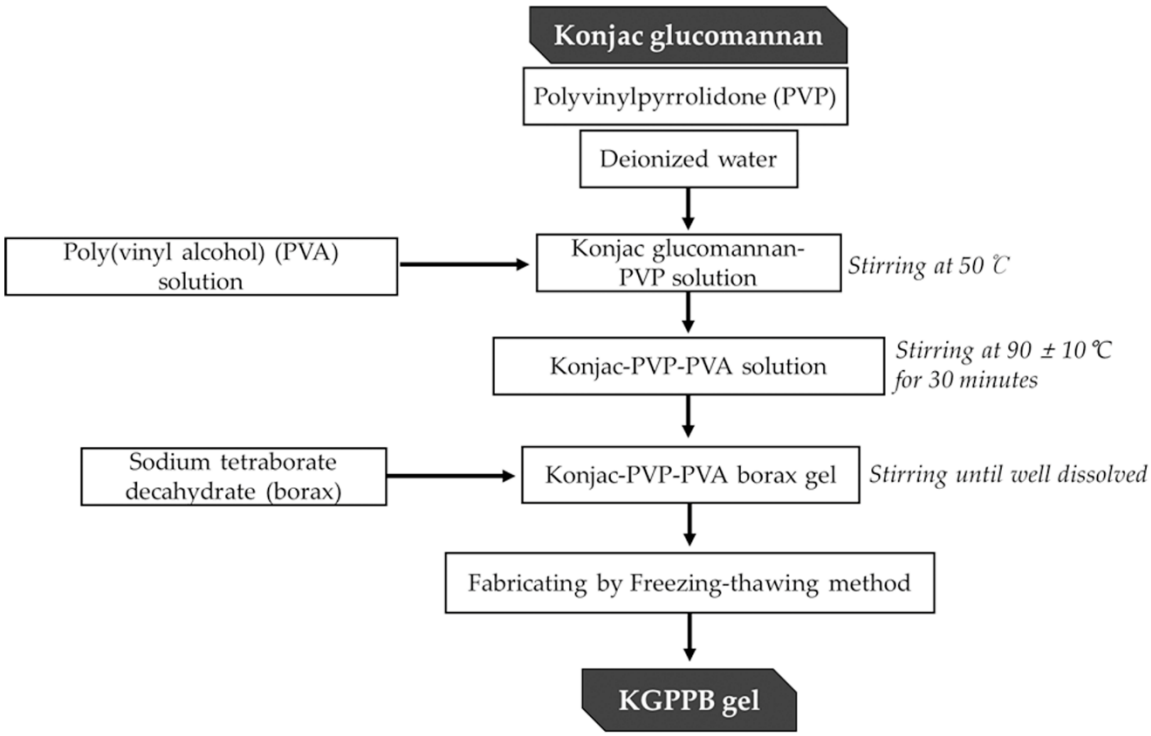

Figure 61. A schematic diagram of steps involved in preparing KGPPB gel.

4.3.2. Gel Characterization

By FTIR-ATR, after cross-linking, the hydrogen bonding influences of PVP and PVA, assigned to C-O and O-H bending, were attributed to 1095 cm^{-1} (Figure 62a). Notably, the C-N stretching vibrations of the PVP ring of pyrrolidone were observed at 1280-1305 cm^{-1} (Erizal et al. 2013; Subramanian et al. 2014; Huang et al. 2017). In the 1500-1200 cm^{-1} range, a band appeared at 1420 cm^{-1}, which could be attributed to the asymmetric relaxation signal of the B-O-C stretching after cross-linking of hydroxyl groups and borate ions (Spoljaric et al. 2014; Song et al. 2019b). The network structure of the KGPPB hydrogel observed by SEM is presented in Figure 62b. KGPPB F-T0, which is without an F-T cycle, appeared as a compact and non-uniform network structure. As the freeze-thaw (F-T) cycles increased, it was evident that the removal of water from the hydrogel and the number of distribution of smaller pores increased (Huang et al. 2017).

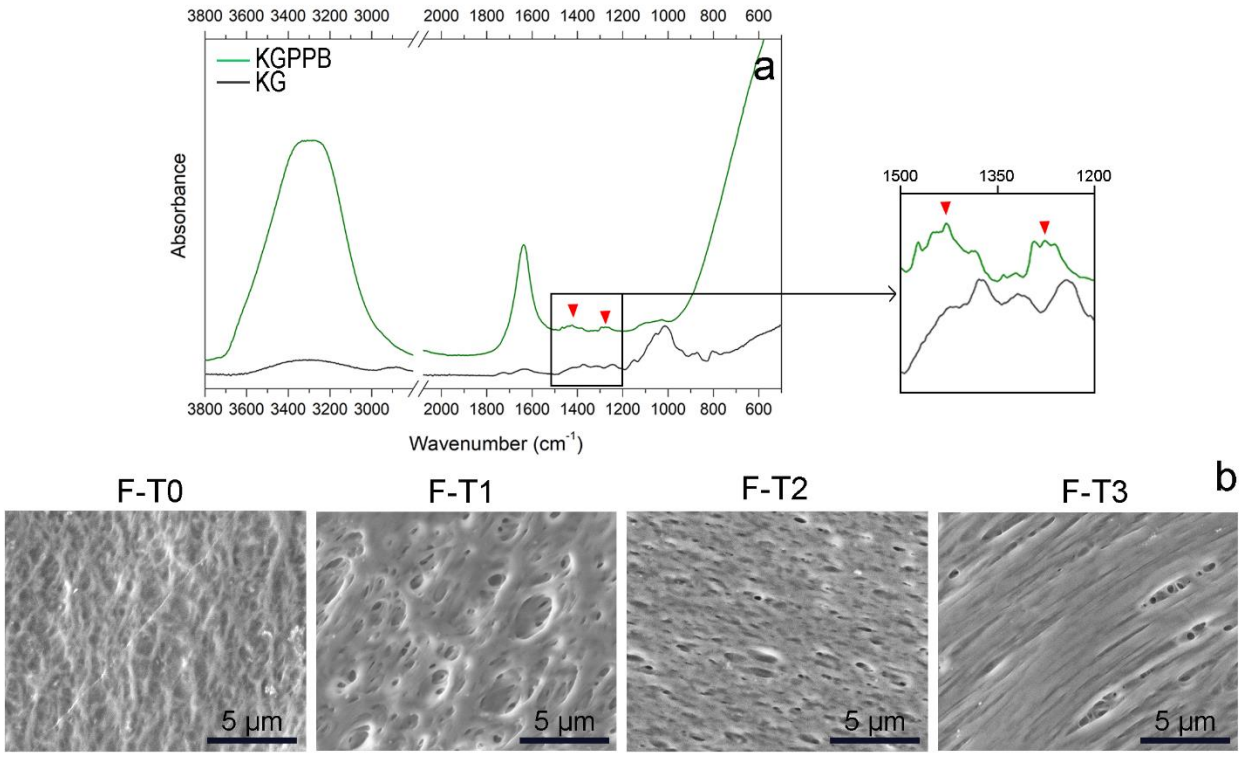

Figure 62. FTIR spectrum of the konjac glucomannan-polyvinyl alcohol- polyvinylpyrrolidone-borax formulated gel (KGPPB) and pure konjac glucomannan (KG) (a). Markers for interactions of hydroxyl groups and borate ions and C-N stretching of PVP (triangle) are displayed. SEM images of KGPPB gels of each freezing-thawing (F-T) cycle, F-T0, F-T1, F-T2, and F-T3 are acquired in a high vacuum with secondary electrons (b).

The mechanical properties of the gels were measured by comparing the KGB with the KGPPB gel after different cycles (F-T0, F-T1, F-T2 and F-T3) in order to understand the influence of freezing-thawing on the mechanical strength and resilience of the gel (Figure 63). For all KGPPB gels, both hardness and Young's modulus were lower than those of the KGB gel (Figure 63). By repeating the F-T cycle, the hardness of the KGPPB gel increased (Figure 63a). When the F-T cyclic process is performed at freezing temperature (F), the ice crystal formation process disrupts the physically cross-linked polymer chains and rearranges them into higher cross-linking densities (Islam and Oyen 2022). This may have increased the hardness of KGPPB. The Young's modulus value is significantly lower than that of the KGB gel, probably due to the high elasticity of the PVA polymer (Figure 63b). However, when comparing F-T0 and F-T3, the result showed a slight increase in the F-T3 value, which means

that it became a tighter hydrogel due to the increase in network density while still keeping its elasticity high, as it still has a lower value than the KGB gel. Also, from the stress-strain curve, strain deformation appears to increase steadily as the F-T cycle increases, whereas, at F-T3, strain arrest is reached, showing both elastic and plastic deformation characteristics (Figure 63c).

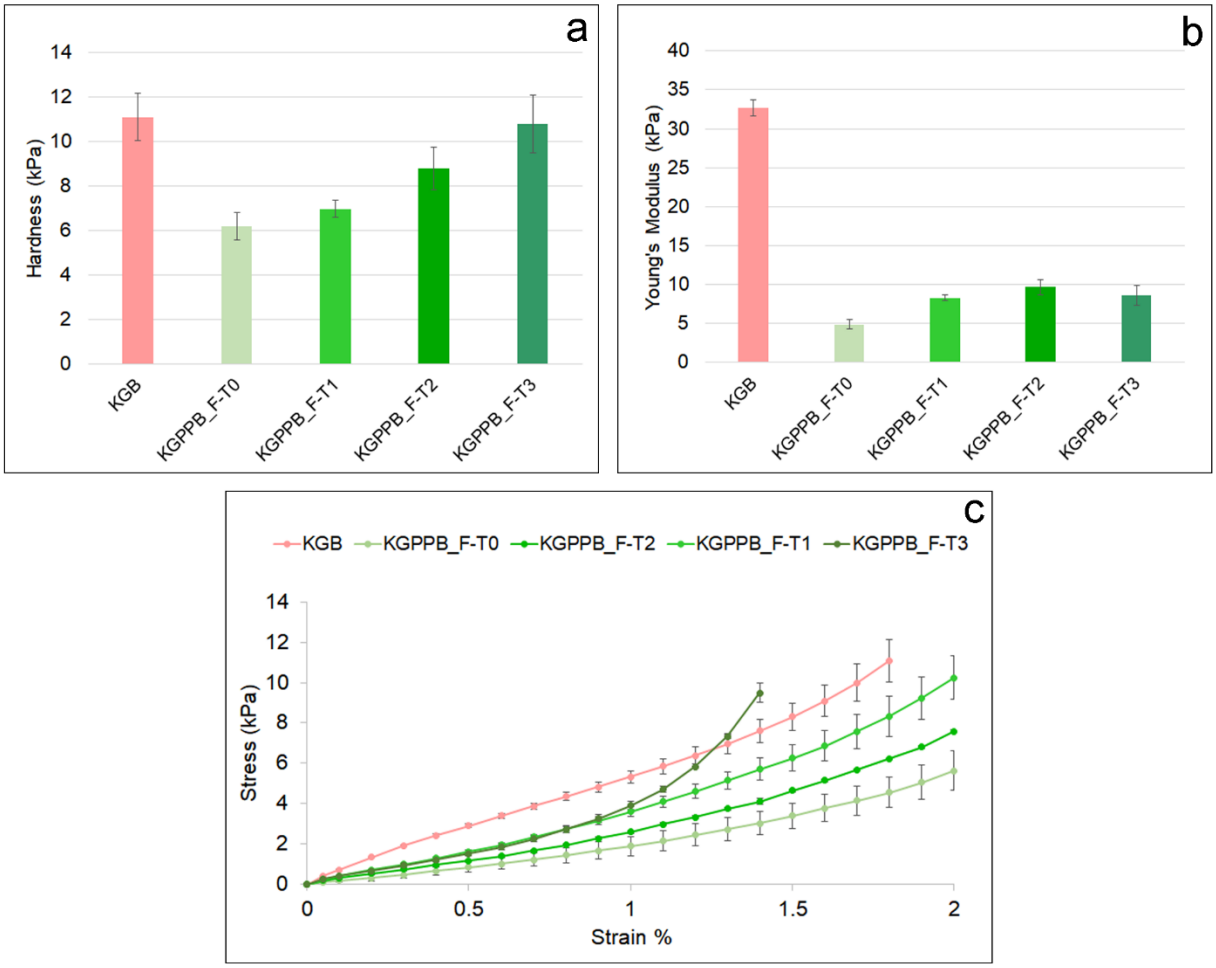

Figure 63 Mechanical properties determined by compressive test (mean value ± s.d.; n = 5): hardness (kPa) (a), Young's Modulus (kPa) (b), and stress-strain curve (c).

The moisture properties of KGPPB gels with F-T cycle processing (KGPPB_F-T1 and KGPPB_F-T3) with the conventional agar gel are summarized in Table 14.

The newly formulated KGPPB gels showed high hydrophilicity and water loading compared to the KGB gel, possibly due to the increased hydrogen bonding due to the introduction of

PVA. It is also worth noting that water release was lower than agar and KGB gel despite the high water-loading capacity.

Table 14. Moisture properties of KGPPB gels (KGPPB_F-T1, KGPPB_F-T3), KGB and agar: equilibrium moisture content (EWC), swelling capacity (SC), and water release (WR). Mean values and standard deviations were calculated on five iterations

Gel	EWC (%)	SC (%)	WR (mg/cm^2)
KGPPB_F-T1	93.7 (± 0.2)	$(1.5 \pm 0.1) \times 10^3$	13.8 (± 2.0)
KGPPB_F-T3	96.3 (± 1.0)	$(2.7 \pm 0.6) \times 10^3$	14.8 (± 2.0)
KGB	82.9 (± 2.7)	$(1.8 \pm 0.4) \times 10^2$	15.6 (± 1.5)
Agar	95.6 (± 0.3)	$(2.2 \pm 0.2) \times 10^3$	29.3 (± 2.5)

Overall, the KGPPB gel appeared remarkably elastic, with a high loading capacity and retention capable of controlling liquid diffusion. In addition, the high pliability could lead to a problem of gel residue when cleaning applications on uneven surfaces, but we employed an F-T cycle formation to improve this point and increase the hardness of this gel while maintaining the elastic property. In this regard, KGPPB_F-T3 was shown to be the most suitable condition for the application.

4.4. Konjac-Polyphenols

This section was carried out in collaboration with the University of Milan Bicocca. The target of forming this gel was to develop a mechanically improved gel with antioxidant properties. Since a hydrogel, which contains a high number of water molecules, may be susceptible to fungal contamination (Mohamed and Al-mehbad 2013; Kopka et al. 2023), and since a conservation intervention often takes a considerable amount of time, a gel cleaning system that can have a considerably long shelf life is required. But at the same time, as this cleaning

system will be used by conservators, a biocompatible and environmentally friendly system is needed.

For this purpose, we experimented with two different polyphenols derived from Softwood Kraft Lignin (SKL) and *Vitis vinifera* (Vv) in an attempt to find an effective cross-linking agent, which improves the functional and mechanical properties of konjac. Softwood Kraft Lignin (SKL) is a type of lignin derived from softwood, widely produced from paper and pulp industry. SKL consists of complex phenolic structures and is known to have characteristics of being low-cost, antioxidant, antimicrobial, and UV protection (Gierer 1980; Crestini et al. 2017). *Vitis vinifera* is a grapevine that contains phenolic molecules and is highly soluble in water. Additionally, it provides antioxidant and UV protection. (Pérez-Navarro et al. 2019; Watrelot and Norton 2020; Zhen et al. 2021). Both SKL and Vv are bio-based, environmentally friendly, and sustainable raw materials, which have been applied to food, biomass, drug delivery, etc. (Nazzaro et al. 2022; Villanueva et al. 2023; Rathod et al. 2023).

Polyphenols are a type of compound with a phenyl chemical structure combined with two or more phenolic groups. We have designed a process for self-polymerization of polyphenols by functionalizing them with epichlorohydrin (ECH). This process involves the binding of the epoxy ring to the deprotonated oxygen of the polyphenol (Figure 64a), resulting in the opening of the ring and subsequent binding to other polyphenol molecules (Figure 64b). This self-polymerization is advantageous for polyphenols because they have a smaller molecular size, which can lead to residue concerns. This formulation was performed on only 25% and 50% of the OH phenolic group content of each SKL (SKL25 and SKL50) and Vv (Vv25 and Vv50) to retain some of the phenol properties. Afterward, the partially etherified polyphenols (SKL25, SKL50, Vv25, and Vv50) were chemically crosslinked with konjac. In addition to forming a desired gel consistency, borax was added for the interchain crosslinking. Figure 64 presents the expected formulation of SKL with ECH (Figure 64a) and konjac hydrogel with partially etherified polyphenols (Figure 64b).

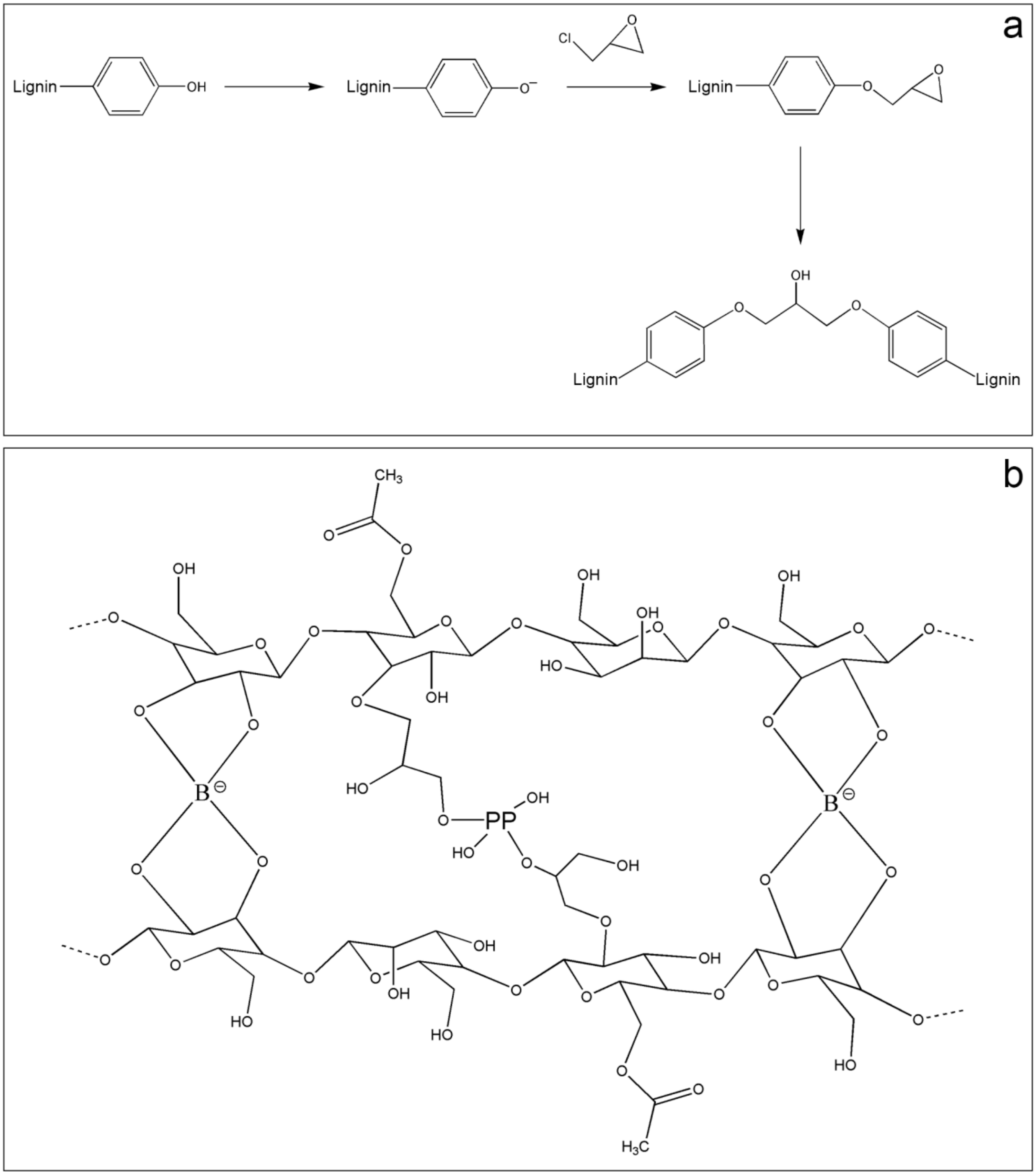

Figure 64. Expected functionalization reaction between Soft Kraft Lignin (SKL) and epichlorohydrin (ECH) (a), and crosslink of konjac with partially etherified polyphenols and borate ions (B) (b).

4.4.1. Gel Preparation

As described in section 4.4., the polyphenols (PP) hydroxyl groups were etherified by linkages with epichlorohydrin (ECH). SKL and Vv functionalized with ECH (25% and 50% of the phenolic groups transformed into ether groups) were prepared at the University of Milano Bicocca. The corresponding materials were named SKL25, SKL50, Vv25 and Vv50. Subsequently, a konjac hydrogel was prepared with a weight ratio of konjac to the partially etherified polyphenols (SKL25, SKL50, Vv25 and Vv50) of 95:5 and 98:2 in 20 ml water. The partially etherified polyphenols were dispersed in Milli-Q water (0.1% and 0.04% w/v) and the dispersion was sonicated for 10 minutes. Afterwards, konjac (1.9% and 1.96% w/v) was added and stirred with a magnetic stirrer at 350 rpm. As a final step, 0.2 g borax was added and stirred until a uniform hydrogel was formed. The hydrogels were left in a water bath at 50 °C for 45 minutes and then stored at ~4 °C temperature. Details of the formulation composition with raw materials and chemical substances are in Tables 15 and Table 16. All these preparation steps are described in Figure 65.

Table 15. Composition of the formulated konjac (KG) gel with SKL and partially etherified polyphenols (SKL25 and SKL50), and borax (B)

Acronym	Water (mL)	Konjac (g)	Borax (g)	SKL(g)	SKL25 (g)	SKL50 (g)
KGB-SKL	20	0.392	0.2	0.02	/	/
KGB-SKL25	20	0.392	0.2	/	0.02	/
KGB-SKL50	20	0.392	0.2	/	/	0.02

Table 16. Composition of the formulated konjac (KG) gel with Vv and partially etherified polyphenols (Vv25 and Vv50), and borax (B)

Acronym	Water (mL)	Konjac (g)	Borax (g)	Vv (g)	Vv25 (g)	Vv50 (g)
KGB-Vv	20	0.392	0.2	0.02	/	/
KGB-Vv25	20	0.392	0.2	/	0.02	/
KGB-Vv50	20	0.392	0.2	/	/	0.02

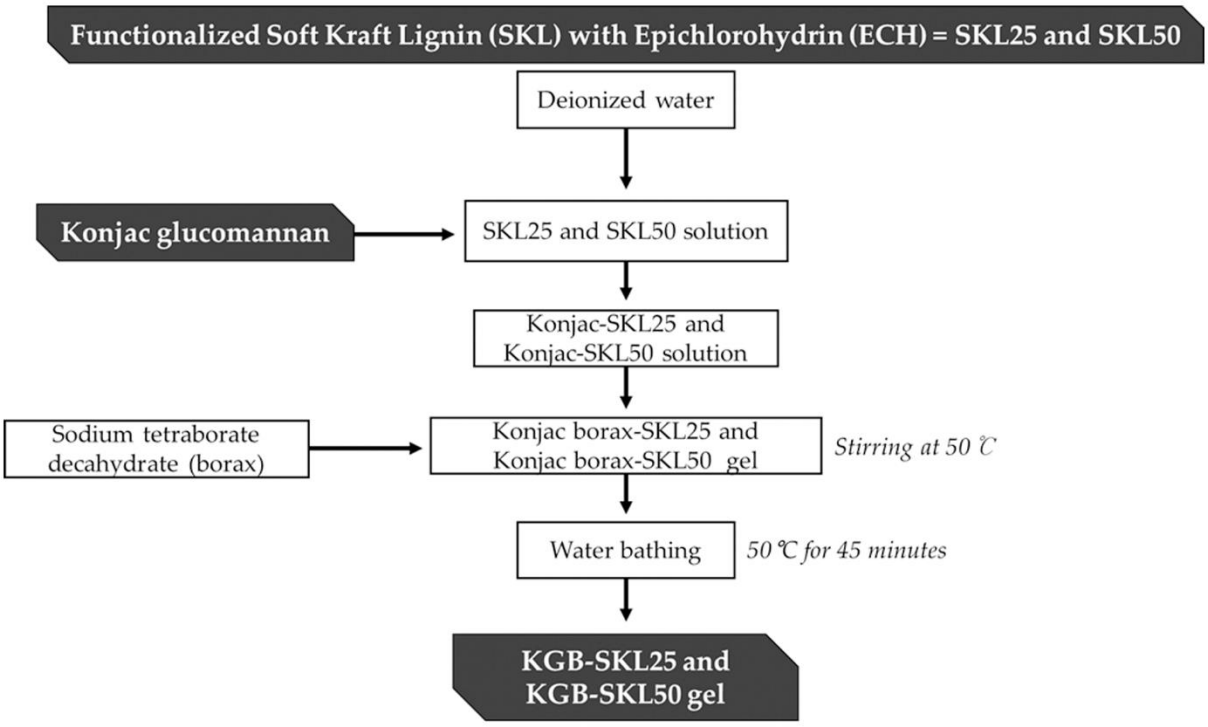

Figure 65. A schematic diagram of steps involved in preparing KGB-SKL25 and KGB-SKL50 gel. The same preparation steps were carried out on KGB-Vv25 and KGB-Vv50.

4.4.2. Gel Characterization

Analysis were performed to confirm the polyphenol etherification at the University of Milan Bicocca. The description of morphological characteristics and moisture properties of the formulated hydrogel is first introduced in the konjac hydrogel with SKL and then with Vv.

The SEM image provided information on the three-dimensional heterogeneous and granular structure of KGB-SKL50 complex aggregation (Figure 66). The average diameter of the interconnected pores was 15 μm, which is small compared to the ~200 μm of the KGB gel presented in Figure 48. This porous feature also explains the moisture properties, showing a relatively high swelling and solvent retention capacity compared to the KGB gel (Table 17). This could be due to the capillary force: numerous small pores (in this case, the KGB-SKL50 gel) allow water to be effectively trapped due to the capillary force, resulting in a higher water retention and swelling capacity.

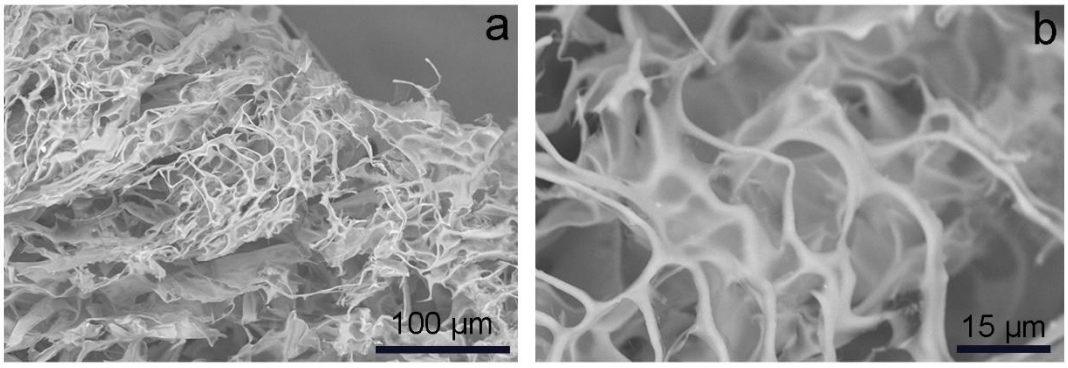

Figure 66. The SEM image of KGB-SKL50 was acquired in standard secondary electrons (a and b).

Table 17. Moisture properties of KGB-SKL, -SKL25, and -SKL50 gels, KGB, and agar: equilibrium moisture content (EWC) and swelling capacity (SC). Mean values and standard deviations were calculated on four iterations

Classification	EWC (%)	SC (%)
KGB-SKL	94.7 (± 0.7)	1.8 (± 0.1) × 10^3
KGB-SKL25	95.2 (± 0.4)	2.0 (± 0.1) × 10^3
KGB-SKL50	94.9 (± 0.1)	1.9 (± 0.0) × 10^3
Agar	95.6 (± 0.2)	2.2 (± 0.1) × 10^3
KGB	94.4 (± 0.4)	1.7 (± 0.1) × 10^3

Meanwhile, the KGB-Vv50 was shown as an irregular surface with inhomogeneous porous structures (Figure 67). The enlarged image in Figure 67b provided information on the porous structure as a slightly irregular texture rather than a deep porous structure when comparing the image with the KGB-SKL50 gel in Figure 65. Likewise, the moisture properties did not provide a significantly different value compared to the KGB gel (Table 18).

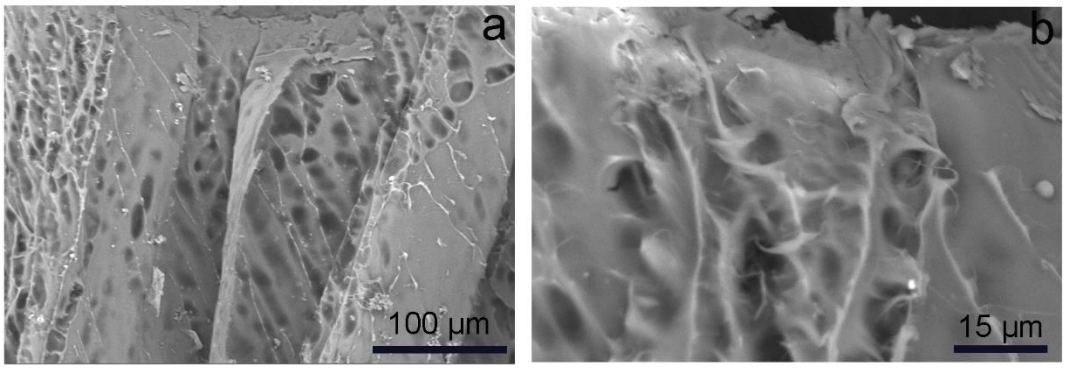

Figure 67. SEM image of KGB-Vv50 acquired in standard secondary electrons (a and b).

Table 18. Moisture properties of KGB-Vv, -Vv25, and -SVv50 gels, KGB, and agar: equilibrium moisture content (EWC) and swelling capacity (SC). Mean values and standard deviations were calculated on four iterations.

Classification	EWC (%)	SC (%)
KGB-Vv	94.2 (± 0.9)	1.6 (± 0.2) × 10^3
KGB-Vv25	95.5 (± 0.2)	2.1 (± 0.0) × 10^3
KGB-Vv50	94.4 (± 0.3)	1.7 (± 0.6) × 10^3
Agar	95.6 (± 0.2)	2.2 (± 0.1) × 10^3
KGB	94.4 (± 0.4)	1.7 (± 0.1) × 10^3

Overall, SKL and Vv were successfully formulated with Konjac. The SEM image allowed us to observe the 3D structure of the gel and the alignment result with the moisture properties. However, to achieve our goal, we plan to further incorporate the characterization of gel properties, such as mechanical properties, and tests on antioxidant and UV activity. Furthermore, both SKL and partially etherified Vv polyphenols showed promising applicability. Therefore, we decided to proceed with a pilot application study in the next section 4.4.3. Due to the similar characteristics of the gels, we decided to apply only one gel (KGB-Vv25) for the pilot application study.

4.4.3. Cleaning Application and Evaluation of the Efficacy

The KGB-Vv25 was applied to soiled and sweat-dispersed WM and EAM (detailed preparation methods are described in sections 2.2.1. and 2.2.2.). To be used for cleaning, the KGB-Vv25s were separately immersed in the 2% v/v solution of ecosurf^{TM} EH-9 for 3 hours to make them ready for use. The cleaning was performed for a single application in 5 minutes and the dried swab was rolled over the surface once to remove dissolved contaminants.

4.4.3.1. XRF

A description of the elemental composition of WM, EAM, synthetic soil, and sweat is given in Section 3.2.2.3.

After cleaning the soiled-WM and soiled-EAM with the KGB-Vv25 gel, the calcium counts were reduced the most, which could indicate the removal of the cement and kaolin components of the soiling mixture (Figure 68a). Comparing the result counts of both soiled-EAM and soiled-WM, it was observed that the reduction of the elemental counts was relatively greater in the cleaned areas of the soiled-EAM (Figure 68b). Furthermore, it is worth noting that, in general, cleaning with agar showed higher counts of Ca, K, and Fe on both soiled-WM and soiled-EAM. This could be due to the fact that KGB-Vv25 showed a softer consistency than agar gel.

The cleaning application on the sweat-WM with KGB-Vv25 and agar gel showed significant removal, which could be due to the hydrophobic surface of the WM, which eased the removal (see detailed explanation in section 3.2.2.1. and 3.2.2.2) (Table 19). On the other hand, after sweat-EAM cleaning, the KGB-Vv25 did not give significant removal, whereas the agar gel showed lower Cl counts.

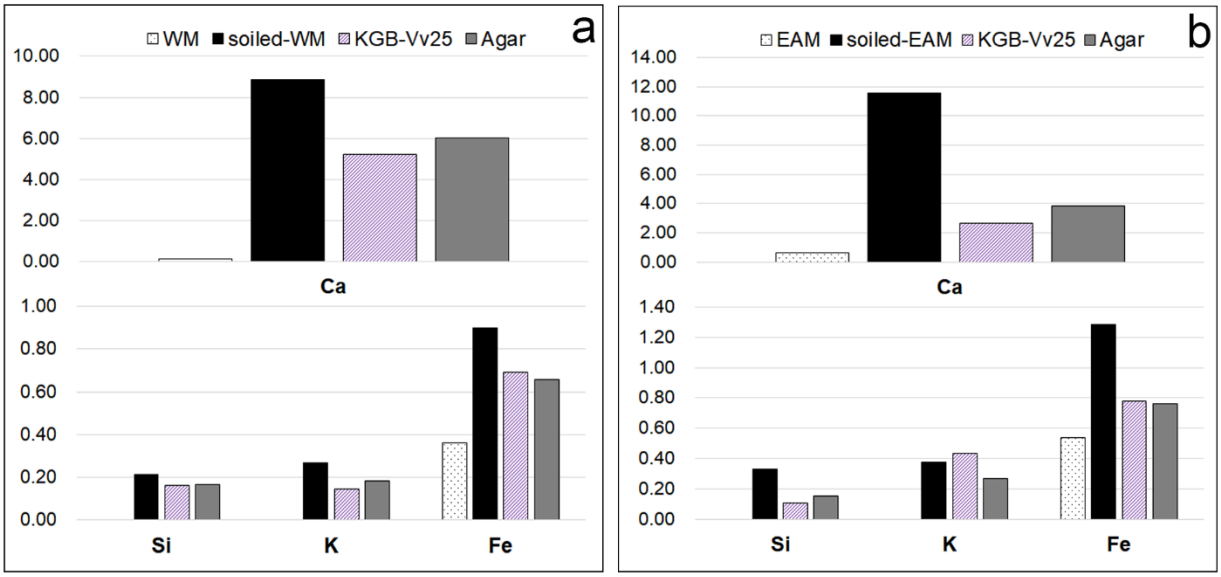

Figure 68. Normalized Ca, Si, K, and Fe counts were detected on (a) WM and (b) EAM. Different bars correspond to plain (WM and EAM) and with soiling deposits treated mock-ups (soiled-WM and soiled-EAM) and after applications of KGB-Vv25 and agar gel. XRF values correspond to the net area counts of the Kα peak of each element normalized to time and the mean of the entire dataset of Rh-Kα peak net area counts, with the related standard deviation.

Table 19. Normalized Cl (Kα) counts on sweat-WM and sweat-EAM, before (control) and after cleaning applications by KGB-Vv25 and agar gel

Mock-Up	Control	KGB-Vv25	Agar
Sweat-WM	10.42	0.47	0.43
Sweat-EAM	4.29	4.04	2.90

4.4.3.2. ER-FTIR

ER-FTIR was performed with XRF analysis to monitor the change in interface characteristics after cleaning. The significant band of soiled and sweat-dispersed WM and EAM was studied previously in section 3.2.2.4. Therefore, this section will discuss the results obtained after cleaning with the KGB-Vv25 gel. The bands attributed to kaolin at 1040, 1000, and 915 cm^{-1} and calcium carbonate at 875 cm^{-1} decreased in intensity, both on the soiled WM and soiled EAM surfaces (Figures 69 and 70). At the same time, the bands contributing to the layer underneath were more recognizable, in this case, the oil-colophony surface for WM and the wood surface for EAM.

The disappearance of sweat-related bands was visibly detected after cleaning the sweat-WM with KGB-Vv25 and agar gel (Figure 70). The results are not presented for sweat-EAM, as it was difficult to detect the difference between before and after cleaning, as described in sections 3.2.2.4. and 4.2.2.4.

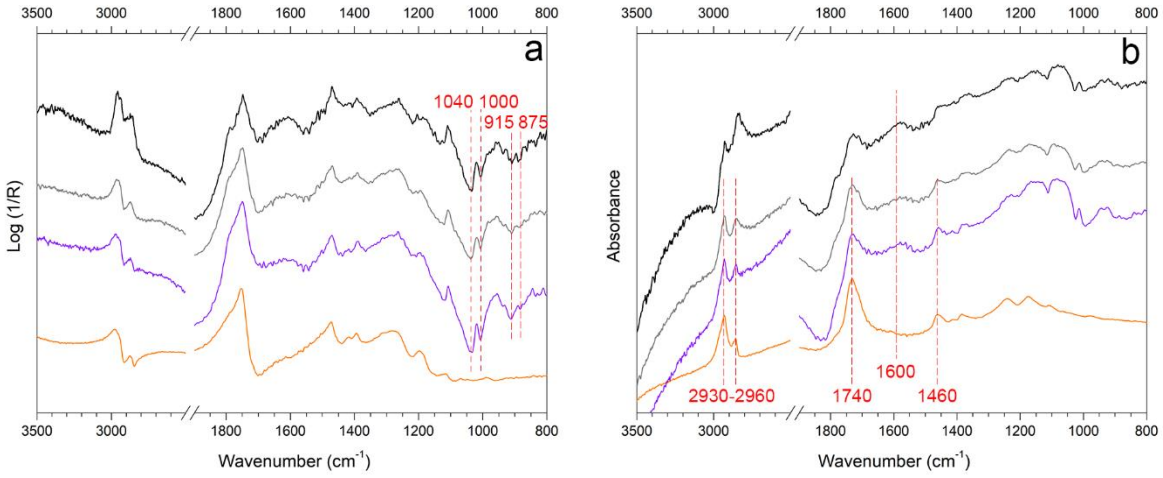

Figure 69. ER-FTIR spectra in (a) pseudo-absorbance and (b) after Kramers-Kronig transform of soiled-WM (black), area cleaned with KGB-Vv25 (purple), agar (grey), and a reference of WM (orange). The marker bands selected for identifying the soiling mixture are reported.

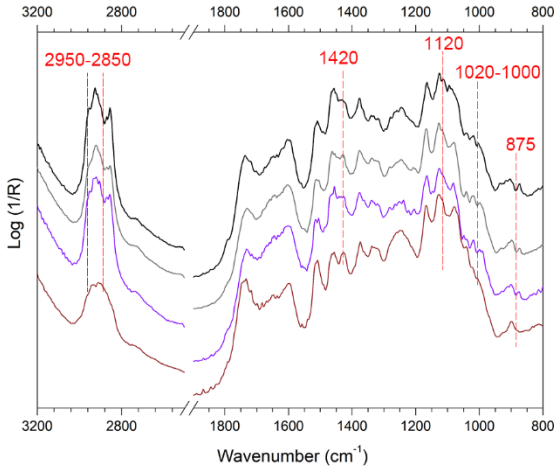

Figure 70. ER-FTIR spectra in pseudo-absorbance acquired on soiled-EAM (black), area cleaned with KGB-Vv25 (purple), agar (grey), and a reference of EAM (brown). The marker bands selected for identifying the soiling mixture are reported.

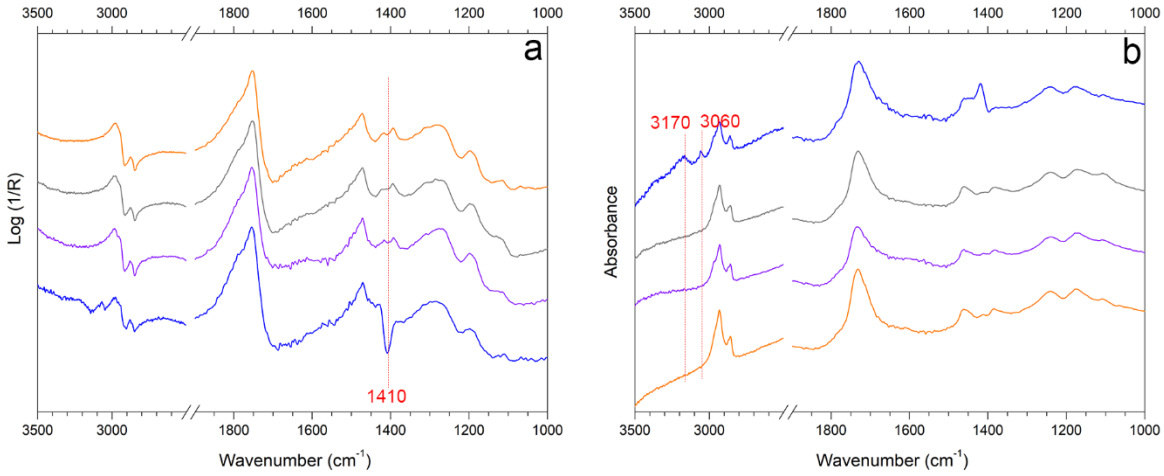

Figure 71. Reflection FTIR spectra in (a) pseudo-absorbance and (b) after Kramers-Kronig transform of WM (orange) and sweat-WM (blue) cleaned with KGB-Vv25 (purple) and agar (grey). The marker bands selected for identifying synthetic sweat components are reported.

4.5. Evaluation and Optimisation of Konjac-based Gels

The konjac-based gels studied in this study (Sections 4.1., 4.2. and 4.4.) were evaluated using the rating scale described in Section 2.5. Subsequently, the characteristics of the konjac-based gels and the cleaning results of each gel after cleaning soiled and sweat mockups were evaluated (Section 4.3. KGPPB gel is excluded from this study because it was not used to clean these mockups), as presented in Figure 72.

The KGB and KGB-Vv25 gels appeared to have a soft and elastic consistency. Notably, cross-linking with partially self-polymerized polyphenols (KGB-Vv) created small pores, causing the gel to absorb a lot of water by capillary action, with a 10% increase in water uptake compared to the KGB gel; in this regard, KGB-Vv25 showed lower water retentivity than KGB.

After cleaning soiled mockups (Figure 72a,b), KGB and KGB-Vv25 gels showed effective cleaning efficacy on both WM and EAM surfaces. In particular, KGB showed high efficacy, which could be related to the fact that KGB gel has a flexible consistency and can easily clean soil particles on irregular surfaces. After cleaning the sweat mockups (Figure 66c,d), no difference was found in the cleaning efficacy of the gel between the agar gel, KGB or KGB-Vv25, but better removal was shown when cleaning the hydrophobic surface of the sweat-WM than on the hydrophilic surface of the sweat-EAM.

Overall, KGB gel showed a wider star diagram than agar and KGB-Vv25, particularly representing the effectiveness of removing soil particles.

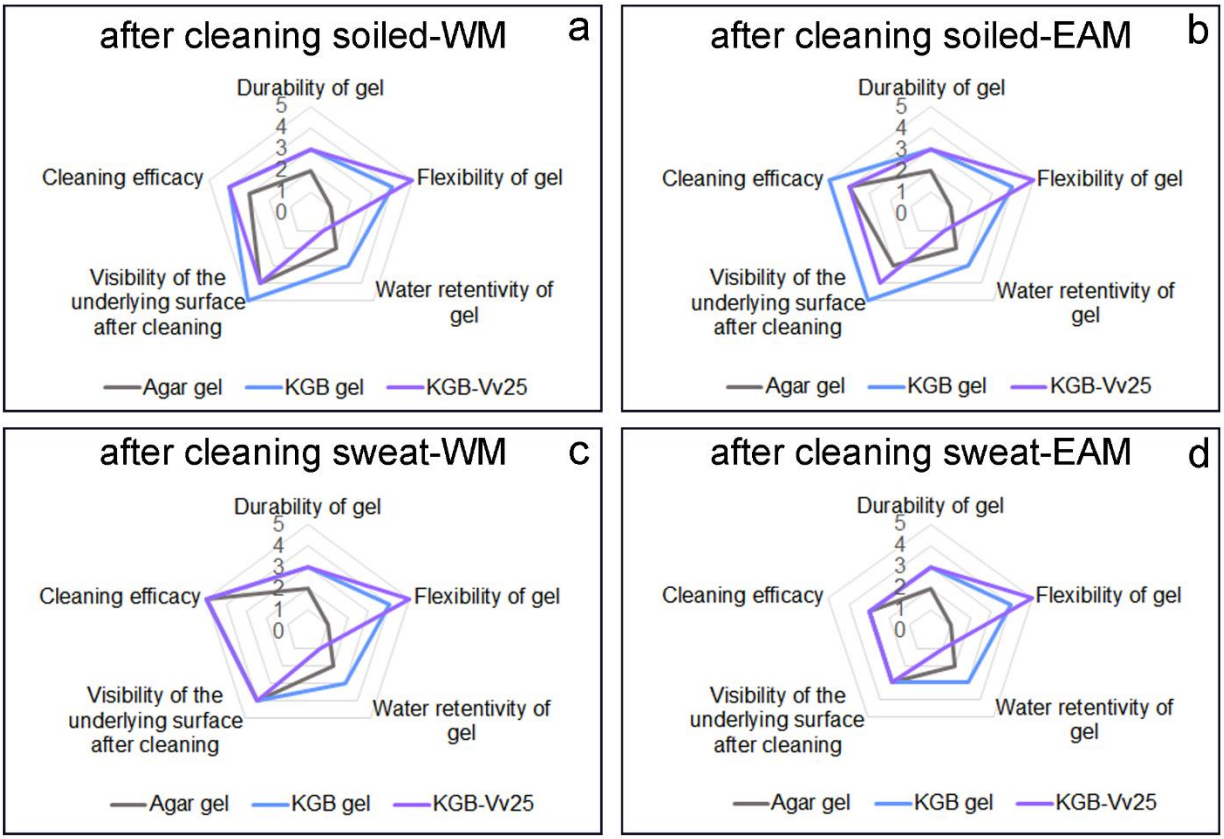

Figure 72. Star diagrams comparing the results of agar, KGB and KGB-Vv25 gel characteristics and cleaning evaluation after cleaning soiled-WM (a) and soiled-EAM (b), sweat-WM (c), and sweat-EAM (d).

Chapter 5.

General Conclusion and Further Perspectives

The research for this thesis focuses not only on the formulation and development of the gel but also on analytical approaches to both Western and East Asian mock-ups in order to understand the cleaning effectiveness on differently featured surfaces on which the colloidal gel system has never been tested before (e.g., on Nakdong technique treated surface).

The gel formulations are based on alginate and konjac glucomannan polysaccharides. These materials were chosen due to their natural origin, bio-compatibility, and long history of use in traditional medicine and food. However, despite their promising properties, they have not been widely explored for conservation purposes, particularly for cleaning.

During the research, sodium alginate showed the typical cross-linking character. Therefore, it was necessary to improve the methodology by testing different cations and preparation methods. The study started with the most widely used cross-linking formulation of alginate in the medical, food and pharmaceutical fields, namely calcium alginate (CA) prepared in film form. Based on this CA gel, we successfully developed the alginate gel functionalized with 3-glycidoxypropyltrimethoxysilane and ionically cross-linked with calcium ions (CA-GPTMS) and the alginate functionalized with pentaerythritol tris[3-(1-aziridinyl)propionate] and ionically cross-linked with calcium ions (CA-XAMA7). In the end, we cross-linked this alginate into a physically cross-linked gel and a chemically cross-linked gel, greatly improving the retentivity of the gel, which could underline its use on water-sensitive surfaces such as wood and paper.

As for konjac, it is a polysaccharide that has the ability to absorb a large amount of water and generally has a soft consistency. For this reason, improvement studies have been conducted with different chemical components together with konjac polymers, including borax, polyvinyl alcohol (PVA), polyvinylpyrrolidone (PVP) and various polyphenols, to improve gel characteristics such as mechanical and moisture properties. The konjac was first formulated with borax by interconnecting the hydrogen bonds, and with regard to PVA and PVP, an attempt was made to form an interpenetrating polymer network (IPN), which combines and makes the networks coexist. For polyphenolic agents containing abundant phenolic hydroxyls, we functionalized with epichlorohydrin (ECH) and chemically cross-linked with konjac polymers. Each of KGB (konjac-borax), KGPPB (konjac-PVA-PVP-borax), KG-SKL (konjac-soft kraft lignin polyphenol) and KG-Vv (konjac-*vitis vinifera* polyphenol) showed distinctive behavior and a strong correlation with mechanical and moisture properties.

Our application approach was to analyze the effectiveness of cleaning by using a non-invasive method. Thanks to comprehensive analytical techniques, even though the mock-ups and case studies presented surfaces with different characteristics, such as hydrophilic surface (EAM treated with the nakdong technique), hydrophobic surface (WM varnished with oil and colophony), highly swelling surface (wood with glue and contrabass fragments with old glue), the overall technique provided us with high confidence in providing cleaning efficacy.

Ultimately, the innovative gel formulation based on sodium alginate and konjac polysaccharides, CA-GPTMS, CA-XAMA7 and KGPPB made it possible to control the solvent release on the wood surface and achieve gradual swelling on the wooden surface. At the same time, due to the different forms, such as alginate-based gel in film form and konjac-based gel in soft form, the soft konjac gel showed a remarkable ability to remove soiling particles from uneven surfaces.

The research work allowed us to gain insight into the two materials, sodium alginate and konjac glucomannan, and their applications for Western and East Asian musical instruments. In this research, we applied our innovative hydrogels to specific surfaces of historical musical instruments in Western and East Asian countries. Going forward, we plan to conduct trials to explore the application of our hydrogels to other types of surfaces, such as those treated with natural or organic pigments mixed with animal glue, lacquers, and oil-treated surfaces. Further, these potential areas will be taken into account other surface layers and the various undesirable materials or contaminants we have to consider. These contaminants may include synthetic adhesives, coatings, improperly restored paintings on musical instruments and soiling on delicate decorative areas such as gilded or mother-of-pearl surfaces. Further research will include a comprehensive study of solvents and their effects on the materials under investigation. Several ideas are already underway, starting with the Italy-Korea Scientific and Technological Cooperation Project for 2023-2025, promoted by the Italian Ministry of Foreign Affairs and International Cooperation (MAECI) and the International Cooperation Bureau of the Korean Ministry of Science and ICT (MSIT). We have also broadened the field of investigation to include not only wooden artifacts but also textile works of art. We believe that this project, which was a first step, can expand and give more prospects for future investigations.

Bibliography

- Abasalizadeh F, Moghaddam SV, Alizadeh E, et al (2020) Erratum: Alginate-based hydrogels as drug delivery vehicles in cancer treatment and their applications in wound dressing and 3D bioprinting (Journal of Biological Engineering (2020) 14: 8 DOI: 10.1186/s13036-020-0227-7). J Biol Eng 14:1–22. https://doi.org/10.1186/s13036-020-00239-0
- Abbasi G, Saini A, Goosey E, Diamond ML (2016) Product screening for sources of halogenated flame retardants in Canadian house and office dust. Sci Total Environ 545–546:299–307. https://doi.org/10.1016/j.scitotenv.2015.12.028
- Adams RD (2021) Adhesive Bonding, 2nd edi. Elsevier, London
- Ahmed HE (2011) Strategy for preservation of ptolemaic wrapped mummy's linen in tuna el-gebel excavation, Egypt. A case study. Int J Conserv Sci 2:155–164
- Ai J, Li K, Li J, et al (2021) Super flexible, fatigue resistant, self-healing PVA/xylan/borax hydrogel with dual-crosslinked network. Int J Biol Macromol 172:66–73. https://doi.org/10.1016/j.ijbiomac.2021.01.038
- Akihiko Nishikawa (2009) Introduction to materials related to Shosoin treasures, imitations of wood lacquerwork owned by Tokyo National Museum-《正倉院宝物関連資料紹介》東京国立博物館所蔵木漆工模造品. Tokyo
- Albano M, Comelli D, Fiocco G, et al (2022) Chemical modification of wood induced by the traditional making procedures of bowed string musical instruments: the effect of alkaline treatments. Herit Sci 10:76. https://doi.org/10.1186/s40494-022-00718-1
- Albano M, Grassi S, Fiocco G, et al (2020) A Preliminary Spectroscopic Approach to Evaluate the Effectiveness of Water- and Silicone-Based Cleaning Methods on Historical Varnished Brass. Appl Sci 10:3982. https://doi.org/10.3390/app10113982
- Al-Emam E, Motawea AG, Janssens K, Caen J (2019) Evaluation of polyvinyl alcohol–borax/agarose (PVA–B/AG) blend hydrogels for removal of deteriorated consolidants from ancient Egyptian wall paintings. Herit Sci 7:22. https://doi.org/10.1186/s40494-019-0264-z

- Al-Emam E, Soenen H, Caen J, Janssens K (2020) Characterization of polyvinyl alcohol-borax/agarose (PVA-B/AG) double network hydrogel utilized for the cleaning of works of art. Herit Sci 8:1–15. https://doi.org/10.1186/s40494-020-00447-3
- Al-Musa S, Abu Fara D, Badwan AA (1999) Evaluation of parameters involved in preparation and release of drug loaded in crosslinked matrices of alginate. J Control Release 57:223–232. https://doi.org/10.1016/S0168-3659(98)00096-0
- Alonso-Sande M, Teijeiro-Osorio D, Remuñán-López C, Alonso MJ (2009) Glucomannan, a promising polysaccharide for biopharmaceutical purposes. Eur J Pharm Biopharm 72:453–462. https://doi.org/10.1016/j.ejpb.2008.02.005
- Alves A, Schwanninger M, Pereira H, Rodrigues J (2006) Analytical pyrolysis as a direct method to determine the lignin content in wood: Part 1: Comparison of pyrolysis lignin with Klason lignin. J Anal Appl Pyrolysis 76:. https://doi.org/10.1016/j.jaap.2005.11.004
- Badita CR, Aranghel D, Burducea C, Mereuta P (2020) Characterization of sodium alginate based films. Rom J Phys 65:1–8
- Baglioni P, Bonelli N, Chelazzi D, et al (2015) Organogel formulations for the cleaning of easel paintings. Appl Phys A 121:857–868. https://doi.org/10.1007/s00339-015-9364-0
- Baglioni P, Chelazzi D (eds) (2013) Nanoscience for the Conservation of Works of Art. The Royal Society of Chemistry, Cambridge
- Baij L, Hermans J, Ormsby B, et al (2020) A review of solvent action on oil paint. Herit Sci 8:1–23. https://doi.org/10.1186/s40494-020-00388-x
- Barclay RL (ed) (1997) The care of historic musical instruments. Canadian Conservation Institute and the museums & galleries comission, Scotland
- Bartoletti A, Barker R, Chelazzi D, et al (2020a) Reviving WHAAM! a comparative evaluation of cleaning systems for the conservation treatment of Roy Lichtenstein's iconic painting. Herit Sci 8:1–31. https://doi.org/10.1186/s40494-020-0350-2
- Bartoletti A, Maor T, Chelazzi D, et al (2020b) Facilitating the conservation treatment of Eva Hesse's Addendum through practice-based research, including a comparative evaluation of novel cleaning systems. Herit Sci 8:1–27. https://doi.org/10.1186/s40494-020-00378-z
- Bennett JM (1993) Recent developments in surface roughness characterization. Eng Opt 6:1–9

- Bertasa M, Canevali C, Sansonetti A, et al (2021) An in-depth study on the agar gel effectiveness for built heritage cleaning. J Cult Herit 47:12–20. https://doi.org/10.1016/j.culher.2020.10.007
- Bezur A, Lee L, Loubser M, Trentelman K (2020) Handheld XRF in Cultural Heritage: A Practical Workbook for Conservators. Getty Conservation Institute
- Boccalon E, Nocchetti M, Pica M, et al (2019) Composite sodium alginate-ion exchangers as cleaning systems for the removal of gypsum efflorescences. Appl Clay Sci 181:. https://doi.org/10.1016/j.clay.2019.105216
- Boccalon E, Nocchetti M, Pica M, et al (2021) Hydrogels: A 'stepping stone' towards new cleaning strategies for biodeteriorated surfaces. J Cult Herit 47:1–11. https://doi.org/10.1016/j.culher.2020.07.008
- Bonaduce I, Ribechini E, Modugno F, Colombini MP (2016) Analytical approaches based on gas chromatography mass spectrometry (GC/MS) to study organic materials in artworks and archaeological objects. Top. Curr. Chem. 374
- Bonelli N, Montis C, Mirabile A, et al (2018) Restoration of paper artworks with microemulsions confined in hydrogels for safe and efficient removal of adhesive tapes. Proc Natl Acad Sci 115:5932–5937. https://doi.org/10.1073/pnas.1801962115
- Bonelli N, Poggi G, Chelazzi D, et al (2019) Poly(vinyl alcohol)/poly(vinyl pyrrolidone) hydrogels for the cleaning of art. J Colloid Interface Sci 536:339–348. https://doi.org/10.1016/j.jcis.2018.10.025
- Bravo I (2023) Tailoring Cleaning Systems for the Removal of Bronze Paint and Soiling From a J.M.W. Turner Gilded Frame. J Am Inst Conserv 62:240–263. https://doi.org/10.1080/01971360.2022.2111498
- Bruce Carlson, Fausto Cacciatori CC (2006) Il DNA degli Amati-The Amatis' DNA. Una dinastia di liutai a Cremona. cremona
- Brus J, Urbanova M, Czernek J, et al (2017) Structure and Dynamics of Alginate Gels Cross-Linked by Polyvalent Ions Probed via Solid State NMR Spectroscopy. Biomacromolecules 18:2478–2488. https://doi.org/10.1021/acs.biomac.7b00627
- Bucur V (2016) Handbook of Materials for String Musical Instruments. Springer International Publishing, Switzerland 2016

- Campanella L, Angeloni R, Cibin F, et al (2021) Capsulated essential oil in gel spheres for the protection of cellulosic cultural heritage. Nat Prod Res 35:116–123. https://doi.org/10.1080/14786419.2019.1616726
- Canevali C, Fasoli M, Bertasa M, et al (2016) A multi-analytical approach for the study of copper stain removal by agar gels. Microchem J 129:249–258. https://doi.org/10.1016/j.microc.2016.07.007
- Caruso MR, D'Agostino G, Milioto S, et al (2023) A review on biopolymer-based treatments for consolidation and surface protection of cultural heritage materials. J Mater Sci 58:12954–12975. https://doi.org/10.1007/s10853-023-08833-5
- Casoli A, Cremonesi P, Isca C, et al (2013) Evaluation of the effect of cleaning on the morphological properties of ancient paper surface. Cellulose 20:2027–2043. https://doi.org/10.1007/s10570-013-9975-6
- Cazzaniga I, Gargano M, Invernizzi C, et al (2021) A Multi-Analytical Non-Invasive Approach to Aqueous Cleaning Systems in Treatments on Bowed String Musical Instruments. Coatings 11:150. https://doi.org/10.3390/coatings11020150
- Chaudhary J, Thakur S, Sharma M, et al (2020) Development of biodegradable agar-agar/gelatin-based superabsorbent hydrogel as an efficient moisture-retaining agent. Biomolecules 10:1–13. https://doi.org/10.3390/biom10060939
- Chen P, Wang S, Huang C, et al (2007) New crosslinked polymer from a rapid polymerization of acrylic acid with triaziridine-containing compound. J Appl Polym Sci 104:809–815. https://doi.org/10.1002/app.25548
- Chen Y, Song C, Lv Y, Qian X (2019) Konjac glucomannan/kappa carrageenan interpenetrating network hydrogels with enhanced mechanical strength and excellent self-healing capability. Polymer (Guildf) 184:. https://doi.org/10.1016/j.polymer.2019.121913
- Chen Y, Zou C, Mastalerz M, et al (2015) Applications of micro-fourier transform infrared spectroscopy (FTIR) in the geological sciences—A Review. Int. J. Mol. Sci. 16:30223–30250
- Chua M, Baldwin TC, Hocking TJ, Chan K (2010) Traditional uses and potential health benefits of Amorphophallus konjac K. Koch ex N.E.Br. J Ethnopharmacol 128:268–278. https://doi.org/10.1016/j.jep.2010.01.021

- Chuang JJ, Huang YY, Lo SH, et al (2017) Effects of pH on the Shape of Alginate Particles and Its Release Behavior. Int J Polym Sci 2017:. https://doi.org/10.1155/2017/3902704
- Connell LS, Gabrielli L, Mahony O, et al (2017) Functionalizing natural polymers with alkoxysilane coupling agents: Reacting 3-glycidoxypropyl trimethoxysilane with poly(γ-glutamic acid) and gelatin. Polym Chem 8:1095–1103. https://doi.org/10.1039/c6py01425a
- Courard L, Nelis M (2003) Surface analysis of mineral substrates for repair works: roughness evaluation by profilometry and surfometry analysis. Mag Concr Res 55:355–366. https://doi.org/10.1680/macr.2003.55.4.355
- Cremonesi P (2012) Rigid Gels and Enzyme Cleaning. Smithson Contrib to Museum Conserv 3:179–183
- Cremonesi P (2016) Surface cleaning? Yes, freshly grated Agar gel, please. Stud Conserv 61:362–367. https://doi.org/10.1179/2047058415Y.0000000026
- Cremonesi PAG (2019) Gel rigidi polisaccaridici per il trattamento dei manufatti artistici. Il prato, Padova
- Crestini C, Lange H, Sette M, Argyropoulos DS (2017) On the structure of softwood kraft lignin. Green Chem 19:4104–4121. https://doi.org/10.1039/C7GC01812F
- Cushman M (1992) Science for Conservators, Vol. 2: Cleaning. Taylor and Francis, London
- Daudin-Schotte M, Bisschoff M, Joosten I, et al (2013) Dry Cleaning Approaches for Unvarnished Paint Surfaces. New Insights into Clean Paint 209–219
- De Chiffre L, Lonardo P, Trumpold H, et al (2000) Quantitative Characterisation of Surface Texture. CIRP Ann 49:635–652. https://doi.org/10.1016/S0007-8506(07)63458-1
- Di Napoli B, Franco S, Severini L, et al (2020) Gellan Gum Microgels as Effective Agents for a Rapid Cleaning of Paper. ACS Appl Polym Mater 2:2791–2801. https://doi.org/10.1021/acsapm.0c00342
- Di Tullio V, Pigliapochi R, Zumbulyadis N, et al (2023) Dynamics of diffusion, evaporation, and retention of organic solvents in paints by unilateral NMR and HR-MAS NMR spectroscopy. Microchem J 190:108582. https://doi.org/10.1016/j.microc.2023.108582

- Dien AE (2007) Early Chinese Civilization. In: Early Chinese Civilization Series. Yale university press/New Haven & London, United States of America
- Domingues J, Bonelli N, Giorgi R, Baglioni P (2014) Chemical semi-IPN hydrogels for the removal of adhesives from canvas paintings. Appl Phys A 114:705–710. https://doi.org/10.1007/s00339-013-8150-0
- Donati I, Holtan S, Mørch YA, et al (2005) New Hypothesis on the Role of Alternating Sequences in Calcium−Alginate Gels. Biomacromolecules 6:1031–1040. https://doi.org/10.1021/bm049306e
- Dost AA (1996) Monitoring surface and airborne inorganic contamination in the workplace by a field portable X-ray fluorescence spectrometer. Ann Occup Hyg 40:589–610. https://doi.org/10.1016/0003-4878(96)00016-6
- Draget K, Smidsrød O, Skjåk-Bræk G (2005) Alginates form algae. In: Steinbüchel A, Rhee SK (eds) Polysaccharides and polyamides in the food iindustries: properties, production and patents. WILEY-VCH Verlag GmbH & Co. KGaA, Weinheim, pp 1–30
- Duncan TT, Chan EP, Beers KL (2021) Quantifying the 'press and peel' removal of particulates using elastomers and gels. J Cult Herit 48:236–243. https://doi.org/10.1016/j.culher.2020.11.004
- Ebnesajjad S (2010) Surface and Material Characterization Techniques. Elsevier Inc.
- Echard J, Bertrand L (2010) Complementary spectroscopic analyses of varnishes of historical musical instruments. Spectrosc Eur 22:2–5
- Erizal E, Tjahyono T, PP D, Darmawan D (2013) Synthesis of Polyvinyl Pirrolidone (PVC) /K-Carrageenan Hydrogel Prepared by Gamma Radiation Processing As a Function of Dose and PVP Concentration. Indones J Chem 13:41–46. https://doi.org/10.22146/ijc.21324
- Feidenhans'l NA, Hansen P-E, Pilný L, et al (2015) Comparison of optical methods for surface roughness characterization. Meas Sci Technol 26:085208. https://doi.org/10.1088/0957-0233/26/8/085208
- Fellin M, Negri M, Zanuttini R (2014) Multi-elemental analysis of wood waste using energy dispersive X-ray fluorescence (ED-XRF) analyzer. Eur J Wood Wood Prod 72:199–211. https://doi.org/10.1007/s00107-013-0766-4

- Fernando IPS, Lee WW, Han EJ, Ahn G (2020) Alginate-based nanomaterials: Fabrication techniques, properties, and applications. Chem Eng J 391:123823. https://doi.org/10.1016/j.cej.2019.123823
- Fiocco G, Grassi S, Invernizzi C, et al (2021a) Chemometric tools to investigate complex synchrotron radiation FTIR micro-spectra: focus on historical bowed musical instruments. ACTA IMEKO 10:201. https://doi.org/10.21014/acta_imeko.v10i1.836
- Fiocco G, Invernizzi C, Grassi S, et al (2021b) Reflection FTIR spectroscopy for the study of historical bowed string instruments: Invasive and non-invasive approaches. Spectrochim Acta - Part A Mol Biomol Spectrosc 245:118926. https://doi.org/10.1016/j.saa.2020.118926
- Fiocco G, Invernizzi C, Rovetta T, et al (2021c) Surfing through the coating system of historic bowed instruments: a spectroscopic perspective. Spectrosc Eur 19. https://doi.org/10.1255/sew.2021.a8
- G. O. Phillips, P. A. Williams (2009) Handbook of hydrocolloids. Woodhead publishing limited and CRS press LLC, cambridge
- Gabriele F, Bruno L, Casieri C, et al (2022) Application and Monitoring of Oxidative Alginate–Biocide Hydrogels for Two Case Studies in "The Sassi and the Park of the Rupestrian Churches of Matera." Coatings 12:. https://doi.org/10.3390/coatings12040462
- Gabriele F, Tortora M, Bruno L, et al (2021) Alginate-biocide hydrogel for the removal of biofilms from calcareous stone artworks. J Cult Herit 49:106–114. https://doi.org/10.1016/j.culher.2021.02.009
- Gabrielli L, Connell L, Russo L, et al (2014) Exploring GPTMS reactivity against simple nucleophiles: Chemistry beyond hybrid materials fabrication. RSC Adv 4:1841–1848. https://doi.org/10.1039/c3ra44748k
- Gabrielli L, Russo L, Poveda A, et al (2013) Epoxide opening versus silica condensation during sol-gel hybrid biomaterial synthesis. Chem - A Eur J 19:7856–7864. https://doi.org/10.1002/chem.201204326
- Gadelmawla ES, Koura MM, Maksoud TMA, et al (2002) Roughness parameters. J Mater Process Technol 123:133–145. https://doi.org/10.1016/S0924-0136(02)00060-2

- Gaggero G, Delucchi M, Allegretta G, et al (2021) Interaction of sodium alginate thickener with components of architectural water-based coatings. Prog Org Coatings 151:106016. https://doi.org/10.1016/j.porgcoat.2020.106016
- Galatis P, Boyatzis S, Theodorakopoulos C (2012) Removal of a synthetic soiling mixture on mastic, shellac & Laropal® K80 coatings using two hydrogels. e-Preservation Sci 9:72–83
- Gao S, Guo J, Nishinari K (2008a) Thermoreversible konjac glucomannan gel crosslinked by borax. Carbohydr Polym 72:315–325. https://doi.org/10.1016/j.carbpol.2007.08.015
- Gao S, Guo J, Wu L, Wang S (2008b) Gelation of konjac glucomannan crosslinked by organic borate. Carbohydr Polym 73:498–505. https://doi.org/10.1016/j.carbpol.2007.12.013
- Garbacz A, Courard L, Kostana K (2006) Characterization of concrete surface roughness and its relation to adhesion in repair systems. Mater Charact 56:281–289. https://doi.org/10.1016/j.matchar.2005.10.014
- Geiringer K (1978) Instruments in the history of western music. Oxford university press, New york
- Gierer J (1980) Chemical aspects of kraft pulping. Wood Sci Technol 14:241–266. https://doi.org/10.1007/BF00383453
- Gorel F (2010) Assessment of agar gel loaded with micro-emulsion for the cleaning of porous surfaces. CeROArt 1–10. https://doi.org/10.4000/ceroart.1827
- Gueidão M, Vieira E, Bordalo R, Moreira P (2021) Available green conservation methodologies for the cleaning of cultural heritage: an overview. Estud Conserv e Restauro 0: https://doi.org/10.34632/ecr.2020.10679
- Gulotta D, Saviello D, Gherardi F, et al (2014) Setup of a sustainable indoor cleaning methodology for the sculpted stone surfaces of the Duomo of Milan. Herit Sci 2:1–13. https://doi.org/10.1186/2050-7445-2-6
- Gulrez SKH, Al-assaf S, Phillips GO (2011) Hydrogels: Methods of Preparation. In: Carpi PA (ed) Progress in Molecular and Environmental Bioengineering – From Analysis and Modeling to Technology Applications. InTech, pp 117–150
- Gurikov P, Smirnova I (2018) Non-conventional methods for gelation of alginate. Gels 4:. https://doi.org/10.3390/gels4010014

- Gwangju KNM of (2002) Gwanju Sinchando jeoseupji-低濕地 IV. Gwangju
- Haraguchi R, Oishi Y, Narita T (2023) Macroscopic Pattern Formation of Alginate Gels in a Two-Dimensional System. Gels 9:444. https://doi.org/10.3390/gels9060444
- Heller C, Ellerbrock RH, Roßkopf N, et al (2015) Soil organic matter characterization of temperate peatland soil with FTIR-spectroscopy: Effects of mire type and drainage intensity. Eur J Soil Sci 66:847–858. https://doi.org/10.1111/ejss.12279
- Huang M, Hou Y, Li Y, et al (2017) High performances of dual network PVA hydrogel modified by PVP using borax as the structure-forming accelerator. Des Monomers Polym 20:505–513. https://doi.org/10.1080/15685551.2017.1382433
- Huang YC, Chu HW, Huang CC, et al (2015) Alkali-treated konjac glucomannan film as a novel wound dressing. Carbohydr Polym 117:778–787. https://doi.org/10.1016/j.carbpol.2014.10.047
- Hughes A, Sullivan M (2016) Targeted Cleaning of Works on Paper: Rigid Polysaccharide Gels and Conductivity in Aqueous Solutions. B Pap Gr Annu 35:30
- Hurler J, Engesland A, Poorahmary Kermany B, Škalko-Basnet N (2012) Improved texture analysis for hydrogel characterization: Gel cohesiveness, adhesiveness, and hardness. J Appl Polym Sci 125:180–188. https://doi.org/10.1002/app.35414
- Ibrahim NA, Nada AA, Eid BM (2018) Polysaccharide-Based Polymer Gels and Their Potential Applications. pp 97–126
- Impaprasert R, Piyarat S, Sophontanakij N, et al (2017) Rehydration and textural properties of dried konjac noodles: Effect of alkaline and some gelling agents. Horticulturae 3:. https://doi.org/10.3390/horticulturae3010020
- Invernizzi C, de Ferri L, Comite V, et al (2022) Correlation between surface roughness and spectral features in IR-reflection spectroscopy. Microchem J 172:. https://doi.org/10.1016/j.microc.2021.106874
- Invernizzi C, Fichera GV, Licchelli M, Malagodi M (2018a) A non-invasive stratigraphic study by reflection FT-IR spectroscopy and UV-induced fluorescence technique: The case of historical violins. Microchem J 138:273–281. https://doi.org/10.1016/j.microc.2018.01.021

- Invernizzi C, Fiocco G, Iwanicka M, et al (2020a) Non-invasive mobile technology to study the stratigraphy of ancient Cremonese violins: OCT, NMR-MOUSE, XRF and reflection FT-IR spectroscopy. Microchem J 155:104754. https://doi.org/10.1016/j.microc.2020.104754
- Invernizzi C, Fiocco G, Iwanicka M, et al (2020b) Surface and Interface Treatments on Wooden Artefacts: Potentialities and Limits of a Non-Invasive Multi-Technique Study. https://doi.org/10.3390/coatings
- Invernizzi C, Rovetta T, Licchelli M, Malagodi M (2018b) Mid and near-infrared reflection spectral database of natural organic materials in the cultural heritage field. Int J Anal Chem 2018:. https://doi.org/10.1155/2018/7823248
- Ishizone T, Takata T, Kobayashi M (2003) Synthesis of new crosslinkable polymers by chemoselective polymerizations of 2-(1-aziridinyl)ethyl methacrylate. J Polym Sci Part A Polym Chem 41:1335–1340. https://doi.org/10.1002/pola.10663
- Islam MR, Oyen ML (2022) Mechanical characterization of hydrogels. In: Li H, Silberschmidt V (eds) The Mechanics of Hydrogels. Elsevier
- Jan van den Berg K, Bonaduce I, Burnstock A, et al (2019) Conservation of Modern Oil Paintings. Springer International Publishing
- Jang HJ, Lee JT, Yoon HJ (2015) Aziridine in polymers: A strategy to functionalize polymers by ring-opening reaction of aziridine. Polym Chem 6:3387–3391. https://doi.org/10.1039/c5py00266d
- Janus J, Fauxpoint G, Arntz Y, et al (2010) Surface roughness and morphology of three nanocomposites after two different polishing treatments by a multitechnique approach. Dent Mater 26:416–425. https://doi.org/10.1016/j.dental.2009.09.014
- Jiang Y, Pang X, Deng Y, et al (2019) An alginate hybrid sponge with high thermal stability: Its flame retardant properties and mechanism. Polymers (Basel) 11:. https://doi.org/10.3390/polym11121973
- Johnson HM (2004) The Koto: A Traditional Instrument in Contemporary Japan. Hotei
- Kanth A, Singh M, Pandey SC (2018) Optimizing the Rigidity of Gellan and Agar Gels for of Conservation Science. Int J Conserv Sci 9:451–462

- Karoyo AH, Wilson LD (2021) A Review on the Design and Hydration Properties of Natural Polymer-Based Hydrogels. Materials (Basel) 14:1095. https://doi.org/10.3390/ma14051095
- Kasprzok L, Fabbri D, Rombolà AG, et al (2020) Identification of organic materials in historical stringed instruments by off-line analytical pyrolysis solid-phase microextraction with on-fiber silylation and gas chromatography-mass spectrometry. J Anal Appl Pyrolysis 145:. https://doi.org/10.1016/j.jaap.2019.104727
- Keefe MH, Ormsby B (2011) Art and Industry: Novel Approaches to the Evaluation and Development of Cleaning Systems for Artists' Acrylic Latex Paints Cleaning Modern Oil Paints View project ESCAPE: Expert System for Characterization using AMDIS Plus Excel View project
- Kim BG (2010) A study on the improvement and manufacture method of traditional musical instrument on the basis of Akhakgwebeom. Soc Kangwon Prov Folk 339–378
- Kolya H, Kang C-W (2021) Hygrothermal treated paulownia hardwood reveals enhanced sound absorption coefficient: An effective and facile approach. Appl Acoust 174:107758. https://doi.org/10.1016/j.apacoust.2020.107758
- Kopka B, Kost B, Wrześniewska J, et al (2023) Supramolecular poly(vinyl alcohol)-based hydrogels containing quercetin for bacterial and fungal elimination. Eur Polym J 187:111881. https://doi.org/10.1016/j.eurpolymj.2023.111881
- Korea National gugak center (2014) Musical instrument of Korea 1-Hangook gukakki. Dolbege-돌베개, Seoul
- Lämmlein SL, Mannes D, Van Damme B, et al (2019) The influence of multi-layered varnishes on moisture protection and vibrational properties of violin wood. Sci Rep 9:1–9. https://doi.org/10.1038/s41598-019-54991-5
- Lee C, Jung H, Chung Y (2021) Functional Characteristics of Nakdong Technique Treated on Paulownia Wood Surface. J Korean Wood Sci Technol 49:82–92. https://doi.org/10.5658/WOOD.2021.49.1.82
- Li C-P, Weng M-C, Huang S-L (2020) Preparation and Characterization of pH Sensitive Chitosan/3-Glycidyloxypropyl Trimethoxysilane (GPTMS) Hydrogels by Sol-Gel Method. Polymers (Basel) 12:1326. https://doi.org/10.3390/polym12061326

- Li J, Wu Y, He J, Huang Y (2016) A new insight to the effect of calcium concentration on gelation process and physical properties of alginate films. J Mater Sci 51:5791–5801. https://doi.org/10.1007/s10853-016-9880-0
- Li Q, Hu Y, Zhang B (2021) Hydrophilic ZnO Nanoparticle-Based Antimicrobial Coatings for Sandstone Heritage Conservation. ACS Appl Nano Mater 4:13908–13918. https://doi.org/10.1021/acsanm.1c03224
- Li Z, Su Y, Xie B, et al (2015) A novel biocompatible double network hydrogel consisting of konjac glucomannan with high mechanical strength and ability to be freely shaped. J Mater Chem B 3:1769–1778. https://doi.org/10.1039/c4tb01653j
- Licchelli M, Malagodi M, Somaini M, et al (2013) Surface treatments of wood by chemically modified shellac. Surf Eng 29:121–127. https://doi.org/10.1179/1743294412Y.0000000069
- Licchelli M, Marzolla SJ, Poggi A, Zanchi C (2011) Crosslinked fluorinated polyurethanes for the protection of stone surfaces from graffiti. J Cult Herit 12:34–43. https://doi.org/10.1016/j.culher.2010.07.002
- Liu XY, Timar MC, Varodi AM, Yi SL (2016) Effects of Ageing on the Color and Surface Chemistry of Paulownia Wood (P. elongata) from Fast Growing Crops. BioResources 11:9400–9420. https://doi.org/10.15376/biores.11.4.9400-9420
- Lotfipour F, Mirzaeei S, Maghsoodi M (2012) Evaluation of the effect of cacl2 and alginate concentrations and hardening time on the characteristics of Lactobacillus acidophilus loaded alginate beads using response surface analysis. Adv Pharm Bull 2:71–78. https://doi.org/10.5681/apb.2012.010
- Ma S, Zhu P, Wang M (2019) Effects of konjac glucomannan on pasting and rheological properties of corn starch. Food Hydrocoll 89:234–240. https://doi.org/10.1016/j.foodhyd.2018.10.045
- Majdar RE, Crestini C, Lange H (2020) Lignin Fractionation in Segmented Continuous Flow. ChemSusChem 13:4735–4742. https://doi.org/10.1002/cssc.202001138
- Manivannan M, Rajendran S (2011) Investigation of inhibitive action of urea-Zn2+ system in the corrosion control of carbon steel in sea water INVESTIGATION OF INHIBITIVE ACTION OF UREA-ZN 2+ SYSTEM IN THE CORROSION CONTROL OF CARBON STEEL IN SEA WATER

- Mansur HS, Sadahira CM, Souza AN, Mansur AAP (2008) FTIR spectroscopy characterization of poly (vinyl alcohol) hydrogel with different hydrolysis degree and chemically crosslinked with glutaraldehyde. Mater Sci Eng C 28:539–548. https://doi.org/10.1016/j.msec.2007.10.088
- Mantha S, Pillai S, Khayambashi P, et al (2019) Smart Hydrogels in Tissue Engineering and Regenerative Medicine. Materials (Basel) 12:3323. https://doi.org/10.3390/ma12203323
- Martínez-Domingo MÁ, Calero Castillo AI, Vivar García E, Valero EM (2020) Evaluation of Cleaning Processes Using Colorimetric and Spectral Data for the Removal of Layers of Limewash from Medieval Plasterwork. Sensors 20:7147. https://doi.org/10.3390/s20247147
- Mastrangelo R, Chelazzi D, Poggi G, et al (2020) Twin-chain polymer hydrogels based on poly(vinyl alcohol) as new advanced tool for the cleaning of modern and contemporary art. Proc Natl Acad Sci U S A 117:7011–7020. https://doi.org/10.1073/pnas.1911811117
- Mazzuca C, Micheli L, Carbone M, et al (2014) Gellan hydrogel as a powerful tool in paper cleaning process: A detailed study. J Colloid Interface Sci 416:205–211. https://doi.org/10.1016/j.jcis.2013.10.062
- Mazzuca C, Poggi G, Bonelli N, et al (2017) Innovative chemical gels meet enzymes: A smart combination for cleaning paper artworks. J Colloid Interface Sci 502:153–164. https://doi.org/10.1016/j.jcis.2017.04.088
- Mohamed NA, Al-mehbad NY (2013) Novel terephthaloyl thiourea cross-linked chitosan hydrogels as antibacterial and antifungal agents. Int J Biol Macromol 57:111–117. https://doi.org/10.1016/j.ijbiomac.2013.03.007
- Montain SJ, Cheuvront SN, Lukaski HC (2007) Sweat Mineral-Element Responses During 7 h of Exercise-Heat Stress. Int J Sport Nutr Excercise Metab 17:574–582
- Moretti P, Iwanicka M, Melessanaki K, et al (2019) Laser cleaning of paintings: in situ optimization of operative parameters through non-invasive assessment by optical coherence tomography (OCT), reflection FT-IR spectroscopy and laser induced fluorescence spectroscopy (LIF). Herit Sci 7:1–12. https://doi.org/10.1186/s40494-019-0284-8

- Moretti P, Rosi F, Miliani C, et al (2020) Non-invasive reflection FT-IR spectroscopy for on-site detection of cleaning system residues on polychrome surfaces. Microchem J 157:105033. https://doi.org/10.1016/j.microc.2020.105033
- Murray Campbell, Clive Greated AM (2004) Musical Instruments: History, Technology, and Performance of Instruments of Western Music. Oxford University Press, New York
- Naga N, Takenouchi T, Nakano T (2022) Ring-Opening Polymerization of Triaziridine Compounds in Water: An Extremely Facile Method to Synthesize a Porous Polymer through Polymerization-Induced Phase Separation. ACS Macro Lett 603–607. https://doi.org/10.1021/acsmacrolett.2c00110
- Nataraj Di, Reddy N (2020) Chemical Modifications of Alginate and Its Derivatives. Int J Chem Res 4:1–17. https://doi.org/10.22159/ijcr.2020v4i1.98
- Nazzaro F, Fratianni F, De Feo V, et al (2022) Polyphenols applications in food industry sector. In: Technologies to Recover Polyphenols from AgroFood By-products and Wastes. Elsevier, pp 301–336
- Ni Y, Lin W, Mu RJ, et al (2019) Microfluidic fabrication of robust konjac glucomannan-based microfiber scaffolds with high antioxidant performance. J Sol-Gel Sci Technol 214–220. https://doi.org/10.1007/s10971-018-4881-x
- Nussinovitch A (2005) Production, properties, and applications of hydrocolloid cellular solids. Mol Nutr Food Res 49:195–213. https://doi.org/10.1002/mnfr.200400032
- Oliver K V., Maréchal A, Rich PR (2016) Effects of the hydration state on the mid-infrared spectra of urea and creatinine in relation to urine analyses. Appl Spectrosc 70:983–994. https://doi.org/10.1177/0003702816641263
- Ormsby B, Keefe M, Phenix A, et al (2016) Mineral spirits-based microemulsions: A novel cleaning system for painted surfaces. J Am Inst Conserv 55:12–31. https://doi.org/10.1080/01971360.2015.1120406
- Papageorgiou SK, Kouvelos EP, Favvas EP, et al (2010) Metal-carboxylate interactions in metal-alginate complexes studied with FTIR spectroscopy. Carbohydr Res 345:469–473. https://doi.org/10.1016/j.carres.2009.12.010
- Paques JP, Sagis LMC, van Rijn CJM, van der Linden E (2014) Nanospheres of alginate prepared through w/o emulsification and internal gelation with nanoparticles of CaCO3. Food Hydrocoll 40:182–188. https://doi.org/10.1016/j.foodhyd.2014.02.024

- Passaretti A, Cuvillier L, Sciutto G, et al (2021) Biologically derived gels for the cleaning of historical and artistic metal heritage. Appl Sci 11:. https://doi.org/10.3390/app11083405
- Patterson MJ, Galloway SDR, Nimmo MA (2000) Variations in Regional Sweat Composition in Normal Human Males. Exp Physiol 85:869–875. https://doi.org/10.1111/j.1469-445X.2000.02058.x
- Pawar SN, Edgar KJ (2012) Alginate derivatization: A review of chemistry, properties and applications. Biomaterials 33:3279–3305. https://doi.org/10.1016/j.biomaterials.2012.01.007
- Pedersen IS (2018) Composite Hydrogels of Alginate and Cellulose Nanofibrils A study of mechanical properties
- Pellegrini D, Duce C, Bonaduce I, et al (2016) Fourier transform infrared spectroscopic study of rabbit glue/inorganic pigments mixtures in fresh and aged reference paint reconstructions. Microchem J 124:31–35. https://doi.org/10.1016/j.microc.2015.07.018
- Pérez-Navarro J, Izquierdo-Cañas PM, Mena-Morales A, et al (2019) Phenolic compounds profile of different berry parts from novel Vitis vinifera L. red grape genotypes and Tempranillo using HPLC-DAD-ESI-MS/MS: A varietal differentiation tool. Food Chem 295:350–360. https://doi.org/10.1016/j.foodchem.2019.05.137
- Petrella G, Mazzuca C, Micheli L, et al (2016) A new sustainable and innovative work for paper artworks cleaning process: Gellan hydrogel combined with hydrolytic enzymes. Int J Conserv Sci 7:273–280
- Phenix A, Sutherland K (2001) The cleaning of paintings: effects of organic solvents on oil paint films. Stud Conserv 46:47–60. https://doi.org/10.1179/sic.2001.46.supplement-1.47
- Phillips GO, Williams PA (2009) Handbook of Hydrocolloids: Second Edition
- Pirkkalainen K, Peura M, Leppänen K, et al (2012) Simultaneous X-ray diffraction and X-ray fluorescence microanalysis on secondary xylem of Norway spruce. Wood Sci Technol 46:1113–1125. https://doi.org/10.1007/s00226-012-0474-y
- Pollens S (2015) The Manual of Musical Instrument Conservation. Cambridge university press

- Prati S, Volpi F, Fontana R, et al (2018) Sustainability in art conservation: A novel bio-based organogel for the cleaning of water sensitive works of art. In: Pure and Applied Chemistry. Walter de Gruyter GmbH, pp 239–251
- Rathod NB, Elabed N, Punia S, et al (2023) Recent Developments in Polyphenol Applications on Human Health: A Review with Current Knowledge. Plants 12:1217. https://doi.org/10.3390/plants12061217
- Reyes-Peces M V., Pérez-Moreno A, De-Los-santos DM, et al (2020) Chitosan-gptms-silica hybrid mesoporous aerogels for bone tissue engineering. Polymers (Basel) 12:1–24. https://doi.org/10.3390/polym12112723
- Riedo C, Caldera F, Poli T, Chiantore O (2015) Poly(vinylalcohol)-borate hydrogels with improved features for the cleaning of cultural heritage surfaces. Herit Sci 3:. https://doi.org/10.1186/s40494-015-0053-2
- Rodriguez JM, Curtis R V., Bartlett DW (2009) Surface roughness of impression materials and dental stones scanned by non-contacting laser profilometry. Dent Mater 25:500–505. https://doi.org/10.1016/j.dental.2008.10.003
- Rosciardi V, Chelazzi D, Baglioni P (2022) "Green" biocomposite Poly (vinyl alcohol)/starch cryogels as new advanced tools for the cleaning of artifacts. J Colloid Interface Sci 613:697–708. https://doi.org/10.1016/j.jcis.2021.12.145
- Rosiak P, Latanska I, Paul P, et al (2021) Modification of Alginates to Modulate Their Physic-Chemical Properties and Obtain Biomaterials with Different Functional Properties. Molecules 26:7264. https://doi.org/10.3390/molecules26237264
- Rovetta T, Invernizzi C, Licchelli M, et al (2018) The elemental composition of Stradivari's musical instruments: new results through non-invasive EDXRF analysis. X-Ray Spectrom 47:159–170. https://doi.org/10.1002/xrs.2825
- Rubinstein M, Colby RH (2003) Polymer Physics. Oxford University Press, New York
- Sadowski Ł, Czarnecki S, Hoła J (2016) Evaluation of the height 3D roughness parameters of concrete substrate and the adhesion to epoxy resin. Int J Adhes Adhes 67:3–13. https://doi.org/10.1016/j.ijadhadh.2015.12.019
- Sahoon C (1990) Our histrorical musical instruments-Woori yet akki. Daewonsa, Seoul

- Said NS, Sarbon NM (2022) Physical and Mechanical Characteristics of Gelatin-Based Films as a Potential Food Packaging Material: A Review. Membranes (Basel) 12:442. https://doi.org/10.3390/membranes12050442
- Samorì C, Galletti P, Giorgini L, et al (2016) The Green Attitude in Art Conservation: Polyhydroxybutyrate–based Gels for the Cleaning of Oil Paintings. ChemistrySelect 1:4502–4508. https://doi.org/10.1002/slct.201601180
- Sansonetti A, Bertasa M, Canevali C, et al (2020) A review in using agar gels for cleaning art surfaces. J Cult Herit 44:285–296. https://doi.org/10.1016/j.culher.2020.01.008
- Schellmann NC (2007) Animal glues: a review of their key properties relevant to conservation. Stud Conserv 52:55–66. https://doi.org/10.1179/sic.2007.52.supplement-1.55
- Scott CL (2012) The use of agar as a solvent gel in objects conservation. AIC Objects Spec Gr Postprints 19:71–83
- Smets A, De Vis K, Ortega-Saez N (2019) A challenging treatment of an 18th century embroidered textile using gel cleaning in combination with decamethylcyclopentasiloxane (D5) silicone solvent barriers. Conserv Património 31:41–52. https://doi.org/10.14568/cp2018023
- Solberg A, Draget KI, Schatz C, Christensen BE (2023) Alginate Blocks and Block Polysaccharides: A Review. Macromol Symp 408:1–5. https://doi.org/10.1002/masy.202200072
- Song C, Lv Y, Qian K, et al (2019) Preparation of konjac glucomannan–borax hydrogels with good self-healing property and pH-responsive behavior. J Polym Res 26:. https://doi.org/10.1007/s10965-019-1702-z
- Spinella A, Malagodi M, Saladino ML, et al (2017) A step forward in disclosing the secret of stradivari's varnish by NMR spectroscopy. J Polym Sci Part A Polym Chem 55:3949–3954. https://doi.org/10.1002/pola.28782
- Spoljaric S, Salminen A, Luong ND, Seppälä J (2014) Stable, self-healing hydrogels from nanofibrillated cellulose, poly(vinyl alcohol) and borax via reversible crosslinking. Eur Polym J 56:105–117. https://doi.org/10.1016/j.eurpolymj.2014.03.009

- Spyros A (2016) Liquid-State NMR in Cultural Heritage and Archaeological Sciences. In: Webb GA (ed) Modern Magnetic Resonance. Springer International Publishing, Cham, pp 1–12
- Stagno V, Ciccola A, Curini R, et al (2021) Non-Invasive Assessment of PVA-Borax Hydrogel Effectiveness in Removing Metal Corrosion Products on Stones by Portable NMR. Gels 7:265. https://doi.org/10.3390/gels7040265
- Stanciu MD, Coşereanu C, Dinulică F, Bucur V (2020) Effect of wood species on vibration modes of violins plates. Eur J Wood Wood Prod 78:785–799. https://doi.org/10.1007/s00107-020-01538-5
- Sterling DA, Lewis RD, Luke DA, Shadel BN (2000) A Portable X-Ray Fluorescence Instrument for Analyzing Dust Wipe Samples for Lead: Evaluation with Field Samples. Environ Res 83:174–179. https://doi.org/10.1006/enrs.2000.4058
- Stulik D, Miller D, Khanjian H, et al (2004) Solvent Gels for the Cleaning of Works of Art: The Residue Question. Getty Conservation Institute
- Subramanian UM, Kumar SV, Nagiah N, Sivagnanam UT (2014) Fabrication of Polyvinyl Alcohol-Polyvinylpyrrolidone Blend Scaffolds via Electrospinning for Tissue Engineering Applications. Int J Polym Mater Polym Biomater 63:476–485. https://doi.org/10.1080/00914037.2013.854216
- Szabó L, Gerber-Lemaire S, Wandrey C (2020) Strategies to functionalize the anionic biopolymer na-alginate without restricting its polyelectrolyte properties. Polymers (Basel) 12:. https://doi.org/10.3390/POLYM12040919
- Takamura A, Watanabe K, Akutsu T, Ozawa T (2018) Soft and Robust Identification of Body Fluid Using Fourier Transform Infrared Spectroscopy and Chemometric Strategies for Forensic Analysis. Sci Rep 8:. https://doi.org/10.1038/s41598-018-26873-9
- Tetreault J (2003) Airborne pollutants in museums galleries, archives: risk assessment, control strategies, and preservation management. Canadian conservation institute, Ottawa
- The Nuclear Magnetic Resonance Society of Japan (2018) Experimental Approaches of NMR Spectroscopy. Springer Singapore, Singapore
- Tirat S, Echard JP, Lattuati-Derieux A, et al (2017) Reconstructing historical recipes of linseed oil/colophony varnishes: Influence of preparation processes on application properties. J Cult Herit 27:S34–S43. https://doi.org/10.1016/j.culher.2017.08.001

- Tireni L, Charta A, Berzioli M, Casoli A (2011) Evaluation of cleaning and chemical stabilization of paper treated with a rigid hydrogel of gellan gum by means of chemical and physical analyses Conservation and Restoration of Cultural Heritage View project VIL Visible Induced Luminescence View project
- Tironi A, Trezza MA, Irassar EF, Scian AN (2012) Thermal Treatment of Kaolin: Effect on the Pozzolanic Activity. Procedia Mater Sci 1:343–350. https://doi.org/10.1016/j.mspro.2012.06.046
- Tran T-N, Mauro C Di, Graillot A, Mija A (2020) Chemical Reactivity and the Influence of Initiators on the Epoxidized Vegetable Oil/Dicarboxylic Acid System. Macromolecules 53:2526–2538. https://doi.org/10.1021/acs.macromol.9b02700
- Umney N, Rivers S (2003) Conservation of furniture. Butterworth-Heinemann, Burlington
- Valtierra N, Courtenay LA, López-Polín L (2020) Microscopic analyses of the effects of mechanical cleaning interventions on cut marks. Archaeol Anthropol Sci 12:. https://doi.org/10.1007/s12520-020-01153-8
- Vázquez-de la Fuente I, Barbier I, Puente-Muñoz S, et al (2023) Looking for Novel Natural Gels to Improve Cleaning Methods for Bronze Leachates on Marble. Gels 9:. https://doi.org/10.3390/gels9110843
- Vicini S, Castellano M, Mauri M, Marsano E (2015) Gelling process for sodium alginate: New technical approach by using calcium rich micro-spheres. Carbohydr Polym 134:767–774. https://doi.org/10.1016/j.carbpol.2015.08.064
- Vicini S, Mauri M, Wichert J, Castellano M (2017) Alginate gelling process: Use of bivalent ions rich microspheres. Polym Eng Sci 57:531–536. https://doi.org/10.1002/pen.24552
- Vigani B, Valentino C, Cavalloro V, et al (2021) Gellan-Based Composite System as a Potential Tool for the Treatment of Nervous Tissue Injuries: Cross-Linked Electrospun Nanofibers Embedded in a RC-33-Loaded Freeze-Dried Matrix. Pharmaceutics 13:164. https://doi.org/10.3390/pharmaceutics13020164
- Vigani, B.; Valentino, C.; Sandri, G.; Caramella, C.M.; Ferrari, F.; Rossi S (2022) Spermidine crosslinked gellan gum-based “hydrogel nanofibers” as potential tool for the treatment of nervous tissue injuries: a formulation study. Int. J. Nanomedicine

- Vilas-Boas C, Carvalhal F, Pereira B, et al (2020) One step forward towards the development of eco-friendly antifouling coatings: Immobilization of a sulfated marine-inspired compound. Mar Drugs 18:. https://doi.org/10.3390/md18100489
- Villanueva X, Zhen L, Ares JN, et al (2023) Effect of chemical modifications of tannins on their antimicrobial and antibiofilm effect against Gram-negative and Gram-positive bacteria. Front Microbiol 13:. https://doi.org/10.3389/fmicb.2022.987164
- Volpi F (2017) Green Strategies for the Cleaning of Works of Art Setting Up of an Analytical Protocol for the Evaluation of Cleaning. Alma Mater Studiorum Università di Bologna. DOI 10.6092/unibo/amsdottorato/8050
- Volpi F, Fiocco G, Rovetta T, et al (2021) New Insights on the Stradivari "Coristo" Mandolin: A Combined Non-Invasive Spectroscopic Approach. Appl Sci 11:11626. https://doi.org/10.3390/app112411626
- Vueva Y, Connell LS, Chayanun S, et al (2018) Silica/alginate hybrid biomaterials and assessment of their covalent coupling. Appl Mater Today 11:1–12. https://doi.org/10.1016/j.apmt.2017.12.011
- Wang L, Mu RJ, Lin L, et al (2019) Bioinspired aerogel based on konjac glucomannan and functionalized carbon nanotube for controlled drug release. Int J Biol Macromol 133:693–701. https://doi.org/10.1016/j.ijbiomac.2019.04.148
- Wang L-X, Lee A-R, Yuan Y, et al (2020) Preparation and FTIR, Raman and SEM characterizations of konjac glucomannan-KCl electrogels. Food Chem 331:127289. https://doi.org/10.1016/j.foodchem.2020.127289
- Warda J, Brückle I, Bezúr A, Kushel D (2007) Analysis of Agarose, Carbopol, and Laponite gel poultices in paper conservation. J Am Inst Conserv 46:263–279. https://doi.org/10.1179/019713607806112260
- Watrelot AA, Norton EL (2020) Chemistry and Reactivity of Tannins in Vitis spp.: A Review. Molecules 25:2110. https://doi.org/10.3390/molecules25092110
- Wegst UGK (2006) Wood for sound. Am J Bot 93:. https://doi.org/10.3732/ajb.93.10.1439
- Weththimuni ML, Canevari C, Legnani A, et al (2016) Experimental characterization of oil-colophony varnish: a preliminary study. Int J Conserv Sci 813–826

- Weththimuni ML, Milanese C, Licchelli M, Malagodi M (2021) Improving the Protective Properties of Shellac-Based Varnishes by Functionalized Nanoparticles. Coatings 11:419. https://doi.org/10.3390/coatings11040419
- Wilder T (2010) The conservation, restoration, and repair of stringed instruments and their bows, Vol. 2. IPCI-Canada, Montreal
- Williams MAK, Foster TJ, Martin DR, et al (2000) A molecular description of the gelation mechanism of konjac mannan. Biomacromolecules 1:440–450. https://doi.org/10.1021/bm005525y
- Witono JR, Noordergraaf IW, Heeres HJ, Janssen LPBM (2014) Water absorption, retention and the swelling characteristics of cassava starch grafted with polyacrylic acid. Carbohydr Polym 103:325–332. https://doi.org/10.1016/j.carbpol.2013.12.056
- Wolbers R (2000) Cleaning Painted Surfaces, Aqueous Methods. Archetype, London
- Wolbers RC (1992) The use of a synthetic soiling mixture as a means for evaluating the efficacy of aqueous cleaning materials on painted surfaces. Conserv Restaur des biens Cult Rev l'ARAAFU 22–29
- Yamauchi A (2001) Section 1 - Gels: Introduction. In: Gels Handbook. Elsevier, USA, pp 4–12
- Yang D, Yuan Y, Wang L, et al (2017) A Review on Konjac Glucomannan Gels: Microstructure and Application. Int J Mol Sci 18:2250. https://doi.org/10.3390/ijms18112250
- Yeung ZLL, Kwok RCW, Yu KN (2003) Determination of multi-element profiles of street dust using energy dispersive X-ray fluorescence (EDXRF). Appl Radiat Isot 58:339–346. https://doi.org/10.1016/S0969-8043(02)00351-2
- Yoshikawa S, Waltham C (2014) Woods for Wooden Musical Instruments. J Acoust Soc Am 122:568–573. https://doi.org/10.13140/2.1.5067.1369
- Yu Y gyeon, Han G, Lee H soo, Han KS (2021) Study on the Gel Cleaning System for Removal of Poly (vinyl acetate) Fixative of the Mural Paintings of the Payathonzu Temple in Bagan, Myanmar (I) - Focusing on Properties and Removability of Gel Cleaners -. J Conserv Sci 37:370–379. https://doi.org/https://doi.org/10.12654/JCS.2021. 37.4.06
- Zaman HU, Beg MDH (2013) Preparation and properties of sodium alginate films. J Polym Eng 33:829–836. https://doi.org/10.1515/polyeng-2013-0146

- Zhang J, Hu Y, Li Y (2018) Gel Chemistry. Springer Singapore, Singapore
- Zhang T, de Vries R, Xu X, et al (2021) Microstructural changes during alkali- and heat induced gelation of konjac glucomannan. Food Hydrocoll 114:. https://doi.org/10.1016/j.foodhyd.2020.106552
- Zhen L, Lange H, Crestini C (2021) An Analytical Toolbox for Fast and Straightforward Structural Characterisation of Commercially Available Tannins. Molecules 26:2532. https://doi.org/10.3390/molecules26092532
- Zhou Y, Jiang R, Perkins WS, Cheng Y (2018) Morphology evolution and gelation mechanism of alkali induced konjac glucomannan hydrogel. Food Chem 269:80–88. https://doi.org/10.1016/j.foodchem.2018.05.116
- Zhuang J, Li M, Pu Y, et al (2020) Observation of potential contaminants in processed biomass using fourier transform infrared spectroscopy. Appl Sci 10:. https://doi.org/10.3390/app10124345
- Zörner A, Oertel S, Schmitz B, et al (2017) Determination of the Selectivity of Printed Wearable Sweat Sensors. In: Proceedings of the 10th International Joint Conference on Biomedical Engineering Systems and Technologies. SCITEPRESS - Science and Technology Publications, pp 81–87

List of Figures

Figure 1. Example 1), schematic drawing of physical phenomena occurring simultaneously while cleaning glue on wood with solvent (water). 24
Figure 2. Example 2), schematic drawing of physical phenomena occurring simultaneously while cleaning dust on wood with a solvent (water). 26
Figure 3. Classification of gelation mechanism (Rubinstein and Colby 2003). 28
Figure 4. Schematic description of the preparation and reconstruction of wooden mock-ups representative of (a) East Asian and (b) Western musical instrument finishing treatments. 39
Figure 5. Sketch of the internal side of the double bass front plate and the detached fragment images in VIS (up) and UV (down). 40
Figure 6. Three different junction zones by calcium ion with alginate. MG/MG, GG/GG, and GG/MG junctions are made up of chains of M-block and G-block (Donati et al. 2005). 53
Figure 7. A different block structure in alginate. The M-block represents β-D-mannuronic acid and G-block represents α-L-guluronic acid (G) (Pawar and Edgar 2012). 53
Figure 8. Different gelation methods of diffusion and internal setting methods (Draget et al. 2005). 54
Figure 9. Gelation of alginate with calcium ion formed in egg-shell structure, and after leaving for 10 min on the surface of WM, the solvent diffused (a). Gelation of alginate with calcium ion (b) and with aluminum (c) in thin form gel. 56
Figure 10. Expected reaction between alginate polymer and calcium ions (Al-Musa et al. 1999). 56
Figure 11. A schematic diagram of steps involved in preparing CA gel. 57
Figure 12. FTIR spectrum of the Ca-alginate formulated gel (CA) and pure sodium alginate (SA) (a). Markers for electrostatic interactions of carboxylate groups and calcium ions (red dotted line). SEM image of CA gel (b) acquired in high vacuum with secondary electrons. 58
Figure 13. Stereomicroscopy images of WM (a), soiled-WM (b), EAM (c), and soiled-EAM (d) mock-ups. 61

Figure 14. Stereomicroscopy images after the cleaning application on soiled-WM by CA gel at different application times CA_1 (a) and CA_3 (b), and on soiled-EAM by CA_1 (c) and CA_3 (d). 61
Figure 15. 3D heat maps of soiled-WM (a) cleaned by CA_3 (b). The colour range represents the different heights (in microns) of the details present on the sample surface. Considered roughness values of Sa (d), Ssk (e), and Sv (f) on the different areas of soiled−WM cleaned by different gels and application time CA_1, CA_3, and Agar_3. 62
Figure 16. 3D heat maps of soiled-EAM (a) cleaned by CA_3 (b). The colour range represents the different heights (in microns) of the details present on the sample surface. Considered roughness values of Sa (d), Ssk (e), and Sv (f) on the different areas of soiled−EAM cleaned by different gels and application time CA_1, CA_3, and Agar_3. 63
Figure 17. Stereomicroscopy images of sweat-WM (a) and sweat-EAM (b). 3D heat map of sweat-EAM (c). The color range represents the different heights (in microns) of the details present on the sample surface. Considered roughness values of Sa (d), Ssk (e), and Sv (f) on the different areas of sweat−EAM cleaned by different gels and application time CA_1, CA_3, and Agar_3. 64
Figure 18. Normalized Ca, Si, K, and Fe counts were detected on (a) WM and (b) EAM. Different bars correspond to plain (WM and EAM) and with soiling deposits treated mock-ups (soiled-WM and soiled-EAM) and after 1, 2, and 3 applications of CA gel (CA_1, CA_2, CA_3). XRF values correspond to the net area counts of the Kα peak of each element normalized to time and the mean of the entire dataset of Rh-Kα peak net area counts, with the related standard deviation. 67
Figure 19. Cleaning efficacy values obtained on soiled-WM, soiled-EAM, and CA gels were applied 1 to 3 times repeatedly. The percentage of cleaning efficacy was calculated based on the counts of calcium markers. 68
Figure 20. Cleaning efficacy values obtained on sweat-WM and sweat-EAM and CA gels were applied 1 to 3 times repeatedly. The percentage of cleaning efficacy was calculated based on the counts of chloride markers. 69
Figure 21. ER-FTIR spectra in (a) pseudo-absorbance and (b) after Kramers-Kronig transform of soiled-WM (black), area cleaned with Agar_3 (grey), CA_3 (red) and, a reference of WM (orange). The marker bands selected for identifying the soiling mixture are reported. 70

Figure 22. ER-FTIR spectra in pseudo-absorbance were acquired on soiled-EAM (black), area cleaned with Agar_3 (grey), CA_3 (red), and a reference of EAM (brown). The marker bands selected for identifying the soiling mixture are reported. 72
Figure 23. Reflection FTIR spectra in (a) pseudo-absorbance and (b) after Kramers-Kronig transform of WM (orange) and sweat-WM (blue) cleaned with Agar_3 (grey) and CA_3 (red). The marker bands selected for identifying synthetic sweat components are reported..... 72
Figure 24. Expected reaction between alginate polymer and GPTMS and calcium ion. 74
Figure 25. A schematic diagram of steps involved in preparing CA-GPTMS gel. 75
Figure 26. Liquid state ^{1}H-NMR of sodium alginate and GPTMS (SA-GPTMS). 76
Figure 27.HSQC NMR spectrum of sodium alginate functionalized with GPTMS..... 76
Figure 28. FTIR spectrum of the Ca-alginate-GPTMS gel formulated in sodium alginate monomer and GPTMS molar ratios respectively in SA: GPTMS = 1: 2 (CA-GPTMS_2), pure sodium alginate (SA) and GPTMS reactants (a). Markers for electrostatic interactions of carboxylate groups and calcium ions (red dotted line), siloxane groups (triangle), and epoxy groups of GPTMS (asterisk) are displayed. SEM image of CA-GPTMS_2 gel film acquired in high vacuum with secondary electrons (b) and its EDS spectrum (c). 78
Figure 29. Mechanical properties determined by tensile test (mean value ± s.d.; n = 5): tensile strength (a) and elongation at break (b). Stress-strain curves of CA, CA-GPTMS_1, _2 and _4 gels. 79
Figure 30. Water dispersion tests after CA-GPTMS (a), CA (b), and agar (c) gel loaded with 2,7-dichlorofluorescein solution and applied on the filter paper. The black square represents the area of the applied gel (1x1 cm), while the red line qualitatively indicates the water dispersion..... 80
Figure 31. SEM-EDS acquired in low vacuum by secondary electrons Tescan detector on wood surface before (a), and after CA-GPTMS_2 gel application (b), and corresponding elemental analysis after cleaning (c). 82
Figure 32. Observation of the cross-sections of the fresh mock-up (a) by stereomicroscope: before cleaning process: the average surface area of 200 µm, after cleaning with CA-GPTMS_2 (b): the average surface area of 25 µm, after cleaning with agar (c): the average surface area of 25 µm. Observation of the cross-section of the aged mock-up (d) by stereomicroscope: before cleaning process: the average surface area of 200 µm, after cleaning with CA-GPTMS_2 (e): the average surface area of 45 µm, after cleaning with agar: the average surface area of 60 µm (f). 83

Figure 33. The ER-FTIR spectra of after Kramers-Kronig transform of fresh (a) and aged (b) wood-animal glue mock-up (orange), cleaned with agar (grey) and CA-GPTMS_2 (green), and wood (brown). The marker bands of animal glue are represented in a dotted red line while those of wood are represented with brown arrows. 84
Figure 34. Images of the wooden fragment plate of the double bass, area before cleaning (a), during cleaning with the CA-GPTMS_2 (b), right after the 20 min application (c), after cleaning (d), and ER-FTIR spectra after Kramers-Kronig transform acquired before (black) and after (green) cleaning area with CA-GPTMS_2 (e). The marker bands of the animal glue are represented in a dotted red line and the wood is represented in brown arrows..... 85
Figure 35. Expected reaction between alginate polymer, XAMA 7 and calcium ion. 86
Figure 36. A schematic diagram of steps involved in preparing CA-XAMA7 gel. 87
Figure 37. Liquid state ^{1}H-NMR of sodium alginate (SA), XAMA®7, and sodium alginate functionalized with XAMA®7 (SA-XAMA7). 88
Figure 38. 2D-COSY NMR spectrum of sodium alginate functionalized with XAMA®7 (SA-XAMA7). Blue and green lines, respectively point out the connections between protons b, d, e, and f. 89
Figure 39. Thermogravimetric analysis (TGA) (a) curves of CA and CA-XAMA7 gels in different ratios..... 89
Figure 40. FTIR spectrum of the Ca-alginate-XAMA7 formulated gel in sodium alginate monomer and XAMA®7 molar ratios respectively in SA: XAMA®7 = 1: 1(CA-XAMA7_1), pure sodium alginate (SA) and XAMA®7 reactants. Markers for electrostatic interactions of carboxylate groups and calcium ions (red dotted line), ester groups (triangle), and methylene derivation from XAMA®7 (asterisk) are displayed. SEM image of CA-XAMA7_1 gel film acquired in high vacuum with secondary electrons (b). 90
Figure 41. Mechanical properties determined by tensile test (mean value ± s.d.; n = 5): tensile strength (a) and elongation at break (b). fresh and aged gel of CA and CA-XAMA7_1 tensile strength (c) and Elongation at break (d). 91
Figure 42. XRF heat maps on sweat-WM after cleaning with CA-XAMA7_1 with deionized water and with different surfactants tween® 20 and ecosurf™ EH-9 The color range represents high to low counts of chlorine marker. 93

Figure 43. Star diagrams comparing the results of agar and CA gel characteristics and cleaning evaluation after cleaning soiled-WM (a) and -EAM (b) and agar, CA gel, and CA-XAMA7 gel characteristics and cleaning evaluation after cleaning sweat-WM (c) and -EAM (d). 95
Figure 44. The structure of β-1,4-linked D-glucose and D-mannose repeating units in konjac glucomannan (Williams et al. 2000). 99
Figure 45. Image of alkaline konjac gel (a) and konjac-borax gel. 100
Figure 46. Expected reaction between konjac polymer and borate ions (Song et al. 2019). 100
Figure 47. A schematic diagram of steps involved in preparing KGB gel. 101
Figure 48. FTIR spectrum of the konjac glucomannan-borax formulated gel (KGB) and pure konjac glucomannan (KG) (a). Markers for interactions of hydroxyl groups and borate ions (triangle) are displayed. SEM image of KGB gel acquired in standard secondary electrons (b). 102
Figure 49. Stress–strain curves of fresh and aged KGB gel (a) and agar gel (b). 103
Figure 50. Stereomicroscopy images after the cleaning application on soiled-WM by KGB gel at different application times KGB_1 (a) and KGB_3 (b), and on soiled-EAM by KGB_1 (c) and KGB_3 (d). 105
Figure 51. 3D heat maps of soiled-WM cleaned by KGB_1 (a) and KGB_3 (b). The color range represents the different heights (in microns) of the details present on the sample surface. Considered roughness values of Sa (c), Ssk (d), and Sv (e) on the different areas of soiled−WM cleaned by different gels and application time KGB_1, KGB_3, and Agar_3. 105
Figure 52. 3D heat maps of soiled-EAM cleaned by KGB_1 (a) and KGB_3 (b). The color range represents the different heights (in microns) of the details present on the sample surface. Considered roughness values of Sa (c), Ssk (d), and Sv (e) on the different areas of soiled−WM cleaned by different gels and application time KGB_1, KGB_3, and Agar_3. 106
Figure 53. 3D heat maps of sweat-EAM cleaned by KGB_1 (a) and KGB_3 (b). The color range represents the different heights (in microns) of the details present on the sample surface. Considered roughness values of Sa (c), Ssk (d), and Sv (e) on the different areas of soiled−WM cleaned by different gels and application time KGB_1, KGB_3, and Agar_3. 107
Figure 54. Normalized Ca, Si, K, and Fe counts were detected on (a) WM and (b) EAM. Different bars correspond to plain (WM and EAM) and with soiling deposits treated mock-ups (soiled-WM and soiled-EAM) and after 1, 2, and 3 applications of KGB gel (KGB_1, KGB_2, KGB_3). XRF

values correspond to the net area counts of the Kα peak of each element normalized to time and the mean of the entire dataset of Rh-Kα peak net area counts, with the related standard deviation. 110
Figure 55. Cleaning efficacy values obtained on soiled-WM and soiled-EAM and KGB gels were applied 1 to 3 times repeatedly. The percentage of cleaning efficacy was calculated based on the counts of calcium markers. 110
Figure 56. Cleaning efficacy values obtained on sweat-WM, sweat-EAM, and KGB gels were applied 1 to 3 times repeatedly. The percentage of cleaning efficacy was calculated based on the counts of chloride markers. 111
Figure 57. ER-FTIR spectra in (a) pseudo-absorbance and (b) after Kramers-Kronig transform of soiled-EAM (black), area cleaned with Agar_3 (grey), KGB_3 (red) and, a reference of WM (orange). The marker bands selected for identifying the soiling mixture are reported. 112
Figure 58. ER-FTIR spectra in pseudo-absorbance acquired on soiled-EAM (black), area cleaned with Agar_3 (grey), KGB_3 (red), and a reference of EAM (brown). The marker bands selected for identifying the soiling mixture are reported. 112
Figure 59. Reflection FTIR spectra in (a) pseudo-absorbance and (b) after Kramers-Kronig transform of WM (orange) and sweat-WM (blue) cleaned with Agar_3 (grey) and KGB_3 (red). The marker bands selected for identifying synthetic sweat components are reported. 113
Figure 60. Expected reaction between konjac glucomannan, polyvinyl alcohol (PVA), polyvinylpyrrolidone (PVP), and sodium tetraborate decahydrate (borax). 114
Figure 61. A schematic diagram of steps involved in preparing KGPPB gel. 115
Figure 62. FTIR spectrum of the konjac glucomannan-polyvinyl alcohol- polyvinylpyrrolidone-borax formulated gel (KGPPB) and pure konjac glucomannan (KG) (a). Markers for interactions of hydroxyl groups and borate ions and C-N stretching of PVP (triangle) are displayed. SEM images of KGPPB gels of each freezing-thawing (F-T) cycle, F-T0, F-T1, F-T2, and F-T3 are acquired in a high vacuum with secondary electrons (b). 116
Figure 63 Mechanical properties determined by compressive test (mean value ± s.d.; n = 5): hardness (kPa) (a), Young's Modulus (kPa) (b), and stress-strain curve (c). 117
Figure 64. Expected functionalization reaction between Soft Kraft Lignin (SKL) and epichlorohydrin (ECH) (a), and crosslink of konjac with partially etherified polyphenols and borate ions (B) (b). 120

Figure 65. A schematic diagram of steps involved in preparing KGB-SKL25 and KGB-SKL50 gel. The same preparation steps were carried out on KGB-Vv25 and KGB-Vv50. 122
Figure 66. The SEM image of KGB-SKL50 was acquired in standard secondary electrons (a and b). 123
Figure 67. SEM image of KGB-Vv50 acquired in standard secondary electrons (a and b). 124
Figure 68. Normalized Ca, Si, K, and Fe counts were detected on (a) WM and (b) EAM. Different bars correspond to plain (WM and EAM) and with soiling deposits treated mock-ups (soiled-WM and soiled-EAM) and after applications of KGB-Vv25 and agar gel. XRF values correspond to the net area counts of the Kα peak of each element normalized to time and the mean of the entire dataset of Rh-Kα peak net area counts, with the related standard deviation. 126
Figure 69. ER-FTIR spectra in (a) pseudo-absorbance and (b) after Kramers-Kronig transform of soiled-WM (black), area cleaned with KGB-Vv25 (purple), agar (grey), and a reference of WM (orange). The marker bands selected for identifying the soiling mixture are reported. 127
Figure 70. ER-FTIR spectra in pseudo-absorbance acquired on soiled-EAM (black), area cleaned with KGB-Vv25 (purple), agar (grey), and a reference of EAM (brown). The marker bands selected for identifying the soiling mixture are reported. 128
Figure 71. Reflection FTIR spectra in (a) pseudo-absorbance and (b) after Kramers-Kronig transform of WM (orange) and sweat-WM (blue) cleaned with KGB-Vv25 (purple) and agar (grey). The marker bands selected for identifying synthetic sweat components are reported. 128
Figure 72. Star diagrams comparing the results of agar, KGB and KGB-Vv25 gel characteristics and cleaning evaluation after cleaning soiled-WM (a) and soiled-EAM (b), sweat-WM (c), and sweat-EAM (d). 130

List of Tables

Table 1. Diverse gels application in the cultural heritage field 30
Table 2. Mechanical properties of gels determined by tensile testing (mean value ± s.d.; n = 3). ANOVA one-way, Multiple Range Test ($p \leq 0.05$): different symbols (*, **, #, °, §, §§) indicate statistically different data. AUC: Area Under the stress–strain curve. 59
Table 3. Moisture properties of SA and KG gels used for the cleaning test, namely equilibrium moisture content (EWC), swelling capacity (SC), and water release (WR). The average values and the related standard deviations were determined by repeating the experiment five times. D.W. = distilled water 60
Table 4. Color coordinates L*, a*, and b* were measured on WM and EAM and with the soiling mixture (soiled-WM and soiled-EAM). After cleaning with CA gel by repeating applications, the average values and the related standard deviations were achieved by repeating the measurement five times. Standard deviation values are given in brackets. The overall chromatic variation (△E*) was calculated between the areas before and after cleaning the soiled-WM and soiled-EAM by repeating cleaning trials using CA gels 65
Table 5. Normalized Cl (Kα) counts on sweat-WM and sweat-EAM, before (control) and after different cleaning applications with SA and KG. 68
Table 6. Reflection FTIR band assignment in the range 4000-800 cm^{-1} identified on EAM and WM and on the soiling mixture and sweat dispersed on the mock-ups. For the derivative bands marked with an asterisk (*), the value refers to the maximum of the band after the application of KK transformations. Inv. = inverted band (Restrahlen) in the pseudo-absorbance spectra 71
Table 7. Moisture properties of CA-GPTMS gels, CA, and agar: equilibrium moisture content (EWC), swelling capacity (SC), and water release (WR). Mean values and standard deviations were calculated on five repetitions 80
Table 8. Moisture properties of CA-XAMA7 gels, CA, and agar: equilibrium moisture content (EWC), swelling capacity (SC), and water release (WR). Mean values and standard deviations were calculated on five iterations 92

Table 9. Mechanical properties of gels determined by compressive test (mean value ± s.d.; n = 3). ANOVA one-way ($p < 0.05$), Multiple Range Test: different symbols indicate statistically different data. AUC: Area Under the stress–strain curve. 103
Table 10. Moisture properties of SA and KG gels used for the cleaning test, namely equilibrium moisture content (EWC), swelling capacity (SC), and water release (WR). The average values and the related standard deviations were determined by repeating the experiment five times. D.W. = distilled water. 104
Table 11. Color coordinates L*, a*, and b* were measured on WM and EAM and with the soiling mixture (soiled-WM and soiled-EAM). After cleaning with KGB gel by repeating applications, the average values and the related standard deviations were achieved by repeating the measurement five times. Standard deviation values are given in brackets. The overall chromatic variation (△E*) was calculated between the areas before and after cleaning the soiled-WM and soiled-EAM by repeating cleaning trials using KGB gels. 108
Table 12 Normalized Cl (Kα) counts on sweat-WM and sweat-EAM, before (control) and after different cleaning applications with KGB gel 111
Table 13. Moisture properties of KGPPB gels (KGPPB_F-T1, KGPPB_F-T3), KGB and agar: equilibrium moisture content (EWC), swelling capacity (SC), and water release (WR). Mean values and standard deviations were calculated on five iterations 118
Table 14. Composition of the formulated konjac (KG) gel with SKL and partially etherified polyphenols (SKL25 and SKL50), and borax (B) 121
Table 15. Composition of the formulated konjac (KG) gel with Vv and partially etherified polyphenols (Vv25 and Vv50), and borax (B). 121
Table 16. Moisture properties of KGB-SKL, -SKL25, and -SKL50 gels, KGB, and agar: equilibrium moisture content (EWC) and swelling capacity (SC). Mean values and standard deviations were calculated on four iterations. 123
Table 17. Moisture properties of KGB-Vv, -Vv25, and -SVv50 gels, KGB, and agar: equilibrium moisture content (EWC) and swelling capacity (SC). Mean values and standard deviations were calculated on four iterations. 124
Table 18. Normalized Cl (Kα) counts on sweat-WM and sweat-EAM, before (control) and after cleaning applications by KGB-Vv25 and agar gel 126

Acknowledgements

I still remember the day in 2020 when I decided to apply for a doctorate program in Italy. I felt a mix of emotions, both worried and nervous about being ready to start a doctorate, especially since the world was facing a pandemic, which created a very different environment from what I had experienced back in Italy in 2019 when I was doing an internship at Arvedi Laboratory. Though, I was also excited about the prospect of gaining new knowledge and meeting new people. Approaching the final stages of my doctoral journey, I now feel excited and relieved to have made some progress in my work. Moreover, during these three years, there have always been people who have supported me with gratitude and open arms, which has kept me going and continuing my work diligently.

I consider myself incredibly lucky to work under the guidance of such great professors. Prof. Maurizio Licchelli always provided unwavering support for my research activities and gave me clear direction. Prof. Marco Malagodi, with his warm heart and firm encouragement, taught me the true meaning of collaboration by involving me in his team. Without these two professors, I guess it would have been impossible to start, work through the problems, and finish my thesis properly.

Most of the work was carried out at the Department of Chemistry Laboratory and the Arvedi Laboratory of Non-Invasive Diagnostics in Cremona of the Interdepartmental Center for Studies and Research for the Conservation of Cultural Heritage (CISRiC) of the University of Pavia. I would like to express my sincere gratitude to Dr. Maduka Weththimuni for her valuable cooperation and for always being available to discuss my concerns or questions. I would also like to extend special thanks to Dr. Francesca Volpi, Dr. Giacomo Fiocco, and Dr. Michela Albano, who provided me with great support and valuable opinions, from whom I learned several ideas and made significant progress in the research project. Furthermore, I would like to express my gratitude to other colleagues at the Arvedi Laboratory and the Department of Chemistry Chiara Dondi, Matteo Ferretti and Dr. Alessando Girella, who supported me professionally and personally. I would like to thank Curzio Merlo and Claudio Canevari for their continued interest and collaborative work on research activities in Cremona.

During my research, I had the opportunity to collaborate with several groups and institutions. I would like to express my sincere gratitude to Prof. Teresa Recca from the Department of Chemistry at the University of Pavia, with whom I collaborated on NMR acquisition, and to Prof. Chiara Milanese from the Department of Chemistry, Division of Physical Chemistry, with whom I collaborated on TGA-DSC analysis. Despite having no prior experience with these analytical techniques, their expert guidance and support were invaluable. Additionally, I sincerely thank Dr. Barbara Vigani and Prof. Silvia Rossi from the Department of Pharmaceutical Sciences, who were always available to help me with gel analysis of mechanical properties which made a huge improvement on the research work.

I would like to express my sincere appreciation to Dr. Francesca di Turo, Prof. Fabio Beltram and Prof. Pasqualantonio Pingue at the National Enterprise for NanoScience and NanoTechnology (NEST) of the Scuola Normale Superiore in Pisa. It was a great opportunity for me to enhance my research section of analytical skills through profilometry analysis. I am pleased to say that I collaborated highly with Prof. Heiko Lange and Elenora Verni at the University of Milan Bicocca, where we worked together on a new gel formulation. Although our time was limited, it was an intense and satisfying experience. I further express my gratitude to ICHEMCO srl (Milan, Italy) and Hubei Yizhi Konjac Co. Ltd (Yichang, China) for providing the essential chemicals for this research work. Without their contribution, it would have been impossible to carry out this study.

My special thanks to Prof. Yongjae Chung. He was my supervisor for six years, from 2013 until 2018, and he remains a constant source of support and guidance for my current and future research. I also extend my heartfelt thanks to Prof. Francesco Canganella for being an incredible mentor to me since our first encounter at the KNUCH and ISCR BILATERAL WORKSHOP in 2017. His words of wisdom and encouragement have always stayed with me.

I would like to acknowledge the immense support I received from my family and friends, without whom this achievement would not have been possible. Being away from them was hard, but their unwavering trust and encouragement kept me going during my three years of research in Italy.

Finally, I thank my reviewers, Prof. Monica Gulmini, Prof. Paola Fermo, and Prof. Chiara Milanese, for their willingness to read the thesis and make suggestions to improve the last stage of the thesis significantly.